UNIVERSITY OF LIVERPOOL

Modelling pattern formation in growing populations of motile bacteria

Thesis submitted in accordance with the requirements of the University of Liverpool for the degree of Doctor in Philosophy by

Valentina-Marina Bucur

FEBRUARY 2025

Contents

List of Figures

List of Tables

Acknowledgements

I would like to express my deepest gratitude to my supervisor, Dr Bakhtier Vasiev, for their unwavering support, guidance, and encouragement throughout the course of this research. I am also immensely grateful to Prof Rachel Bearon for her guidance and help during my PhD. Their expertise, insightful feedback, and patient mentorship have been invaluable to the completion of this thesis.

I would also like to thank EPSRC (Engineering and Physical Sciences Research Council) and NBIC (National Biofilms Innovation Centre) for their financial support, which made this research possible.

Special thanks to my colleagues and fellow researchers at the University of Liverpool, whose collaboration, ideas, and camaraderie have greatly enriched this journey.

Lastly, I would like to thank my family and friends for their unwavering encouragement and support, both emotional and practical, which have been a constant source of strength.

To all who have contributed to this thesis, directly or indirectly, thank you.

Declaration

I declare that the following thesis is my own composition and that it has not been submitted before in application for a higher degree.

Valentina-Marina Bucur

Abstract

Biological pattern formation is one of the most intriguing phenomena in nature. Since bacteria are rarely motionless, simple patterns such as travelling waves and stationary periodic patterns form as a result of cellular movement, including diffusion (movement away from areas of high density) and chemotaxis (movement in response to chemical gradients). Bacterial movement in an originally homogeneous system is due to an instability triggered by random disturbances. In this work, we investigate the conditions for the onset of instability that leads to the formation of stationary periodic patterns, as well as the minimum wavespeed of travelling wavefronts that appear between the steady states of reaction-diffusion-advection systems.

We first consider some reaction-diffusion systems used in population dynamics to illustrate the formation of travelling wavefronts, such as the well-known Fisher-Kolmogorov equation, which is the starting point for our research since it is commonly used to demonstrate the spatial spread of a single biological population. Initially, we investigate the effects of model parameters on the profile of the travelling wavefronts. Then, by assuming that the bacteria produce a chemical agent, we use a modified reaction-diffusion-advection system to examine the effects of chemotaxis on the wavespeed of the travelling wavefronts. Through methods of nonlinear analysis, as well as computational simulations, it has been shown that the wavespeed is highly affected by chemorepulsion. Essentially, bacterial species transition across the medium much faster when the chemical agent produced acts as a repeller. On the other hand, when the chemical agent acts as an attractor and the chemotaxis sensitivity is above a certain threshold value, determined by methods of linear analysis, stationary periodic patterns form behind the travelling wavefront. Characteristics of such patterns are determined using methods of nonlinear Fourier analysis. Assuming the pattern has reached a stationary nonhomogeneous state, the time variable is removed, and we seek Fourier solutions over some modes, which can be used to find information about the amplitude and wavelength of the patterns formed. The effects of model parameters are also investigated, and analytical results are supported by numerical simulations.

We then investigate pattern formation in a system of two interacting species with Lotka-Volterra kinetics. Initially, in the absence of chemotaxis, travelling wavefronts are admitted as solutions to such systems, making the transition from an unstable steady state to a stable one. We show that, in this case, depending on the diffusion and proliferation of the species, wavefronts can move with different speeds when transitioning from the unstable trivial steady state to the

stable coexistence state. More interestingly, when the coexistence steady state is unstable, travelling wavefronts are admitted as solutions, making the transition to one of the stable extinction states. In this case, the minimum wavespeed is determined by investigating the dispersion curve, and the effects of model parameters on the propagation of the species are investigated by both analytical and numerical methods. Additionally, a reaction-diffusion-advection model has also been examined, in which one of the species produces a chemical agent that can act either as a repeller or attractor for the other species. In the case where the chemical agent acts as an attractor, we show that when the coexistence steady state is unstable, the minimum wavespeed of travelling fronts significantly increases with an increase in chemoattraction. Conversely, if the chemical agent acts as a repeller and specific conditions are met, stationary periodic patterns form behind the travelling wavefronts. Similar to the one-species case, characteristics such as amplitude and wavelength are obtained using methods of nonlinear analysis. One of the most interesting patterns that form in a system of two interacting species is stationary periodic patterns triggered by finite amplitude disturbances when the species producing the chemical agent is initially extinct. In this case, methods of linear analysis show that stationary periodic patterns are not initiated by infinitesimal perturbations; however, assuming the perturbation is above a certain threshold value, patterns can emerge.

The outcomes of our research demonstrate that chemotaxis plays a vital role in pattern formation, which occurs during various biological processes such as morphogenesis and population dynamics. In a one-species case, chemoattraction is responsible for the formation of stationary periodic patterns, while chemorepulsion is responsible for faster bacterial propagation across the host medium. In a two-species case, chemorepulsion is responsible for stationary periodic patterns, while chemoattraction results in faster propagation of species. These results can be applied to a range of biological processes, such as understanding the effects of chemotaxis on colonisation in the early stages of biofilm formation, bacterial infections, and wound healing processes.

Thesis Outline

This thesis consists of five chapters.

Chapter 1: Introduction

The first chapter of the thesis introduces the motivation behind this research, which is to understand how bacterial motility affects pattern formation, as well as some basic biological concepts and mathematical methods. Bacteria are among

the most primitive forms of life, and they can respond to a wide range of environmental signals by directing their motion to more favourable conditions. We are interested in examining how chemotaxis, as well as interspecific competition, affects bacterial motility and results in spatial-temporal patterning.

After introducing the general area of research, we provide an introduction to some common biological concepts. Different phenomena are discussed in which pattern formation plays an important role, such as the explanation of animal markings, e.g., the pattern that appears on the skin of the giant puffer fish [144], or the way cells form complex patterns in developing tissue [82]. The effects of chemotaxis on bacterial motion, as well as the differences between chemoattraction and chemorepulsion, are also explained. This is followed by a number of experimental results that show patterns such as travelling waves and stationary spots formed by *E. coli* on a Petri dish [17], as well as patterns in the form of aggregating streams formed by starving populations of *Dictyostelium discoideum* [133].

The biological introduction is followed by mathematical background, which includes the main mathematical methods used in the analysis of systems of ordinary differential equations, as well as partial differential equations. Methods of linear analysis are introduced to investigate some simple mathematical models, such as the Fisher-Kolmogorov equation [33, 62] and the Lotka-Volterra model [76, 135]. Classical Turing pattern analysis is also introduced to find conditions under which stability breaks down, resulting in stationary periodic pattern formation [128]. In addition, Fourier analysis is introduced to obtain information about the characteristics of the pattern. At the end of the chapter, we describe some methods of solving differential equations numerically. These include the classical forward Euler formula for time discretisation, the central scheme for spatial discretisation, and the two-step Lax-Friedrichs method for the advection term [100].

Chapter 2: Travelling wavefronts formed by chemotactically active bacteria

In this chapter, the aim is to understand the formation of travelling wavefronts in a system with one bacterial population, as well as in a system with two interacting species. In both cases, bacteria produce a chemical agent, which can have no effect on the microorganisms, or it can act either as a chemoattractant or chemorepellent, initiating the migration of bacteria due to chemotaxis.

In the first instance, we consider a system with one bacterial species in which the chemical agent has no effect on motility. The partial differential equation describing the change in the density of bacteria over time is the Fisher-Kolmogorov

equation [33], introduced in the first chapter. Since there is no movement due to chemotaxis, the two partial differential equations are decoupled, and hence, travelling wavefronts connect an unstable steady state to a stable one. Moreover, travelling wavefronts also appear in the presence of chemotaxis. If the chemical acts as a chemoattractant and the chemotactic sensitivity is above a certain threshold value, periodic patterns form behind the travelling wavefront. If the chemical acts as a repellent and chemorepulsion is strong enough, the wavespeed of the front is significantly affected by chemotaxis. Using methods of nonlinear analysis, we provide a formula to describe how the wavespeed depends on diffusion, reproduction, and chemorepulsion.

In the second section of the chapter, the formation of travelling wavefronts in a system with two interacting species is considered. In the absence of chemotaxis, this system represents the well-known Lotka-Volterra model [89, 137], in which the only patterns that can be obtained are travelling wavefronts. On the other hand, in the presence of chemotaxis, periodic patterns form behind the travelling wavefronts if chemorepulsion is strong enough. In this section, we have shown the formation of travelling wavefronts moving at different speeds, depending on diffusion and reproduction, as well as wavefronts moving from the unstable coexistence steady state to a stable extinction state if certain conditions on interspecific competition are met.

Chapter 3: Stationary periodic patterns in a one species system

In this chapter, stationary Turing patterns formed by a single bacterial species producing its own chemoattractant are considered and described in detail. This work builds on research conducted by Keller and Segel [58, 59, 60], which investigates patterns formed as a result of a breakdown of stability. In the mathematical model considered, the movement of bacteria is highly dependent on the strength of chemotactic sensitivity. First, using methods of linear analysis, conditions under which stability breaks down and Turing pattern formation is initiated are obtained.

Since classical Turing pattern analysis does not provide any information about the characteristics of the pattern, nonlinear Fourier analysis is used to obtain information about wavelength and amplitude. Assuming a stationary pattern, a system of simultaneous equations is obtained, which can be solved to give solutions as Fourier series over some modes. The effects of model parameters on amplitude and wavelength are also investigated, and analytical results are verified by methods of computational simulations. This work fills existing gaps in the literature regarding the analysis of Turing patterns in a system with one bacterial species producing a chemotactic agent. This chapter has also been

submitted as a paper and is available as a preprint on arXiv [15].

Chapter 4: Stationary periodic patterns in a system of two interacting species

The last research chapter focuses on stationary periodic pattern formation in a system of two interacting bacterial species, where one of the species produces a chemotactic agent for the other. The aim of this chapter is to understand the conditions that lead to the formation of Turing patterns and to obtain characteristics of the patterns, such as wavelength and amplitude.

The simplest case to consider is the emergence of Turing patterns from the coexistence steady state, which is stable in the well-mixed system if both competition rates are smaller than 1. By fixing model parameters and using the Routh-Hurwitz criteria [25], regions in which the stable steady state becomes unstable due to perturbations are identified. These regions are used to investigate the relationship between interspecific competition and chemorepulsion, and how these parameters affect the formation of Turing patterns.

The next part of this chapter involves obtaining information about the characteristics of the patterns using methods of nonlinear Fourier analysis, which is done in a similar manner to the case of a single bacterial population. One of the most important applications of nonlinear Fourier analysis is to demonstrate the emergence of stationary periodic patterns when the species producing the chemical agent is initially extinct. In this instance, methods of linear analysis show that the emergence of patterns is not possible with infinitesimal perturbations; however, using Fourier analysis, as well as computational simulations, we show that patterns form under the influence of finite amplitude disturbances.

Chapter 5: Discussion

In this chapter, the main results of our research, along with further research opportunities, are presented. We discuss the effects of chemotaxis, as well as other model parameters, on pattern formation in a system of one or two interacting bacterial populations. Additionally, the importance of using methods such as linear analysis and nonlinear Fourier analysis to accurately describe the patterns obtained in numerical simulations is highlighted. Finally, we conclude the chapter and the thesis by discussing the significance of this work and potential future research opportunities.

Chapter 1

Introduction

Mathematical modelling is a fundamental method for studying biological pattern formation in populations of motile microorganisms. In this chapter, we provide an overview of the biological and mathematical concepts used throughout this thesis to motivate the research. We begin by introducing the biological properties of microorganisms, as well as the different interactions between two or more species that give rise to spatial patterns, such as travelling wavefronts and stationary Turing patterns. Next, we introduce the main mathematical methods used in this thesis, including linear analysis and nonlinear Fourier analysis, to examine systems of partial differential equations in order to determine conditions for pattern formation, as well as to gain insights into pattern characteristics, such as amplitude and wavelength, in the case of stationary Turing pattern formation. Computational simulations are a valuable part of this research, so in the final section, we describe the numerical algorithm used to illustrate the various types of patterns that emerge in systems involving one species, as well as two interacting species.

1.1 Biological background

This research project is motivated by biological pattern formation, which is one of the most intriguing phenomena in nature. The simplest examples of such patterns are represented by travelling waves and stationary periodic patterns, which occur during various biological processes, including morphogenesis and population dynamics. The formation of these patterns in populations of motile microorganisms, such as *Dictyostelium discoideum* and *E. coli*, has been demonstrated in a number of experimental studies. Conditions for the formation of various types of patterns are commonly addressed in mathematical studies of dynamical systems containing diffusive and advection terms. In this work, we conduct a mathematical study of spatio-temporal patterns forming in a growing population

of chemotactically active bacteria. We consider a single species of bacteria, as well as two interacting species, and we are interested in determining under which conditions we obtain travelling wave solutions [86] or stationary Turing patterns [87]. Pattern formation is a fascinating topic with many applications, as it represents visible outcomes of self-organization. In biology, it explains patterns such as animal markings, for example, the pattern that appears on the skin of the giant pufferfish [144], or the way cells form complex patterns in developing tissue. Additionally, in the very early stages of biofilm formation, many bacterial patterns appear during colonization [56]. Pattern formation also has applications in industry, for example, the formation of temperature hot spots as a result of chemical kinetics and autocatalytic reactions [41]. Patterns appear everywhere in nature, but we are specifically interested in patterns formed by bacterial species in response to concentration gradients.

1.1.1 Bacterial growth

Populations of microorganisms expand through a process called binary fission [57]. During this process, a mother cell doubles in size and then splits into two daughter cells, which are genetically identical, assuming no mutations have occurred. The growth of a population is defined by an increase in the number of cells, rather than their size. The number of cells arising from a group of cells via binary fission can be calculated as follows:

$$N = n \times 2^d, \tag{1.1}$$

where N represents the number of cells at the end of the growth period, n the number of cells at the beginning of the growth period and d the number of divisions. There are four main stages of bacterial growth, which can be seen graphically in Figure 1.1.

The four main phases that affect bacterial growth can be described as follows [57, 107, 127]:

- **Lag phase**: this is the period of time in which bacteria adjust to the environment and go through slow changes, however they are still in the developing phase, so unable to go through binary fission;

- **Log phase**: this is also known as the exponential growth phase, and it is the period of time in which cells divide via binary fission. This period cannot be sustained permanently, since nutrients in the medium will eventually be consumed;

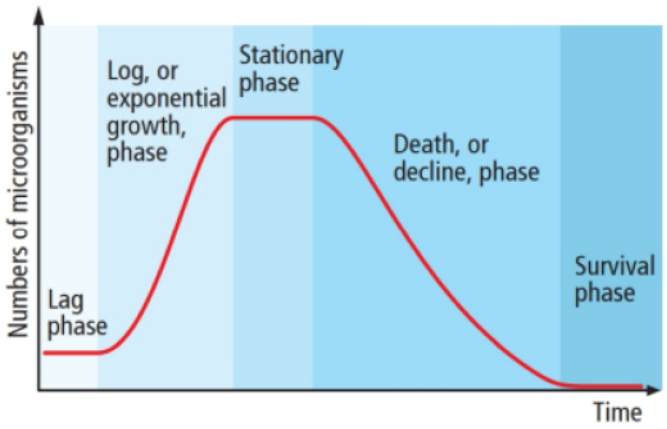

Figure 1.1: ***Bacterial growth curve.*** *This shows the number of microogranisms as time increases affected by four main stages, followed by the survival phase. Figure reproduced from [107].*

- **Stationary phase**: period of time in which growth and death rate are equal due to growth being limited by environmental factors such as nutrients, oxygen, temperature. Population remains constant during this phase;
- **Death phase**: cells start dying due to limitations such as nutrients and oxygen and other harmful factors.

Some cells will also adapt to the harsh environmental conditions and survive under conditions of stress and starvation, however not many species will survive, and population will eventually decay to 0 [55]. It is important to understand the bacterial growth concept, since this is present in the main models considered in this thesis and has a great impact on pattern formation.

1.1.2 Microorganisms motility

Microorganisms, such as bacteria, are known to move independently from unfavourable conditions towards more beneficial areas using metabolic energy. Bacterial motility and interactions between bacteria and their host can result in colonisation, which is crucial for processes such as the early stages of biofilm formation [5] or poorly healing wounds [148], but also for infectious pathogenic processes [91].

Motion depends on the different appendages used for propulsion, but also on the characteristics of the medium. There are various types of movement depending on how bacteria propel themselves: swarming and swimming are done using rotating flagella, twitching is aided by pili, gliding uses motor complexes such as focal adhesion, and sliding is independent of both flagella and pili, as it involves

changing shape and moving across surfaces [22, 148]. A visual representation can be seen in Figure 1.2.

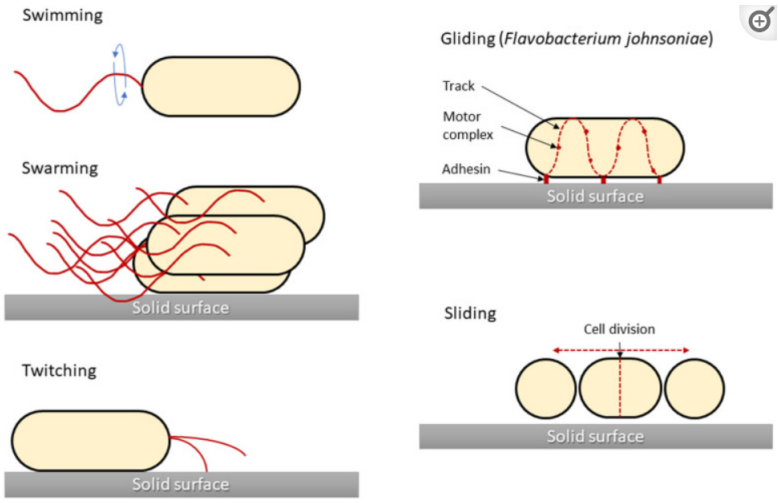

Figure 1.2: ***Different types of bacterial motility, depending on the structures that generate movement (marked by red).*** *Figure reproduced from [148].*

The motion of microorganisms can be described by diffusion when bacteria respond to concentration gradients in a medium, which appears to smooth out any concentration differences. In this case, bacteria move from regions of high concentration to regions of low concentration until the concentration gradient is eventually eliminated. On the other hand, taxis refers to directed motion in response to a stimulus, resulting in high densities of microorganisms in favourable regions. There are different types of taxis. For example, phototaxis is movement towards or away from light [7], magnetotaxis is movement along a magnetic field, which can be used by bacteria for orientation [29], and the type considered most important throughout this thesis is chemotaxis, which is movement in response to chemical gradients [80, 118].

When considering microorganisms, such as bacteria, interacting with a chemical, their motility is highly affected by changes in the concentration field of the chemical agent. This process, known as chemotaxis, represents the chemically directed movement of cells either along the concentration gradient (chemoattraction) or in the opposite direction (chemorepulsion), typically resulting in regions with higher concentration densities [136]. Chemotaxis plays a crucial role in the formation of Turing patterns, which represent regions of high and low densities of bacteria and chemotactic agents. A chemical gradient is required for stability to break down and initiate aggregation [59].

For example, consider a Petri dish with randomly distributed cells. If a drop of chemoattractant is introduced, it can dissolve and diffuse, creating a concentra-

tion gradient. Since the agent acts as a chemoattractant, cells will move along the concentration gradient towards the point where the chemical was first introduced. This is represented graphically in Figure 1.3. The figure also shows three modes of bacterial movement: the bottom bacterium moves by attaching to a surface and crawling by changing and elongating its shape; the middle bacterium moves with the aid of pili; and the top bacterium uses its flagellum to move towards regions of higher chemical concentration.

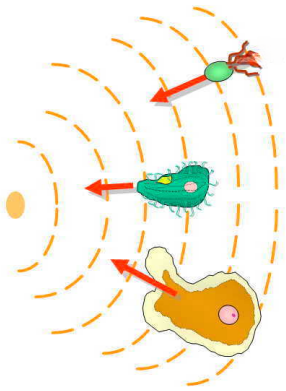

Figure 1.3: ***Organisms moving up the concentration gradient towards the areas of high (chemoattraction) chemical concentrations.*** *The dashed lines represent isolines, where the chemoattractant concentration is constant along the lines and the further away from center the lower the concentration of the chemical is. Modified figure from wikipedia.org/wiki/chemotaxis.*

Chemotaxis is arguably the most important form of taxis, and we have thoroughly investigated its effect on the types of patterns that can form when bacteria respond to chemical concentration gradients. For example, in a one-species system, strong chemoattraction leads to the formation of Turing patterns, while strong chemorepulsion results in faster-moving wavefronts. Conversely, in a two-species system, strong chemorepulsion leads to the formation of Turing patterns, while strong chemoattraction results in faster-moving wavefronts. These results will be explained using methods of linear and nonlinear analysis, as well as computational simulations, in the following chapters.

1.1.3 Interactions between species

Rather than existing as single planktonic cells, microorganisms are more likely to form complex interactive networks. Due to environmental sensing, species in an ecosystem compete for the same limited resources, such as food and space, usually resulting in the fitter individual surviving and reproducing. Competition can be classified into three main categories: intraspecific competition (between individuals of the same species), interspecific competition (between individuals of

different species), and competition between entirely different families [139]. The effects of intraspecific interactions are generally stronger than interspecific ones, since members of the same species are more likely to require the same resources. For example, they consume the same food and favour the same environmental conditions, such as temperature [21]. Moreover, it has been shown that the coexistence of competitive species is only possible when intraspecific competition is stronger than interspecific competition, meaning that species inhibit their own growth more than the growth of other species [38].

When considering the properties of an ecosystem, such as productivity and stability, the effects of interspecific interactions are much more important, as these represent different interactions between the species of a community. Microorganisms can compete for resources such as food and space, inhibit each other by secreting toxins, or even kill each other through direct contact [40]. Coexistence is a fundamental ecological interaction, and when species cannot coexist, dynamics lead to the exclusion of one species, a phenomenon known as the competitive exclusion principle: *"Complete competitors cannot coexist"* [43].

Depending on the effect microorganisms have on each other, both when considering members of the same species, or different species, the most important interactions can be classed as:

- **Competition**: when niches overlap and resources are limited, organisms are in competition with each other in order to survive. Many species compete for food or environmental conditions, such as places with higher or lower temperatures, or places more dense in oxygen [9];

- **Predation**: occurs when an organism, predator, kills and eats another organism, prey. Predators affect an ecosystem directly and indirectly by eating its prey, but also reducing predation by other species. If there would be no predators in an ecosystem, its population would increases exponentially until it reaches its carrying capacity [88];

- **Symbiosis**: this is a long-term interaction between different organisms. There are three main types of symbiosis: mutualism (both species benefit), commensalism (one species benefits and another is not affected) and parasitism (one species benefits and another is harmed) [110].

Understanding the different interactions between organisms is crucial for comprehending how an ecosystem can evolve or how biofilms form in the early stages. In our models, we consider cases of competition and competitive exclusion, but depending on the growth and competition rates of the species involved, the system can be extended to other types of interactions as well. We thoroughly investigate

the effects of interspecific competition and chemotaxis on the interactions and patterns formed in a system of two species, one of which produces a chemotactic agent that affects the other. It will be shown that the most interesting phenomena arise from the disturbance of the coexistence steady state, both in the presence and absence of chemotaxis.

1.1.4 Applications and experiments

Motility is one of the most important characteristics of many species, as it facilitates rapid expansion into previously unoccupied habitats. Expansion is initiated by the sensing of gradients produced by the species themselves and is further enhanced by growth and chemotaxis. Understanding bacterial motility is crucial for many sectors, such as healthcare (e.g., bacterial adaptation and antibiotic resistance) [95], agriculture (e.g., effects of bacteria on plant growth) [129], and the environment (e.g., bacterial motility in lakes) [119].

The aim of this research project is to better understand how bacterial motility and growth can lead to different types of pattern formation. One of the spatial patterns we are most interested in is the formation of travelling waves [17, 11, 37, 49, 58, 86, 87, 137]. Much work has been done on understanding the existence of travelling wave solutions in systems with one or two bacterial populations. The simplest way to describe the spread of a single population is by using the well-known Fisher-Kolmogorov equation [33, 62]. This equation has a wide range of applications; it can be used to describe the spread of animals and insects [86], the propagation of mutant genes [14], and even has applications in nuclear reactor theory [18]. In biology, the Fisher-Kolmogorov equation describes how a population can occupy the entire available medium by moving from one region to another at a constant speed. On the other hand, the Lotka-Volterra model is commonly used to describe the spread of any two interacting species [76, 135] that can diffuse, reproduce, decay, and compete for food and resources. In these models, populations start moving from a certain region in the medium and occupy the entire available space by forming travelling wavefronts that move at a constant speed, making the transition from an unstable steady state to a stable one.

The concept of a 'Turing pattern' was first introduced by Alan Turing in [128]. He examined a system with two substances, or morphogens, that are allowed to diffuse and interact with each other. Mathematically, this is known as a 'reaction-diffusion' system. Initially, in the absence of diffusion, the homogeneous steady state is stable against perturbations. However, if the morphogens both diffuse and interact with each other, the steady state becomes unstable when a random perturbation is introduced. This perturbation drives the system unstable, and patterns such as stripes or spots begin to appear [17, 59, 60, 86, 87]. These

are stationary patterns, meaning that once they are formed, they do not change their characteristics over time. In other words, a system exhibits Turing patterns under the condition of 'local self-enhancement and long-range inhibition' [128, 144]. This concept has been used to investigate the aggregation of amoebae in response to chemical gradients in the concentration of acrasin [59]. Amoebae are unicellular organisms that, after formation, disperse uniformly as if acting under repulsion. When food is present, the amoebae are chemotactically attracted to it, and once the food has been consumed, they again disperse uniformly. After some time, the amoebae start producing a chemical called acrasin, which acts as a chemoattractant and initiates the process of aggregation. A number of collecting spots form, and a slug begins to develop at the centre. This process is explained mathematically in the next section.

There are many experiments examining the motility of bacteria in response to chemical agents, as understanding bacterial response plays an important role in bacterial infections and epidemiology [27]. Many experiments have focused on the study of *E. coli* bacteria, which are primarily found in the human intestine and produce their own chemoattractant, aspartate, leading to a chemotactic aggregative signalling mechanism [130]. Researchers have investigated patterns formed by *E. coli* on a Petri dish due to its simplicity and ease of use [17]. A uniform distribution of food source is placed on the Petri dish with a high density of bacteria in the middle. As bacteria start eating and spreading out, a swarm ring is formed and travels outward as a travelling band. When bacteria in the swarm ring reach maximal capacity, some bacteria are left behind. These start producing their own chemoattractant, aspartate, which results in the formation of aggregates. After some time, the aggregates begin to dissolve as bacteria join the swarm ring and leave behind non-motile bacteria. These non-motile *E. coli* produce the spots pattern seen in Figure 1.4 a. Even though this is similar to one of the models we consider in this thesis, the main difference is that in this system there is one bacterial species and two chemicals: one acting as a food source and one acting as a chemoattractant.

Pseudomonas is a different type of bacteria that is well known for forming biofilms and is preferred by experimentalists due to its adaptation to diverse and challenging conditions [109]. This bacterium can be chemotactically affected by a wide range of chemicals, and its response to concentration changes is mediated by flagella or pili coupled with a well-developed chemosensory system. Its motility has been well studied since it can cause a wide range of infections, such as pneumonia and infections of the gastrointestinal system [10]. In Figure 1.4 b, four spots of bacteria are placed on a Petri dish containing an attractant. The top spot is a non-chemotactic mutant of *Pseudomonas putida*, while the bottom three

spots are the wild-type of the same species, which is chemically attracted to the substance, causing it to spread outward. Experimentalists use *Pseudomonas* to study antimicrobial treatments of infections because it forms dense and persistent biofilms [125].

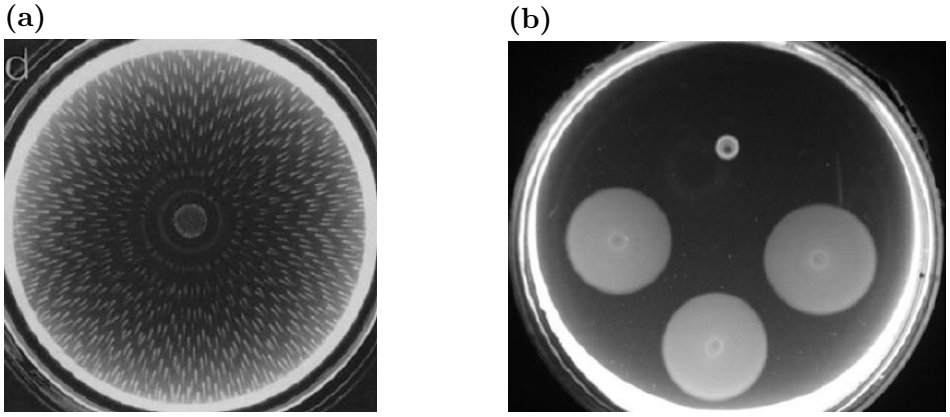

Figure 1.4: ***Stationary patterns formed by growing populations of bacteria in agar.*** ***(a)****: Patterns formed by growing populations of E.coli; the light spots on the Petri dish represent accumulations of bacteria due to the production of chemoattractant. Taken from [17].* ***(b)****: Bacterial colonies formed by growing population of Pseudomonas in response to attractant. Figure reproduced from [109].*

Spatial patterns can also be seen in the aggregation of *Dictyostelium discoideum* (Dd) in response to concentration gradients of cyclic AMP (cAMP) [133]. This is a cellular slime mold that forms an excitable medium for cAMP. Patterns are formed when a starving population of Dd starts moving toward foci to form multicellular structures. Cells appear that spontaneously secrete cAMP, and when a threshold value is reached, neighbouring cells also begin secreting the chemical. In response to the increased concentration of cyclic AMP, Dd starts producing phosphodiesterase, which slowly destroys the cAMP, creating travelling waves. At the same time, on the front of these waves, Dd moves chemotactically towards higher concentrations of cAMP. Figure 1.5 shows patterns formed by Dd in response to cyclic AMP. In Figure 1.5 a, dark-field waves form because aggregating cells communicate through propagating waves of chemoattractant. In Figure 1.5 b, aggregation streams occur due to the dependence of the velocity of cAMP waves on the density of the cells.

The difference between *E. coli* and *Dictyostelium discoideum* is that while the former is a group of bacteria that always produces a chemical agent, the latter is an amoeba species that produces a chemical agent in pulses, rather continuously. In Dd, chemical emissions and amoeba movement occur every few minutes. When one amoeba secretes cAMP, others start moving towards this central amoeba, the

one secreting the most chemicals. Amoebae move toward a high concentration of cyclic AMP for about 60 seconds, then stop until the next secretion begins. This behaviour causes oscillations in the form of waves of cAMP, and this is how aggregation and, hence, pattern formation, are initiated in populations of *Dictyostelium discoideum*.

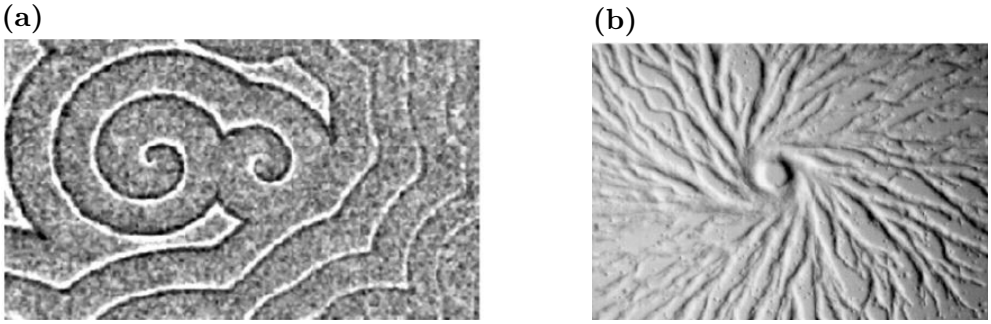

Figure 1.5: ***Patterns formed by the amoeba species Dictyostelium discoideum.*** ***(a)****: Formation of dark-field waves, in which light regions represent elongated cells that move and dark regions represent round cell that do not move.* ***(b)****: Formation of aggregation streams towards a common centre in response to chemical gradients. Figure reproduced from [115].*

Interactions between two or more species also have a significant impact on pattern formation and colonisation, so it is important to understand how these interactions affect species dispersal in response to different stimuli. One application of species interactions is pattern formation and colonisation in the early stages of biofilm formation. Biofilms are communities of many different species of bacteria attached to a surface [102]. Once bacteria are irreversibly attached to a surface, they can proliferate to form a mature biofilm and then disperse. Inside the biofilm, the different species of bacteria reproduce, decay, and interact. Researchers have studied interactions such as competition and predation within the biofilm because of their importance for public healthcare, as they play a crucial role in certain infectious diseases [26, 42, 56]. A particularly challenging topic is studying the formation of biofilms on medical devices, as they were the first clinical biofilm-related infections. Several devices are prone to biofilms, such as intravenous catheters, cardiac pacemakers, and prosthetic heart valves [42]. Due to the interactions between microbial cells and the host product, the biofilm's resistance to microbial agents is not fully understood. Cystic fibrosis and pneumonia are only two examples of biofilm-related diseases. However, understanding biofilms is not only important in healthcare, as they appear everywhere in nature. For example, in Figure 1.6 a, biofilms can be seen forming in hydrothermal hot springs, and similarly, in Figure 1.6 b, we can observe the formation of biofilms in freshwater rivers.

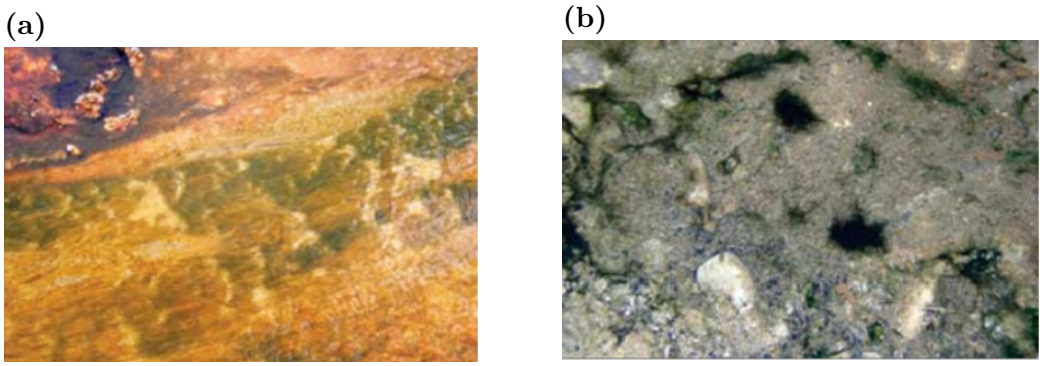

Figure 1.6: ***Examples of biofilms in nature.*** ***(a)****: Formation of filamentous streamers in hydrothermal hot springs due to the fast moving water which is able to mold the morphology of bacteria and algae.* ***(b)****: Formation of periphyton, complex community of algae and bacteria growing on submerged surfaces in fresh water rivers . Figure reproduced from [42].*

In this project, we are interested in the structure formed by cells inside the biofilm, so we investigate the very early stages of biofilm formation [5], when bacteria are very loosely attached to a surface and are still motile. In particular, we are interested in pattern formation, as this shows visible outcomes of self-organization in response to morphogen gradients. These gradients appear as a result of the bacteria diffusing, responding to chemicals, proliferating, decaying, and competing for resources. Interactions between different bacterial species are important in biofilm formation; however, we have not seen any experiments that investigate the interactions we are interested in. Some researchers have looked at interactions between multiple species, but these species are not motile, so their results cannot provide significant data for our study.

Interactions between bacterial species are crucial in the early stages of biofilm formation, but they also have other relevant applications in healthcare, such as bacterial colonisation of the respiratory tract, which is an important cause of morbidity and mortality worldwide [114]. Respiratory tract infections require bacteria to evade the host mucosal system and spread to susceptible sites in the upper airway, where colonisation occurs. Rapid transmission and spread of bacteria are evasion strategies related to bacterial motility and interactions between species.

Another relevant application of interactions between species is understanding population dynamics in ecological systems. For example, one of the most studied interactions of the Lotka-Volterra type is that of red and grey squirrels in the United Kingdom, one reason being the amount of available data. In the early stages of this research, the Lotka-Volterra system has been modified to include a diffusion term that describes the random movement and spatial dispersal of

the squirrels [89]. Under the assumption that grey squirrels have a competitive advantage over red squirrels, it has been shown that the species disperse by forming a wave, with red squirrels at the front of the travelling wave and only grey squirrels behind it. These results have also been expanded to show that both interspecific and intraspecific competition affect the minimal invasion speed; moreover, this cannot be predicted when the former is greater than the latter [47]. In a later paper [48], the existence of travelling fronts between the two steady states in which one of the species is extinct has been investigated and the minimal invasion speed when $D_1/D_2 << 1$ was found. Biologically, this means that if there is no diffusion, the n-species always overcomes the v-species. In [49], it was proved that travelling waves exist with any positive speed when the predator cannot diffuse, and so only the prey is motile. This competitive interaction has also been described using individual-based models to investigate the effects of reproduction, mortality, and competition on the dispersal of red and grey squirrels in a realistic habitat [108]. These models have been used to successfully predict the expansion of grey squirrels in Italy. In addition, the response of the squirrels to a virus has also received significant attention in order to understand the impact of a shared disease and how to better conserve red squirrels [140].

The dynamics of plant communities are another example of species interactions, and in this case, the flux of species in a community has a significant impact on colonisation. Plant species are highly competitive since most of them require the same resources at all stages of their vegetative life cycle [93, 94]. It has been shown that the competitive ability of plants is due to their colonisation and inhibition abilities, which play a vital role in population and community change. Additionally, pattern formation in plant communities is due to plants responding to competition from their neighbours, which influences the distribution and abundance of adult species.

The aim of this biological background section was to introduce the reader to some of the most basic concepts used throughout this PhD thesis, such as bacterial growth and motility, and to highlight the importance of interactions between species and how these characteristics affect dispersal and, consequently, pattern formation. It is clear that understanding bacterial responses to stimuli and how the speed of dispersal is affected is important in many different sectors, such as healthcare and ecology. In the next section, we will introduce the main mathematical methods used for linear and nonlinear analysis, and also present the numerical algorithms employed to support the analytical findings.

1.2 Mathematical background

In this section, we introduce the basic mathematical methods used throughout the thesis to investigate the existence of travelling wave solutions and stationary periodic patterns in a system of one, as well as two interacting bacterial populations. Some of the most fundamental methods employed include transforming a system from a space-time frame ((x,t) coordinates) to another frame that moves at a constant velocity relative to the first frame (z-coordinates) [86, 87], and linearising a system about the steady state to determine its stability when perturbed [124] and understand the existence of Turing patterns [59]. Fourier analysis is also introduced, as it is used to determine characteristics of the Turing pattern, such as amplitude and wavelength.

1.2.1 Logistic growth equation

The simplest way to describe the expansion of a biological population is to say that it grows at a rate proportional to the population density, under the assumption that there is sufficient food and space for growth, and no threat from predators. This can be modelled using the simple ordinary differential equation:

$$\frac{dn}{dt} = rn, \tag{1.2}$$

where n represents the population and r its growth rate coefficient. However, these assumptions are not correct, as populations are constrained by limitations on resources, which means the population can reach a maximum capacity. To account for the reproduction rate declining to zero, the system is modified such that:

$$\frac{dn}{dt} = rn\left(1 - \frac{n}{K}\right), \tag{1.3}$$

where K represents the maximum carrying capacity. This is known as the logistic equation, or the Pearl-Verhulst model [104].

In this thesis, we have used the logistic model to describe the growth of populations of microorganisms, as it is the simplest model that accounts for the fact that a population cannot expand infinitely. For example, in Figure 1.7, we can see that over time, a very small population grows until it reaches its maximum carrying capacity, after which its density remains constant.

1.2.2 Fisher-Kolmogorov equation

The logistic growth model describes the growth of a biological population over time, characterised by the absence of a spatial variable, meaning the population is non-motile. The simplest model that accounts for diffusion, or Brownian motion,

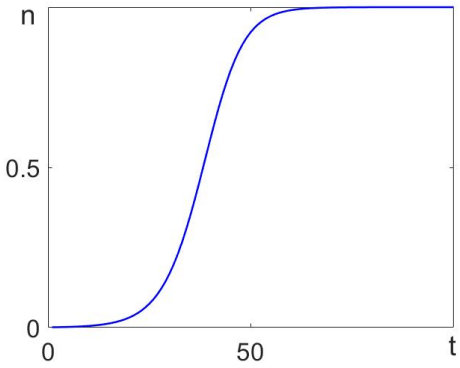

Figure 1.7: ***Solution of the logistic growth equation (1.3).*** *Solution with model parameters $r = 0.1$ and $K = 1$, shows population transitioning from $n = 0.001$ at time $T = 0$ to $n = 1$ as time increases.*

is known as the Fisher-Kolmogorov model, which exhibits travelling wave solutions and can be applied to the spread of any biological population [33, 62, 86]. In its dimensional form, it is:

$$\frac{\partial n}{\partial t} = D\frac{\partial^2 n}{\partial x^2} + kn(1-n), \tag{1.4}$$

where $kn(1-n)$ and $D\dfrac{\partial^2 n}{\partial x^2}$ are the reaction and diffusion terms respectively, while D represents the diffusion coefficient. Nondimensionalisation of mathematical equations has several advantages, such as reducing the number of relevant parameters and removing the need for measuring units in analysis. Further advantages of nondimensionalisation and scaling are discussed in [111]. Introducing the nondimensional parameters:

$$\tilde{t} = kt, \;\; \tilde{x} = x\left(\frac{k}{D}\right)^{1/2},$$

and dropping the tilde, the nondimensional Fisher-Kolmogorov equation becomes:

$$\frac{\partial n}{\partial t} = \frac{\partial^2 n}{\partial x^2} + n(1-n), \tag{1.5}$$

where n represents any biological population which can diffuse and reproduce. This model depends on both space and time, so as the population grows, it moves from an unstable steady state to a stable one.

The main characteristic of travelling waves is that they move in a particular direction with constant speed c [58] and they can be expressed as:

$$n(x,t) = N(z), \text{ where } z = x \pm ct, \tag{1.6}$$

subject to the boundary conditions:

$$\begin{cases} N(\pm\infty) = n_{\pm}, \\ N'(\pm\infty) = 0, \end{cases} \tag{1.7}$$

where $n_{\pm}$ is a constant. If $n_+ = n_-$ then the wave is a travelling pulse and if $n_+ \neq n_-$ then the wave is a travelling front. The steady states of the spatially homogeneous problem $\left(\dfrac{\partial^2 n}{\partial x^2} = 0\right)$ are $n = 0$ and $n = 1$, which are unstable and stable respectively. This means that we seek travelling wave solutions between $0 \leq n \leq 1$. Substituting $N(z)$ into (1.5) gives:

$$-cN' = N'' + N(1 - N). \tag{1.8}$$

First step is to transform the equation into a system of two ODE's:

$$\begin{cases} N' = V, \\ V' = -cV - N(1 - N). \end{cases} \tag{1.9}$$

Then, to obtain the speed of the travelling wave, the system needs to be linearized about the steady states $(N,\ V) = \{(0,\ 0),\ (1,\ 0)\}$. Let $f = N' = V$ and $g = V' = -cV - N(1 - N)$, the Jacobian of the system becomes:

$$J = \begin{pmatrix} f_N & f_V \\ g_N & g_V \end{pmatrix} = \begin{pmatrix} 0 & 1 \\ -1 + 2N & -c \end{pmatrix}. \tag{1.10}$$

Evaluating J at the origin gives:

$$J(0,0) = \begin{pmatrix} 0 & 1 \\ -1 & -c \end{pmatrix}, \tag{1.11}$$

which has eigenvalues $\lambda_{1,2} = \dfrac{-c \pm \sqrt{c^2 - 4}}{2}$. This means that the origin $(0, 0)$ is a stable node if $c^2 \geq 4$ or a stable spiral if $c^2 \leq 4$. Next, evaluating J at $(1, 0)$:

$$J(1,0) = \begin{pmatrix} 0 & 1 \\ 1 & -c \end{pmatrix}, \tag{1.12}$$

which has eigenvalues $\lambda_{1,2} = \dfrac{-c \pm \sqrt{c^2 + 4}}{2}$, meaning that the steady state $(1, 0)$ is a saddle.

If $c^2 < 4$, the origin is a stable spiral, which would result in the population having negative densities. Since this is physically impossible, we require $c \geq c_{min} = 2$. This makes the origin a stable node, so we expect travelling waves between the two steady states.

Figure 1.8 shows the trajectories of system (1.9) in the phase plane for two different values of speed. In Figure 1.8 a, we see that when the speed is $c =$

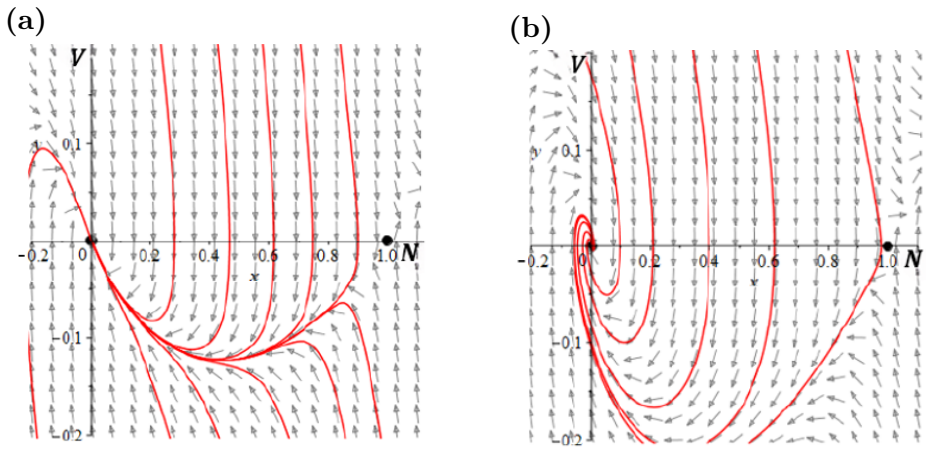

Figure 1.8: ***The phase-plane portrait of system (1.9).*** *Direction field is shown by the gray arrows and the red curves represent represent the phase trajectories.* ***(a)****: Simulation of phase portrait with* $c = c_{min} = 2$*, where steady state* $(0,\ 0)$ *is a stable node.* ***(b)****: Simulation of phase portrait with* $c = 1$*, where steady state* $(0,\ 0)$ *is a stable spiral. The two steady states of the system* $(0,\ 0)$ *and* $(1,\ 0)$ *are represented by the black dots. Figure produced numerically in Maple.*

$c_{min=2}$, the trajectories all converge to the point $(0,\ 0)$, indicating that this is a stable node. However, in Figure 1.8 b, with $c = 1$, the trajectories oscillate around the origin, meaning the point is a stable spiral. This illustrates why we generally require the eigenvalues at the extinction points to be real. Having established the existence of travelling wavefronts with $c_{min} \geq 2$, Figure 1.9 shows the numerical profile of the biological population n as described by the Fisher-Kolmogorov equation (1.5), transitioning from the unstable equilibrium point $n = 0$ to the stable equilibrium point $n = 1$.

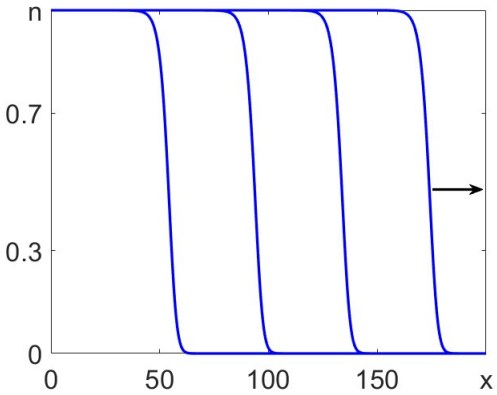

Figure 1.9: ***Profiles of the density of species*** n ***as described by the the Fisher-Kolmogorov equation*** (1.5) ***produced in numerical simulations at times:*** $T = 25,\ 50,\ 75,\ 100$ ***from left to right.***

In this part, we have introduced the simplest method to describe the spatial spread of a single population using the Fisher-Kolmogorov equation. Next, we will introduce the simplest model to describe the spread of two interacting biological populations: the Lotka-Volterra model.

1.2.3 The Lotka-Volterra model

The Lotka-Volterra model is a classical model [76, 135] of first-order, nonlinear partial differential equations that describe the interaction between two or more biological populations. There are three main types of interactions that can occur in a system of two species: competition, which decreases the growth rate of each population; symbiosis, which increases both growth rates; and predator-prey dynamics, where the growth rate of one population is increased while the other's is decreased [56, 86]. Several assumptions are made when using the Lotka-Volterra models, such as: predators can eat continuously and their only food source is the prey, which can also eat continuously and has a limitless food supply; there are no environmental changes; and the rate of change of each population is proportional to its size. The classical and dimensional Lotka-Volterra model that describes the spatial distribution of two interacting populations is [86]:

$$\begin{cases} \dfrac{\partial n}{\partial t} = D_n \dfrac{\partial^2 n}{\partial x^2} + r_1 n \left(1 - \dfrac{n}{k_1} - \dfrac{B_1 v}{k_1}\right), \\ \dfrac{\partial v}{\partial t} = D_v \dfrac{\partial^2 v}{\partial x^2} + r_2 v \left(1 - \dfrac{v}{k_2} - \dfrac{B_2 n}{k_2}\right), \end{cases} \tag{1.13}$$

where n and v represent two interacting bacterial populations, $D_n,\ D_v$ represent the diffusion coefficients, $r_1,\ r_2$ the proliferation rates, $k_1,\ k_2$ the carrying capacities and $b_1,\ b_2$ the interspecific competitive effects of species n and v respectively. To reduce the number of relevant parameters, the system is commonly nondimensionalized using the following substitutions: $\tilde{n} = \dfrac{n}{k_1}, \quad \tilde{v} = \dfrac{v}{k_2}, \quad \tilde{t} = tr_1$ and $\tilde{x} = x\sqrt{\dfrac{r_1}{D_n}}$. Dropping the tilde and using the new nondimensional parameters: $r = r_2/r_1, \quad d = D_v/D_n, \quad b_1 = B_1 k_2/k_1$ and $b_2 = B_2 k_1/k_2$, the nondimensional system is:

$$\begin{cases} \dfrac{\partial n}{\partial t} = \dfrac{\partial^2 n}{\partial x^2} + n(1 - n - b_1 v), \\ \dfrac{\partial v}{\partial t} = d\dfrac{\partial^2 v}{\partial x^2} + rv(1 - v - b_2 n). \end{cases} \tag{1.14}$$

Depending on the signs of the interspecific competitions, $b_{1,2}$, different interactions can be described by the model:

- Competition: $a_{1,2},\ b_{1,2} > 0$, both species compete for food and resources [9, 21];

- Symbiosis: $b_{1,2} < 0$, both species cooperate and coexist [110, 149];
- Predator-Prey: $b_1 = 0$ or $b_2 = 0$, one species feeds on the other [88].

To understand the spatio-temporal distribution of such system, it is important to know what the equilibrium points are and their stability. Clearly, system (1.14) has four equilibrium points:

$$(n,\ v) = \left\{(0,\ 0),\ (1,\ 0),\ (0,\ 1),\ \left(\frac{b_1 - 1}{b_1 b_2 - 1},\ \frac{b_2 - 1}{b_1 b_2 - 1}\right)\right\}, \tag{1.15}$$

and their stability can be determined by evaluating the trace and determinant of the Jacobian evaluated at the equilibrium points, as seen in Figure 1.10.

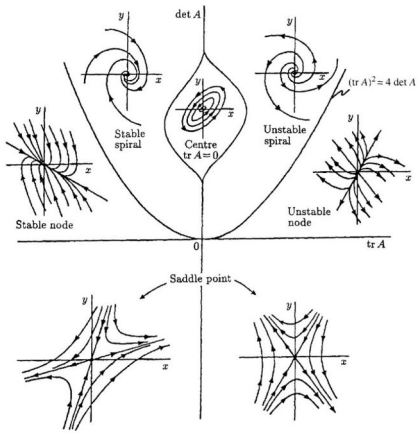

Figure 1.10: ***Poincaré diagram showing stability depending on trace and determinant****. Steady states are stable in the first quadrant and unstable anywhere else. Figure reproduced from [86].*

The Jacobian of the homogeneous case (well-mixed system with no spatial component) is:

$$J_{wm} = \begin{pmatrix} 1 - 2n - b_1 v & -b_1 n \\ -r b_2 v & r(1 - 2v - b_2 n) \end{pmatrix}, \tag{1.16}$$

and the results regarding the stability of the equilibrium points are summarized in Table 1.1.

To look for travelling wave solutions and analyse the stability of the equilibrium points in the nonhomogeneous system, one must first apply the transformations: $n(x,t) = N(z)$ and $v(x,t) = V(z)$ where $z = x - st$ represents a travelling wave moving from left to right with speed s. This gives:

$$\begin{cases} -sN' = N'' + N(1 - N - b_1 V), \\ -sV' = dV'' + rV(1 - V - b_2 N), \end{cases} \tag{1.17}$$

and by letting $N' = U$ and $V' = W$, this results in a system of ordinary differential equations:

$$\begin{cases} N' = U, \\ U' = -sU - N(1 - N - b_1 V), \\ V' = W, \\ W' = \dfrac{1}{d}(-sW - rV(1 - V - b_2 N)), \end{cases} \tag{1.18}$$

which has four steady states:

$$(N,\ U,\ V,\ W) = \left\{ (0,\ 0,\ 0,\ 0),\ (1,\ 0,\ 0,\ 0),\ (0,\ 0,\ 1,\ 0),\ \left(\frac{b_1 - 1}{b_1 b_2 - 1},\ 0,\ \frac{b_2 - 1}{b_1 b_2 - 1},\ 0 \right) \right\}, \tag{1.19}$$

with stabilities given by evaluating the Jacobian:

$$J_{tw} = \begin{pmatrix} 0 & 1 & 0 & 0 \\ -1 + 2N + b_1 V & -s & b_1 N & 0 \\ 0 & 0 & 0 & 1 \\ \dfrac{b_2 r V}{d} & 0 & \dfrac{-r(1 - 2V - b_2 N)}{d} & -\dfrac{s}{d} \end{pmatrix}, \tag{1.20}$$

at each steady state. In addition to stability, by requiring the steady states: $(N,\ U,\ V,\ W) = \{(0,\ 0,\ 0,\ 0),\ (1,\ 0,\ 0,\ 0),\ (0,\ 0,\ 1,\ 0)\}$ to be nodes, rather than spirals (real eigenvalues), one can find the minimum wavespeed requirements for travelling wavefronts transitioning from that specific state. Results requiring stability are summarized in Table 1.1 and results regarding minimum wavespeed are summarized in Table 1.2.

Steady state	Homogeneous	Nonhomogeneous
$(0,\ 0)$	always unstable	always stable
$(1,\ 0)$	stable if $b_2 > 1$ unstable if $b_2 < 1$	always unstable
$(0,\ 1)$	stable if $b_1 > 1$ unstable if $b_1 < 1$	always unstable
$\left(\dfrac{b_1 - 1}{b_1 b_2 - 1},\ \dfrac{b_2 - 1}{b_1 b_2 - 1} \right)$	stable if $b_1,\ b_2 < 1$	unstable if $b_1,\ b_2 < 1$

Table 1.1: ***Stability of the steady states of system*** (1.14) ***as obtained by evaluating Jacobians*** (1.16) ***(homogeneous case) and*** (1.20) ***(nonhomogeneous case) at each steady state.***

Since travelling waves make the transition from unstable to stable steady states, it is clear from Table 1.1 that the simplest waves admitted as solutions to

system (1.14) are waves from the unstable steady states $(n,\ v) = \{(0,\ 0),\ (1,\ 0),\ (0,\ 1)\}$ to the stable coexistence state with speeds as given in Table 1.2. The next step is to show numerical simulations of such profiles in Figure 1.11.

Unstable steady state	$(0,\ 0)$	$(1,\ 0)$	$(0,\ 1)$
Minimum wavespeed	$s_{min} \geq 2\sqrt{dr}$	$s_{min} \geq 2\sqrt{dr(1-b_2)}$	$s_{min} \geq 2\sqrt{dr(1-b_1)}$

Table 1.2: ***Minimum wavespeed requirement for travelling wavefronts to be admitted as solutions to system (1.14), making the transition from specified unstable steady states.***

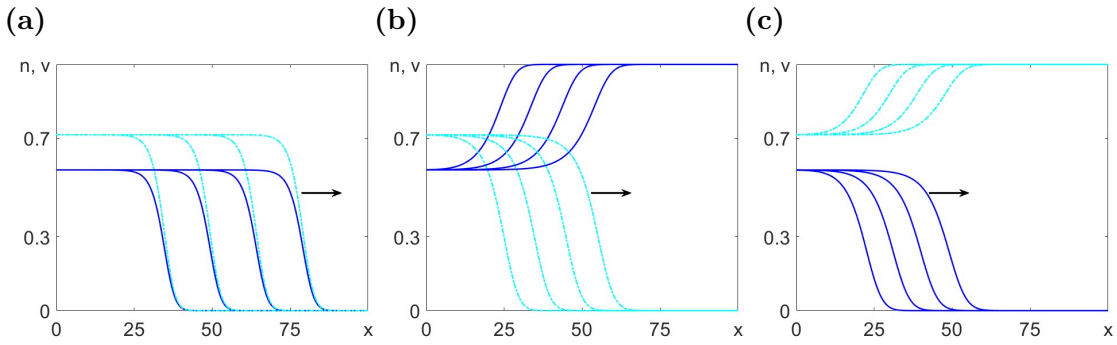

Figure 1.11: ***Travelling wavefronts admitted as solutions to system*** (1.14) ***making the transition to the stable coexistence steady state.*** *Initial conditions:* $(n,\ v)(x,\ 0) = \left(\dfrac{b_1-1}{b_1b_2-1},\ \dfrac{b_2-1}{b_1b_2-1}\right)$, *if* $x < 10$ *and if* $x \geq 10$, $(n,\ v) = (0,\ 0)$ *in* ***(a)***, $(n,\ v) = (1,\ 0)$ *in* ***(b)*** *and* $(n,\ v) = (0,\ 1)$ *in* ***(c)***. *Blue and cyan lines represent the densities of* n *and* v*, respectively, at times:* $T = 10,\ 20,\ 30,\ 40$ *from left to right. Fixed parameters:* $d = 1,\ r = 1,\ b_1 = 0.6,\ b_2 = 0.5$.

As well as the different types of wavefronts admitted as solutions to system (1.14) and their minimum wave speed, their direction of propagation has also been thoroughly investigated [2, 3, 4]. In a system with Lotka-Volterra dynamics, conditions under which diffusion and competition can cause waves to be halted or reversed have been explored. The dependence of wave speed on model parameters in degenerate (one species assumed not to diffuse) and near-degenerate (ratio of diffusion coefficients is small) systems results in three zones of response: in the central zone, the direction of propagation depends on motility, while in the outer two zones it depends on competition [2, 4]. Conditions under which competition

between two species can be controlled by a biocontrol agent have also been investigated. Without altering the competitive strengths or motility of the existing species, it has been shown that the relative strength of the biocontrol agent can slow, stall, or even reverse the advance of one species into the territory of the other [3].

This section has introduced some basic concepts about travelling waves admitted as solutions to the classical non-dimensional Lotka-Volterra system (1.14). In the next chapters, we will investigate the existence of travelling wavefronts, as well as stationary periodic patterns in a system of two competitive species with Lotka-Volterra dynamics interacting with a chemical.

1.2.4 Turing instability

The concept of a 'Turing pattern' was first introduced by Alan Turing in 1952 in his classical paper "The Chemical Basis of Morphogenesis" [128]. Concerned with a system involving two substances, or morphogens, that diffuse and interact with each other from an initially homogeneous state, Turing described pattern formation as an instability of the homogeneous equilibrium triggered by random disturbances. Mathematically, this is known as a 'reaction-diffusion' system, and conditions for the onset of instability can be found using methods of linear analysis. There are three mathematical conditions that a reaction-diffusion system must satisfy to exhibit Turing patterns [86, 87]. First, the non-trivial steady state of two morphogens in a well-mixed system with no spatial variation must be stable against perturbations. The system can be represented by the system of ordinary differential equations:

$$\begin{cases} \dfrac{dn}{dt} = f(n, c), \\ \dfrac{dc}{dt} = g(n, c), \end{cases} \tag{1.21}$$

which represent the rate of change of morphogens concentrations over time as coupled functions. Here, n and c are two chemicals that can interact with each other.

Now, consider the equilibrium point $(n,\ c) = (n_0,\ c_0)$ and a simple perturbation of the form $\tilde{n}, \tilde{c} \approx \exp(\lambda t)$, where λ represents the eigenvalues of the system. Then, the concentration of the morphogens at the perturbed point is:

$$\begin{cases} n = n_0 + \tilde{n}, \\ c = c_0 + \tilde{c}, \end{cases} \tag{1.22}$$

and the system can be linearized about the steady state $(\tilde{n},\ \tilde{c})^T$, such that:

$$\frac{\partial}{\partial t}\begin{pmatrix} \tilde{n} \\ \tilde{c} \end{pmatrix} = J \begin{pmatrix} \tilde{n} \\ \tilde{c} \end{pmatrix}, \tag{1.23}$$

where J is the Jacobian of the system, i.e:

$$J = \begin{pmatrix} f_n & f_c \\ g_n & g_c \end{pmatrix}\Big|_{(\tilde{n},\tilde{c})}. \tag{1.24}$$

For a system to be stable, we know that we require the determinant to be positive and the trace negative. Therefore, here we require:

$$\begin{cases} f_n g_c - f_c g_n > 0, \\ f_n + g_c < 0, \end{cases} \tag{1.25}$$

which provides the first two conditions needed for the homogeneous steady state in the well-mixed system to be stable against perturbations. Next, spatial variation is introduced into the system so that the morphogens can diffuse. The previously stable homogeneous steady state in the well-mixed system needs to become unstable due to random perturbations in the reaction-diffusion system, which is:

$$\begin{cases} \dfrac{\partial n}{\partial t} = D_n \dfrac{\partial^2 n}{\partial x^2} + f(n,c), \\ \dfrac{\partial c}{\partial t} = D_c \dfrac{\partial^2 c}{\partial x^2} + g(n,c). \end{cases} \tag{1.26}$$

Generally, a perturbation of the homogeneous steady state $(n_0,\ c_0)$ is considered to take the form:

$$\begin{cases} n = n_0 + \tilde{n}, \\ c = c_0 + \tilde{c}, \end{cases} \quad \text{where} \quad \begin{cases} \tilde{n} = \sum\limits_i \alpha_i T_{1,i}(\lambda_i t) X_{1,i}(k_i x), \\ \tilde{c} = \sum\limits_i \beta_i T_{2,i}(\lambda_i t) X_{2,i}(k_i x). \end{cases} \tag{1.27}$$

To find out which functions $T_{1,i}(\lambda_i t),\ T_{2,i}(\lambda_i t)$ and $X_{1,i}(k_i x),\ X_{2,i}(k_i x)$ satisfy the system of partial differential equations, consider only the first equation of the homogeneous system and substitute in $n = n_0 + \tilde{n}$, keeping in mind that all the terms vanish at the equilibrium point to obtain:

$$\begin{cases} T'_{1,i} - \lambda_i T_{1,i} = 0 \\ X''_{1,i} - k_i^2 X_{1,i} = 0 \end{cases} \implies \begin{cases} T_{1,i}(t) = \exp(\lambda_i t), \\ X_{1,i}(x) = a_i \cos(k_i x) + b_i \sin(k_i x), \end{cases} \tag{1.28}$$

where a_i and b_i are constants, k_i represents the wavenumber and λ_i are the eigenvalues of the system. Next, since in this work, we require no flux boundary conditions, it is appropriate to apply Neumann boundary conditions for $x \in [0,\ L]$. Therefore, the derivatives of n and c with respect to x need to vanish at the end points $x = 0$ and $x = L$. The derivative of $X_{1,i}(x) = a_i \cos(k_i x) + b_i \sin(k_i x)$ with respect to x evaluated at 0 gives $b_i = 0$, so all the sin coefficients vanish. In addition, applying no flux boundary conditions at $x = L$, gives $L = \dfrac{(2m+1)\pi}{2k_i}$,

where $m = 1, 2, ...$ Same argument also holds for $X_{2,i}(x)$. Since this is valid for all terms of the Fourier series, only one term of the series can be considered to give the most commonly used perturbation:

$$\begin{cases} \tilde{n} = \alpha \exp(\lambda t)\cos(kx), \\ \tilde{c} = \beta \exp(\lambda t)\cos(kx). \end{cases} \tag{1.29}$$

Linearizing the system about $(\tilde{n},\ \tilde{c})^T$:

$$\frac{\partial}{\partial t}\begin{pmatrix} \tilde{n} \\ \tilde{c} \end{pmatrix} = \frac{\partial^2}{\partial x^2}\begin{pmatrix} D_n\tilde{n} - \chi\tilde{c} \\ D_c\tilde{c} \end{pmatrix} + J\begin{pmatrix} \tilde{n} \\ \tilde{c} \end{pmatrix}, \tag{1.30}$$

gives the characteristic matrix:

$$M = \begin{pmatrix} f_n - D_n k^2 & f_c \\ g_n & g_c - D_c k^2 \end{pmatrix}. \tag{1.31}$$

The trace is clearly negative, $trM = -D_n k^2 - D_c k^2 + f_n + f_c < 0$ since $f_n + g_c < 0$ and D_c, D_n positive constants, so for the system to be driven unstable by perturbation, the determinant has to be negative. Let:

$$\det M = (f_n - D_n k^2)(g_c - D_c k^2) - f_c g_n, \tag{1.32}$$

$$\implies \det M = k^4 D_n D_c + k^2(-D_c f_n - D_n g_c) + f_n g_c - g_n f_c, \tag{1.33}$$

which can be used to find the corresponding wavenumbers, k, that drive the system unstable.

Equation (3.5) can be rewritten in parabola form, such that:

$$\det M = ak^4 + bk^2 + c. \tag{1.34}$$

If $b^2 - 4ac > 0$, the parabola has two distinct roots; if $b^2 - 4ac = 0$, then the parabola has one root and if $b^2 - 4ac < 0$, it has no roots. In order to get Turing patterns, the determinant of matrix M needs to be negative, and since $D_n D_c > 0$, this means that $\det M$ has a minimum value, and so, it is negative for all k^2 between the two distinct roots.

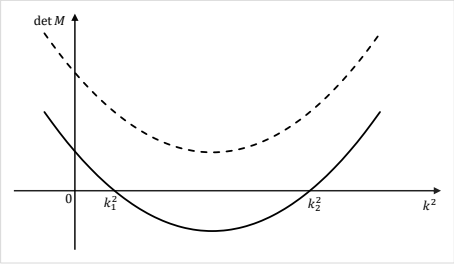

Figure 1.12: ***Plot of*** $\det M$ ***represented by equation (1.34).*** *If* $b^2 - 4ac > 0$*, the parabola has two distinct roots (solid line) and if* $b^2 - 4ac < 0$*, the parabola has no roots (dashed line).*

The roots of equation (3.5) can be expressed as:

$$k_{1,2}^2 = \frac{D_c f_n + D_n g_c \pm \sqrt{(-D_c f_n - D_n g_c)^2 - 4D_n D_c (f_n g_c - g_n f_c)}}{2D_n D_c}, \tag{1.35}$$

which gives two distinct roots if:

$$(-D_c f_n - D_n g_c)^2 > 4D_n D_c (f_n g_c - g_n f_c). \tag{1.36}$$

From (1.25), $f_n g_c - g_n f_c > 0$, so for (1.36) to hold, take the positive root of the left hand side, which gives the condition needed for $\det M < 0$ and for instability to be initiated:

$$D_c f_n + D_n g_c > 2\sqrt{D_n D_c (f_n g_c - g_n f_c)}. \tag{1.37}$$

To summarize, the conditions needed for the onset of instability and hence, formation of Turing patterns, are:

$$\begin{cases} f_n g_c - f_c g_n > 0, \\ f_n + g_c < 0, \\ D_c f_n + D_n g_c > 2\sqrt{D_n D_c (f_n g_c - g_n f_c)}. \end{cases} \tag{1.38}$$

In this section, classical Turing pattern analysis has been introduced in a simple reaction-diffusion system and condidtions for the onset of instability have been obtained. Next, we introduce some well-known mathematical models of chemotaxis.

1.2.5 Mathematical models of chemotaxis

Chemotaxis represents the directed movement of microorganisms in response to gradients in the concentration field of the chemical [136]. Therefore, depending on the microorganism and chemical kinetics, different spatial patterns can be formed. As mentioned in the biological background section, bacterial interactions can produce stationary patterns due to Turing instabilities or travelling waves between two equilibrium points. In this section, we present some of the most important chemotaxis models developed to show pattern formation initiated by chemotaxis.

Consider a system with one reproductive bacterial species, n, and a chemoattractant, c, with diffusive coefficients D_n and D_c, respectively. Chemotaxis can be modelled mathematically by introducing the advection term $\dfrac{\partial}{\partial x}\left(\chi(n,c)\dfrac{\partial c}{\partial x}\right)$, which represents directed motion due to changes in the concentration field of the chemical. $\chi(n,c)$ represents the chemotactic sensitivity of n to c, and it can take different forms [46], depending on the density of bacteria, the concentration of the chemical, or both. The sign of the chemotactic term describes the type of

response: if $\chi > 0$, then the chemical acts as a chemoattractant, and if $\chi < 0$, then the chemical acts as a repellent. Different forms of chemotactic sensitivity, as well as their advantages and disadvantages, are described in Chapter 3 of this thesis.

Mathematically, a model in which a chemical agent affects the motility of a microorganism can be described by the reaction-diffusion-advection system:

$$\begin{cases} \dfrac{\partial n}{\partial t} = D_n \dfrac{\partial^2 n}{\partial x^2} - \dfrac{\partial}{\partial x}\left(\chi(n,c)\dfrac{\partial c}{\partial x}\right) + f(n,c), \\ \dfrac{\partial c}{\partial t} = D_c \dfrac{\partial^2 c}{\partial x^2} + g(n,c), \end{cases} \tag{1.39}$$

where $f(n,c)$ and $g(n,c)$ represent kinetics of n and c, respectively. Under certain conditions, different types of patterns can be admitted as solutions to this system, such as:

- $f(n,c) \neq 0$ and $\chi = 0$, then we get the classical Fisher-Kolmogorov model and expect formation of travelling wavefronts [33, 62];
- $f(n,c) = 0$ and $\chi \neq 0$, then we get the classical Keller-Segel model and expect formation of stationary Turing patterns [59, 60];
- $f(n,c) \neq 0$ and $\chi \neq 0$, then we can get both stationary Turing patterns and travelling wavefronts depending on the kinetics of n and c and parameter values. [46, 128].

In a system where both bacteria and the chemical can diffuse, and the bacteria are chemotactically affected by gradients in the concentration of the chemical, the type of pattern that emerges depends heavily on the kinetics of the system. For example, Turing patterns form when bacteria produce their own chemotactic agent, which acts as an attractant that can decay but is not consumed by the bacteria [59, 60]. On the other hand, if there is a source of chemotactic agent that can be consumed by the bacteria, then travelling bands are formed [58]. Both of these models are described in detail in the following sections.

1.2.6 Turing patterns in systems with chemotaxis

In 1970, Keller and Segel [59] built on work done by Turing in 1952 [128] and described pattern formation as a breakdown of stability in the context of amoebae mediated by acrasin. They considered a homogeneous population of amoebae and a chemical, namely acrasin, which chemotactically affects the amoebae. Acrasin is a chemical substance that can be degraded by an enzyme called acrasinase,

which reacts according to:

$$c + \eta \leftrightarrows C \rightarrow \eta + product, \tag{1.40}$$

where c represents the chemical acrasin and η represents the enzyme acrasinase. They form a complex C, which dissociates into free enzymes plus the degraded product. The change in concentration of amoeba and acrasin per time is:

$$\begin{cases} \dfrac{\partial n}{\partial t} = Q^n - \nabla \cdot J^n, \\ \dfrac{\partial c}{\partial t} = Q^c - \nabla \cdot J^c, \end{cases} \tag{1.41}$$

where n and c represent the amoeba and acrasin concentration, Q^n and Q^c the mass of amoeba and the mass of acrasin, J^n and J^c the flux of amoeba and acrasin, respectively. To write a mathematical model describing the interaction between amoeba and acrasin, Keller has described the different types of interactions in the model. First, the flux of amoeba and acrasin is considered to be of diffusive type:

$$\begin{cases} J^n = \chi(n, c)\nabla c - D_n \nabla n, \\ J^c = -D_c \nabla c, \end{cases} \tag{1.42}$$

where $\chi(n, c)$ is the chemotactic sensitivity of amoeba to acrasin and D_n, D_c are the diffusion coefficients of amoeba and acrasin respectively, also known as Brownian motion or random motion.

To construct a simplified model, assume a homogeneous population of cells and regard aggregation as a manifestation of instability in a uniform distribution of acrasin and acrasinase. In the early stages of life, the uniform distribution is stable, but at some point characteristics change to make the distribution unstable and any spontaneous perturbation can trigger aggregation. The model constructed is:

$$\begin{cases} \dfrac{\partial n}{\partial t} = -\nabla \cdot (\chi(n, c)\nabla c) + \nabla \cdot (D_n \nabla n), \\ \dfrac{\partial c}{\partial t} = \nabla^2 c + hn - pc, \end{cases} \tag{1.43}$$

which describes the interaction between amoeba and acrasin; p represents the decay rate of acrasin and h represents the production of the chemical per amoeba. Assuming the diffusion and chemotactic sensitivity are constant, the model can be simplified such as:

$$\begin{cases} \dfrac{\partial n}{\partial t} = -\chi \nabla^2 c + D\nabla^2 n, \\ \dfrac{\partial c}{\partial t} = \nabla^2 c + hn - pc, \end{cases} \tag{1.44}$$

where χ is the chemotactic sensitivity and D is the ratio between the diffusion of amoeba and acrasin. Conditions for the onset of instability and formation of Turing patterns can be found by looking for solutions near the equilibrium (n_0, c_0) using a perturbation of the form (1.29), as described in the previous section. Substituting (1.29) into (1.44) and linearzing about the equilibrium point gives the characteristic matrix:

$$M = \begin{pmatrix} -Dk^2 & \chi k^2 \\ h & -k^2 - p \end{pmatrix}. \tag{1.45}$$

The trace of M is clearly negative, $trM = -Dk^2 - k^2 - p < 0$, so for instability require:

$$\det M = (-Dk^2)(-k^2 - p) - \chi h k^2 < 0, \tag{1.46}$$

which gives the instability condition:

$$\frac{\chi h}{D(k^2 + p)} > 1, \tag{1.47}$$

and since unstable disturbances grow faster for a sufficiently large medium, assume that $k \to 0$ to get the following instability condition:

$$\frac{\chi h}{Dp} > 1, \tag{1.48}$$

which means that if the chemotactic sensitivity of amoeba to acrasin as well as the production of acrasin per amoebae is higher than the diffusion ratio and the decay rate, then the system is driven unstable by perturbation and aggregation initiated.

This paper describes how the chemotactic effect is long-range, meaning that amoebae respond to small gradients in acrasin. Cells respond to local fluctuations in the concentration of acrasin, which means that even small differences in concentration can be detected. In addition, it has been shown that amoebae become unstable if there is an increase in sensitivity to the acrasin gradient (χ) or the rate of acrasin production (h). However, the cells can also become unstable if there is a decrease in the diffusion coefficient (D) or the decay rate of acrasin (p).

Next, Keller and Segel focused their attention on how cell flux is affected by chemotaxis [60]. When a chemical substance such as acrasin is introduced into the system, a chemotactic event is initiated by the local concentration of acrasin in the vicinity of a cell receptor. Cells that respond to acrasin form individual cell paths, resulting in an average cell flux proportional to the chemical gradient. They also discussed how the range of motion in a given direction is determined by the concentration at the propelling edge. For example, amoebae are propelled by pulling, so their propelling edge is the leading edge, while the propelling edge

for flagellated cells is the lagging edge, as they move by pushing. They provided a general form for the derivation of the flux of cells that follow a Brownian motion model of chemotaxis.

In this section, methods of classical Turing pattern analysis have been used to describe the initiation of aggregation in a system of one species interacting with a chemical agent, in which the chemical is produced by the cell. In the next part, the formation of travelling bands is shown, due to the chemical being consumed by the cell rather than produced.

1.2.7 Travelling bands in systems with chemotaxis

The first part of our research is focused on the analysis of a cell-chemical system. In this system, the interactions between one bacterial species and a chemical are considered to understand the existence of travelling wave solutions. Researchers have looked into the existence of travelling waves in systems with chemotactic activity from different perspectives. In 1971, Keller [58] considered the interaction between *E.coli* and a chemical substrate which acts as an energy source. They looked at patterns formed by *E.coli* placed at one end of a capillary tube containing oxygen and the substrate and observed the formation of travelling bands. This can be represented mathematically as:

$$\begin{cases} \dfrac{\partial n}{\partial t} = \dfrac{\partial}{\partial x}\left(\mu(c)\dfrac{\partial n}{\partial x}\right) - \dfrac{\partial}{\partial x}\left(\chi(n,c)\dfrac{\partial c}{\partial x}\right), \\ \dfrac{\partial c}{\partial t} = D\dfrac{\partial^2 c}{\partial x^2} - kn, \end{cases} \tag{1.49}$$

where n represents the concentration of bacteria; c the concentration of the chemical; $\mu(c)$ measures motility, which can vary with substrate concentration; $\chi(n,c)$ measures the chemical sensitivity of bacteria; D the diffusion of the chemical and k the rate of consumption per cell.

They have taken chemotaxis of the form $\chi(n,c) = n/c$ and have shown that, in this case, travelling bands exist only if chemotaxis is sufficiently strong and the concentration of the food source is always sufficiently high. Motivated by model (1.49) and the biologically unrealistic singularity in the chemotaxis term, a more complicated partial differential equation model based on transport equations from a velocity-jump process has been formulated [143]. This takes into account the turning rate of cells, but also internal metabolic processes such as the response to low nutrient levels and signal transduction. Global existence of travelling wave solutions is proven with and without cell starvation. They later developed a hybrid model which describes bacteria using an individual-based approach and the chemoattractant using a partial differential equation [37]. This model takes into

account signal transduction, as well as the proliferation and death of cells. They have shown that proliferation is necessary for the existence of stationary travelling waves and that reproduction and death have a stabilising effect. To show that the existence of travelling waves is due to chemotaxis and not proliferation, they obtained the expected wave speed in the case of no chemotaxis and observed that this increases as chemotaxis strengthens.

In the models mentioned so far, methods of linear analysis, such as classical Turing instability analysis, have been used to show the formation of spatial patterns such as travelling waves or periodic stationary patterns. Next, we introduce methods of Fourier analysis, which we have used to obtain information about the characteristics of the pattern, such as amplitude and wavelength.

1.2.8 Fourier analysis of stationary solution

In this section, we introduce the method of Fourier analysis, which refers to representing and approximating solutions to equations by sums of trigonometric functions [35, 126]. This method is named after Joseph Fourier, who showed that the study of heat is simplified if the function is represented by a sum of trigonometric functions. His work describes the flow of heat in a thin rectangular plate, where there is no heat loss from either face of the plate and the two long sides are held at a constant temperature set to 0. Heat is then applied to one of the short sides, while the other short side is assumed to be infinitely far away [36]. Mathematically, this can be represented in the wx-plane as a region bounded below by $x = -1$, above by $x = 1$, and to the left by $w = 0$, as shown in Figure 1.13. Let $z(w,\ x)$ represent the temperature at the point $(w,\ x)$; then a temperature of 0 along the two faces of the plate means:

$$z(w,\ -1) = z(w,\ 1) = 0, \quad x > 0, \tag{1.50}$$

and the temperature distribution along the left-hand edge is described by a function of x such as:

$$z(0,\ x) = f(x), \tag{1.51}$$

where $f(x)$ is assumed to be an even function.

Fourier describes heat flow at equilibrium using the partial differential equation:

$$\frac{\partial^2 z}{\partial w^2} + \frac{\partial^2 z}{\partial x^2} = 0, \tag{1.52}$$

which is known as Laplace's equation. Looking for solutions of the form:

$$z = \Phi(w)\psi(x), \tag{1.53}$$

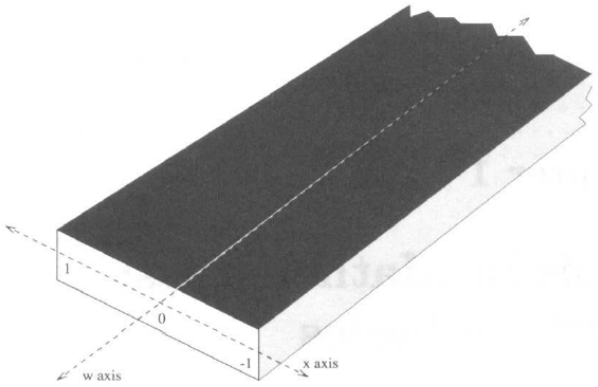

Figure 1.13: ***Representation of Fourier's thin plate to describe heat distribution***. *Figure reproduced from [20].*

this reduces to:

$$\Phi''(w)\psi(x) + \Phi(w)\psi''(x) = 0 \implies \frac{\Phi(w)}{\Phi''(w)} = -\frac{\psi(x)}{\psi''(x)}. \tag{1.54}$$

From (1.50) $\psi(-1) = \psi(1) = 0$, which means $\dfrac{\psi(x)}{\psi''(x)}$ must be negative. Let:

$$\frac{\Phi(w)}{\Phi''(w)} = A, \quad \text{and} \quad \frac{\psi(x)}{\psi''(x)} = -A, \tag{1.55}$$

where A is some positive constant set to be $A = \dfrac{1}{n^2}$. Solving for:

$$\begin{cases} \Phi(w) = c_1 \exp(-nw) + c_3 \exp(-nw), \\ \psi(x) = c_2 \cos(nx) + c_4 \sin(nx), \end{cases} \tag{1.56}$$

where $c_3 = 0$ since temperature approaches 0 as $w \longrightarrow \infty$ and $c_4 = 0$ since ψ is an even function, gives solution:

$$z(w,\ x) = a \exp(-nw) \cos(nx), \tag{1.57}$$

where a and n are unknown constants, and a general solution over all modes takes the form:

$$z(w,\ x) = a_1 \exp(-n_1 w) \cos(n_1 x) + a_2 \exp(-n_2 w) \cos(n_2 x) + a_3 \exp(-n_3 w) \cos(n_3 x) + \ldots \ . \tag{1.58}$$

Since (1.50) holds if and only if n_i is an odd multiple of $\dfrac{\pi}{2}$ and $z(0,\ x) = f(x)$,

this gives:

$$\begin{aligned} f(x) &= a_1 \exp(-n_1 0)\cos(n_1 x) + a_2 \exp(-n_2 0)\cos(n_2 x) + a_3 \exp(-n_3 0)\cos(n_3 x) + ... \\ &= a_1 \cos\left(\frac{\pi}{2}x\right) + a_2 \cos\left(\frac{3\pi}{2}x\right) + a_3 \cos\left(\frac{5\pi}{2}x\right) + ... \\ &= \sum_{m=1}^{\infty} a_m \cos\left(\frac{(2m-1)\pi x}{2}\right), \end{aligned} \tag{1.59}$$

which is a solution to equation (1.52) known as Fourier series solution and where coefficients a_m can be calculated according to the integral:

$$a_m = \int_{-1}^{1} \cos\left(\frac{(2m-1)\pi x)}{2}\right) dx. \tag{1.60}$$

Generally, for any periodic function:

$$f(\theta) = A_0 + \sum_{n=1}^{\infty} [A_n \cos(n\theta) + B_n \sin(n\theta)], \tag{1.61}$$

Fourier series solution coefficients can be calculated according to:

$$\begin{cases} A_0 = \dfrac{1}{\pi}\displaystyle\int_0^{2\pi} f(\theta) d\theta, \\ A_n = \dfrac{1}{\pi}\displaystyle\int_0^{2\pi} f(\theta)\cos(n\theta) d\theta, \\ B_n = \dfrac{1}{\pi}\displaystyle\int_0^{2\pi} f(\theta)\sin(n\theta) d\theta. \end{cases} \tag{1.62}$$

This section has introduced how solutions of partial differential equations can be described by sums of trigonometric functions once equilibrium has been reached and the solutions are stationary. This is a powerful method that we have used throughout this thesis to find characteristics of stationary periodic patterns such as wavelength and amplitude.

1.3 Numerical integration of partial differential equations

In this section, we present methods for integrating partial differential equations that are useful for investigating pattern formation in nonlinear reaction-diffusion systems, as well as nonlinear reaction-diffusion-advection systems. Numerical integration is needed to solve these types of systems since they cannot be solved analytically, and the separation of variables method only works for some of the simplest cases. To address these difficulties, we use finite difference methods to

replace partial differential equations with difference equations and find solutions to such modified systems.

Finite difference methods are commonly used in numerical simulations to approximate derivatives with finite differences by discretizing space and time, finding the solution at each discrete point by solving algebraic equations where first and second derivatives have been obtained using Taylor expansion methods [54, 83, 85]. Typically, a discretized point has index j to represent the x-direction (spatial) and index n to represent the t-direction (temporal) position. To represent a solution using the finite difference method, we represent the function $u(x,\ t)$ by its values at a discrete set of points, such that:

$$\begin{cases} t_n = t_0 + n\Delta t, & \text{where } n = 0, ..., T \\ x_j = a + j\Delta x, & \text{where } j = 0, ..., M, \end{cases} \tag{1.63}$$

where T represent the number of time steps and M the number of mesh points, such that $M = \dfrac{L}{\Delta x}$ for medium length L.

To establish the truncation error in the approximation of a function and approximate its derivatives, one can use Taylor series. For example, the Taylor series expansion of a function $u(x)$ is:

$$\begin{aligned} u(x + \Delta x) &= u(x) + \sum_{m=1}^{\infty} \frac{(\Delta x)^m}{m!} \frac{\partial^m f}{\partial x^m} \\ &= u(x) + \Delta x u'(x) + \frac{\Delta x^2}{2!} u''(x) + \frac{\Delta x^3}{3!} u'''(x) + ... + R, \end{aligned} \tag{1.64}$$

and similarly,

$$u(x - \Delta x) = u(x) - \Delta x u'(x) + \frac{\Delta x^2}{2!} u''(x) - \frac{\Delta x^3}{3!} u'''(x) + ... + R, \tag{1.65}$$

where R represents higher order derivative terms of u in the infinite sum. Rewriting (1.64) to obtain the Taylor series approximation of the first derivative gives:

$$u'(x) = \frac{u(x + \Delta x) - u(x)}{\Delta x} - \frac{\mathbf{\Delta x}}{\mathbf{2!}} \mathbf{u''(x)} - \frac{\mathbf{\Delta x^2}}{\mathbf{3!}} \mathbf{u'''(x)} - ... - \mathbf{R}, \tag{1.66}$$

where the bold terms represent the truncation error, which is the discrepancy betwen the partial derivative and the Taylor approximation, also known as:

$$-\frac{\Delta x}{2!} u''(x) - \frac{\Delta x^2}{3!} u'''(x) - ... - R = O(\Delta x), \tag{1.67}$$

and since $\Delta x >> \Delta x^2 >> \Delta x^3$, this is known as the leading term and contributes to maximal error.

Rewriting (1.66) in terms of index j gives three difference schemes:

$$\begin{cases} \text{Forward difference approximation:} & u'(x) \simeq \dfrac{u_{j+1} - u_j}{\Delta x} + O(\Delta x), \\ \text{Central difference approximation:} & u'(x) \simeq \dfrac{u_{j+1} - u_{j-1}}{2\Delta x} + O(\Delta x), \\ \text{Backward difference approximation:} & u'(x) \simeq \dfrac{u_j - u_{j-1}}{\Delta x} + O(\Delta x). \end{cases} \tag{1.68}$$

Extending to find the second derivative approximation of $u(x)$ gives:

$$u''(x) = \frac{u(x + \Delta x) - 2u(x) + u(x - \Delta x)}{\Delta x^2} + O(\Delta x^2), \tag{1.69}$$

which represents the central difference approximation of the second derivative.

1.3.1 Finite difference methods for diffusive terms

Explicit and implicit numerical methods are two types of schemes used for approximating solutions to differential equations. Explicit schemes involve a direct computation of dependent variables in terms of known quantities and are generally easier to implement, requiring fewer computational resources. However, explicit schemes are also conditionally stable and require smaller time steps. On the other hand, in implicit schemes, dependent variables are computed using coupled sets of equations, often requiring either a matrix or iterative technique. They are harder to implement since they require additional computation, but larger time steps can be used, resulting in less overall computational time [54, 85]. For the numerical results presented in this thesis, we have used explicit schemes since they are relatively fast and much easier to modify for different systems of partial differential equations.

For the numerical approximation of the diffusive term, it is common to use the forward Euler difference approximation for the first-order derivative in time and the central difference approximation for the second-order derivative in space. For example, the one-dimensional heat equation:

$$\frac{\partial u}{\partial t} = D\frac{\partial^2 u}{\partial x^2}, \tag{1.70}$$

can be approximated numerically using the explicit method:

$$u_j^{n+1} = n_j^n + D\frac{\Delta t}{\Delta x^2}\left[u_{j+1}^n - 2u_j^n + u_{j-1}^n\right]. \tag{1.71}$$

Since explicit schemes are conditionally stable, Von Neumann analysis is commonly used to find the stability condition, since coefficients of the difference equations are slowly changing over space and time and can be assumed to be

constant [100]. The independent solutions, or eigenmodes, of the difference equations are considered to be of the form:

$$u_j^n = \epsilon^n \mathrm{e}^{ikj\Delta x}, \tag{1.72}$$

where k is a real spatial wavenumber and $\epsilon = \epsilon(k)$ is a complex number that depends on k. The integer powers of ϵ are responsible for the time dependence of a single eigenmode, which means that the difference equations have exponentially growing modes if $|\epsilon(k)| > 1$, or are said to be unstable. Similarly, according to Von Neumann analysis, a numerical scheme is stable if $|\epsilon(k)| \leq 1$. Substituting (1.72) into (1.71) after a single iteration gives:

$$\epsilon\epsilon^n \mathrm{e}^{ikj\Delta x} = \epsilon^j \mathrm{e}^{ikm\Delta x} + D\frac{\Delta t}{\Delta x^2}\left[\epsilon^n \mathrm{e}^{ikj\Delta x}(\mathrm{e}^{ik\Delta x} + \mathrm{e}^{-ik\Delta x} - 2)\right], \tag{1.73}$$

and the condition for stability:

$$\left|\epsilon = 1 + \frac{2D\Delta t}{\Delta x^2}(i\sin(k\Delta x) - 1)\right| \leq 1, \tag{1.74}$$

which gives:

$$D\frac{\Delta t}{\Delta x^2} \leq \frac{1}{2}, \tag{1.75}$$

showing the explicit scheme (1.71) is conditionally stable.

This section shows that using the forward Euler difference approximation for the first order time derivative and the central difference approximation for the second order derivative in space is a reasonable numerical scheme to use for the numerical integration of the diffusive type terms. Next, we present some schemes that can be used to approximate the advection term, as well as discuss their stability.

1.3.2 Finite difference methods for advection terms

The advection equation is well-known for representing the transport of a substance or morphogen by the bulk motion of a fluid. For example, in this thesis, we consider chemotaxis, which is the directed movement of bacteria in response to concentration gradients of a chemical, and it can be modelled mathematically by the introduction of an advection term. The advection equation is not simple to solve numerically, so in this section, we introduce some finite difference methods for advection terms and discuss their stabilities. Consider the advection equation:

$$\frac{\partial u}{\partial t} = -\chi\frac{\partial u}{\partial x}, \tag{1.76}$$

where χ is a constant.

One way of numerically integrating this equation and approximating its solution using finite difference methods is to use the forward Euler formula for time discretization and the *central scheme* for spatial discretization, which results in a first order accurate method in time [100]. For one iteration, equation (1.76) can be represented by:

$$u_j^{n+1} = u_j^n - \chi \frac{\Delta t}{2\Delta x} \left(u_{j+1}^n - u_{j-1}^n \right). \tag{1.77}$$

Applying Von Neumann analysis by substituting $u_j^n = \epsilon^n \mathrm{e}^{ikj\Delta x}$ into (1.77) gives:

$$\epsilon(k) = 1 - i \frac{\chi \Delta t}{\Delta x} \sin(k\Delta x), \tag{1.78}$$

whose modulus is always greater than 1 for all k, meaning the central scheme is unconditionally unstable.

A more appropriate method is using the *upwind difference scheme* which is first order accurate in space and reads:

$$\begin{cases} u_j^{n+1} = u_j^n - \chi \dfrac{\Delta t}{\Delta x} \left(u_j^n - u_{j-1}^n \right), & \text{if } \chi > 0, \\ u_j^{n+1} = u_j^n - \chi \dfrac{\Delta t}{\Delta x} \left(u_{j+1}^n - u_j^n \right), & \text{if } \chi < 0, \end{cases} \tag{1.79}$$

For constant coefficient χ, applying Von Neumann stability analysis gives amplification factor:

$$\epsilon = 1 - \left| \frac{\chi \Delta t}{\Delta x} \right| (1 - \cos(k\Delta x)) - i \frac{\chi \Delta t}{\Delta x} \sin(k\Delta x) \Longrightarrow \tag{1.80}$$

$$|\epsilon|^2 = 1 - 2 \left| \frac{\chi \Delta t}{\Delta x} \right| \left(1 - \left| \frac{\chi \Delta t}{\Delta x} \right| \right) (1 - \cos(k\Delta x),$$

For stability, require $|\epsilon|^2 \leq 1$ which gives:

$$\frac{|\chi| \, \Delta t}{\Delta x} \leq 1, \tag{1.81}$$

known as the Courant-Friedrichs-Lewy stability condition, or simply the Courant condition [23].

The last method we introduce, which also represents the method used throughout this thesis for the numerical integration of the advection term, is the *Lax-Friedrichs numerical scheme*, or simply the *Lax scheme* [68, 78, 100]. This method fixes the instability in the central scheme by replacing the term u_j^n in the time derivative by its average such that:

$$u_j^n \longrightarrow \frac{1}{2} \left(u_{j+1}^n + u_{j-1}^n \right), \tag{1.82}$$

and (1.77) becomes:

$$u_j^{n+1} = \frac{1}{2}\left(u_{j+1}^n + u_{j-1}^n\right) - \frac{\chi\Delta t}{2\Delta x}\left(u_{j+1}^n - u_{j-1}^n\right). \tag{1.83}$$

Applying Von Neumann analysis gives amplification factor:

$$\epsilon = \cos(k\Delta x) - i\frac{\chi\Delta t}{\Delta x}\sin(k\Delta x), \tag{1.84}$$

which by requiring $|\epsilon|^2 \leq 1$ for stability gives $\dfrac{|\chi|\,\Delta t}{\Delta x} \leq 1$, which again is the Courant condition. One advantage of using such method is that it accounts for numerical dissipation.

For a nonlinear advection equation:

$$u_t + \chi f(u)_x = 0. \tag{1.85}$$

one can use the *second-order Lax-Friedrichs scheme* [13, 51, 112]. Instead of approximating the advection term at each step, it is approximated at each half step such that equation (1.77) becomes:

$$u_j^{n+1} = u_j^n + \chi\frac{\Delta t}{\Delta x}\left[f(u_{j+1/2}^n) - f(u_{j-1/2}^n)\right]. \tag{1.86}$$

Since points $u_{j+1/2}^n$ and $u_{j-1/2}^n$ are not available, they must be approximated using available point values $\{u\}_{j-2}^{j+2}$. Introduce $\hat{f}_{j\pm1/2} \approx f(u_{j\pm1/2}^n)$ such that the nonlinear conservation law becomes:

$$u_j^{n+1} = u_j^n + \chi\frac{\Delta t}{\Delta x}\left(\hat{f}_{j+1/2} - \hat{f}_{j-1/2}\right) = 0. \tag{1.87}$$

To approximate $\hat{f}_{j+1/2}$ and $\hat{f}_{j-1/2}$ using available point values, let:

$$\hat{f}_{j+1/2} = \frac{1}{2}\left[f(u_{j+1/2}^-) + f(u_{j+1/2}^+) - \alpha(u_{j+1/2}^+ - u_{j+1/2}^-)\right], \tag{1.88}$$

and similarly for $\hat{f}_{j-1/2}$,

$$\hat{f}_{j-1/2} = \frac{1}{2}\left[f(u_{j-1/2}^-) + f(u_{j-1/2}^+) - \alpha(u_{j-1/2}^+ - u_{j-1/2}^-)\right], \tag{1.89}$$

where $u_{j\pm1/2}^{\pm}$ represents the approximation of $u_{j\pm1/2}$ from the left and right, and $\hat{f}_{j-1/2}$ can be obtained by taking one full step back from $\hat{f}_{j+1/2}$. Note that the coefficient α is defined such that:

$$\alpha = \max|f'(u)|, \tag{1.90}$$

and it represents numerical dissipation, which is associated with diffusion.

The term $u^+_{j+1/2}$ is approximated from the right using available point values such that:

$$\begin{aligned} u^+_{j+1/2} &= u_{j+1} - \frac{u_{j+2} - u_{j+1}}{2} \\ &= \frac{3u_{j+1} - u_{j+2}}{2}, \end{aligned} \tag{1.91}$$

and similarly,

$$\begin{aligned} u^-_{j+1/2} &= u_j - \frac{u_{j-1} - u_j}{2} \\ &= \frac{3u_j - u_{j-1}}{2}. \end{aligned} \tag{1.92}$$

Note that $u^+_{j-1/2}$ and $u^-_{j-1/2}$ can be constructed in the same way or they can be obtained taking one full step back from $u^+_{j+1/2}$ and $u^-_{j+1/2}$. These approximations can now be substituted into (1.87) to obtain a stable numerical scheme for (1.85).

The Lax-Friedrichs method is a useful numerical scheme for the integration of advection term in model (1.39) in which chemotactic sensitivity is proportional to the density of bacteria and takes the form $\left(\chi u \frac{\partial c}{\partial x}\right)_x$. In this case, u is approximated at each half step according to $\hat{f}_{j\pm1/2}$ and the gradient of the chemical using the central scheme such that:

$$(c_x)^n_j = \frac{c^n_{j+1} - c^n_{j-1}}{2\Delta x}. \tag{1.93}$$

Using the forward Euler difference approximation for time discretization, the central difference approximation for the second order derivative of diffusive term and the Lax-Friedrichs scheme for the chemotactic term, the explicit numerical scheme for the integration of model (1.39) becomes:

$$\begin{cases} u^{n+1}_j = u^n_j + D\dfrac{\Delta t}{\Delta x^2}\left[u^n_{j+1} - 2u^n_j + u^n_{j-1}\right] - \chi\dfrac{\Delta t}{\Delta x}\left[\hat{f}_{j+1/2}(c_x)_{j+1/2} - \hat{f}_{j-1/2}(c_x)_{j-1/2}\right] \\ \qquad\qquad +\Delta t f(u^n_j,\ c^n_j), \\ c^{n+1}_j = c^n_j + \dfrac{\Delta t}{\Delta x^2}\left[c^n_{j+1} - 2c^n_j + c^n_{j-1}\right] + \Delta t g(u^n_j,\ c^n_j), \end{cases} \tag{1.94}$$

with Neumann boundary conditions:

$$\begin{cases} u_x(a,t) = u_x(b,t) = 0, \\ (c_x)_{j=1} = (c_x)_{j=N+1} = 0. \end{cases} \tag{1.95}$$

Note that in our numerical simulations, the coefficient for numerical dissipation is set such that $\alpha = 0$, since this is associated with diffusion and is already taken into account in the model.

Chapter 2

Travelling wave solutions in reaction-diffusion-advection systems

In this chapter, the existence of travelling wave solutions [86, 87] in systems involving one or two interacting bacterial populations is investigated. The chapter begins by introducing the Fisher-Kolmogorov equation and the Lotka-Volterra system, along with methods for determining their respective minimum wave speeds. This is followed by two research sections that explore the spatio-temporal distribution in systems of one and two interacting species, both in the presence and absence of chemotaxis. A key result in Section 2.1 highlights the influence of diffusion and reproduction on the shape of travelling wavefronts, as well as the impact of these parameters on the spatial separation between bacterial species and the chemical agent. Notably, when both diffusion and reproduction are sufficiently small, the density of the bacterial species is approximately equal to the concentration of the chemical agent. Using this result, an analytical equation has been derived for a specific solution $n(z)$ to calculate the minimum wave speed of the travelling waves when the chemical agent acts as a repeller.

Section 2.2 focuses on two interacting bacterial species, one of which produces a chemical agent. In the absence of chemotaxis, it is well established that travelling waves can form between the unstable trivial steady state and the stable coexistence state. Our findings show that the product of diffusion and reproduction determines the minimum wave speed, such that travelling waves can move with different speeds when $Dr \neq 1$. We also demonstrate how these speeds change depending on whether $Dr \lesseqgtr 1$. Furthermore, we address gaps in the literature regarding the minimum wave speed of travelling waves transitioning from the unstable coexistence steady state to one of the stable extinction states, both with and without chemotaxis. To achieve this, we derive the dispersion curve that relates wave speed to wave number. While this approach has previously been

employed to determine the minimum wave speed in reaction-diffusion systems, we extend its application to reaction-diffusion-advection systems. Throughout the chapter, analytical results are supported by computational simulations.

Introduction

Travelling waves are waves that move in a particular direction, with constant speed and fixed shape, making the transition from an unstable steady state to a stable one. They have many applications in science, such as slow and fast combustion waves due to chemical reactions [134], or shock waves in fluid dynamics [117]. Moreover, in mathematical biology, the spatial spread of diffusive microorganisms can be described by travelling wave solutions, which represents the motivation behind this chapter.

The simplest way to describe the spatial distribution of any population with logistic growth that can diffuse is to use the nondimensional Fisher-Kolmogorov equation [33, 62] :

$$\frac{\partial n}{\partial t} = D\frac{\partial^2 n}{\partial x^2} + rn(1-n), \tag{2.1}$$

where n represents the population density, D its diffusion rate and r the proliferation rate. This equation can be transformed into a system of two ordinary differential equations using the ansatz $n(x,t) = N(z)$ and $N' = U$, where $z = x - st$ and s is the speed of the wave travelling from left to right. The transformed system has two equilibrium points, $(N,U) = (0,0), (1,0)$, which are stable and unstable, respectively, and allows the formation of travelling waves between the two steady states. Using methods of linear analysis, one can find the minimum wavespeed requirement by ensuring that the trivial steady state is a node rather than a spiral, to avoid negative concentrations around $(N,U) = (0,0)$, which gives $s_{min} \geq 2\sqrt{Dr}$ [86, 87]. Finding the wavespeed of the front has attracted great attention from researchers, as it provides insight into how fast a bacterial species can be expected to spread across a medium. Since linear analysis provides a minimum wavespeed, rather than an exact speed, much work has been done using a variety of different algebraic methods. An effective method to obtain exact solutions to nonlinear partial differential equations is the direct tanh method, in which the solution is expressed as a sum of hyperbolic functions such that:

$$n(z) = \sum_{i=0}^{m} a_i \tanh^i(kz), \tag{2.2}$$

where k represents the wavenumber and m the order of expansion. The order of expansion is calculated such that $m = \dfrac{d}{h-1}$, where d is the order of the highest derivative term and h the highest nonlinear term. By substituting $n(z)$ into the

Fisher equation and equating coefficients of powers of tanh to zero, it has been shown that, for this solution of type (2.2) to system (2.1), the exact travelling wavespeed is $s = \sqrt{\frac{25Dr}{6}}$, which is about the minimum [64, 121]. It has also been shown that travelling wavefronts exist when the diffusive flux is nonlinear and the wavespeed has been determined explicitly in some special cases [8, 141].

There are many other effective algebraic methods for finding the exact speed of travelling wavefronts such as the Exp-function method, which is used for finding solitary solutions, periodic solutions and compacton-like solutions. In this method, the solution is assumed to take the form:

$$n(z) = \frac{\sum_{i=-c}^{d} a_i \exp(iz)}{\sum_{j=-p}^{q} b_j \exp(jz)}, \tag{2.3}$$

where c and p are obtained by balancing the highest order linear term with the highest order nonlinear term and q and d the lowest order terms. The effectiveness of this method has been proven by applying it to nonlinear PDEs such as the Korteweg-de Vries and the Dodd-Bullough-Mikhailov equations [45], or Burgers-type equations [145], and it has been shown to be a highly effective method for solving equations with higher-order nonlinearity. These types of nonlinear equations and travelling wave solutions can also be found using the sine-cosine method, in which solutions take one of two forms:

$$\begin{cases} n(z) = \alpha \cos^i(kz), \\ \text{or,} \\ n(z) = \alpha \sin^i(kz). \end{cases} \tag{2.4}$$

This method has been proven to give exact solutions in line to those obtained when using the direct tanh method when applied to generalised KdV equations [122] or fifth order nonlinear evolution equations [101]. Another powerful method has been applied to the Kolmogorov-Petrovskii-Piskunov equation [63] in which the solution took the form:

$$n(z) = \sum_{i=0}^{m} a_i (v(z))^i, \tag{2.5}$$

where $v_z = \epsilon(1 - v^2)$ represents the Riccati equation. In this case, if the functions $1,\ v,\ v^2\ ...\ v^m$ are linearly independent, then $m = 1$ [79]. These algebraic methods represent tools that can be used to find exact travelling wavefront solutions to nonlinear partial differential equations when linear analysis does not provide sufficient insight into the existence of travelling wavefronts or their speed, but are not always guaranteed to work for any type of equation or boundary conditions.

The aim of this chapter is to understand the formation of travelling waves in a system of one bacterial species interacting with a chemical. A great deal of

research has been conducted on this subject due to the observation that bacteria seek an optimal environment and can move towards regions of higher or lower concentrations of certain chemical substrates. Keller and Segel first observed that *E. Coli* form bands that can travel at constant speed when placed at one end of a capillary tube containing oxygen and an energy source, in 1971 [58]. To describe this phenomenon of substrate consumption and changes in bacterial density due to diffusion and chemotaxis, they used a set of partial differential equations:

$$\begin{cases} \dfrac{\partial n}{\partial c} = \dfrac{\partial}{\partial x}\left(D(c)\dfrac{\partial n}{\partial x}\right) - \dfrac{\partial}{\partial x}\left(n\chi(c)\dfrac{\partial c}{\partial x}\right), \\ \dfrac{\partial c}{\partial t} = \dfrac{\partial^2 c}{\partial x^2} - p(c)n, \end{cases} \tag{2.6}$$

where $D(c)$ and $\chi(c)$ represent the diffusion and chemotactic sensitivity of bacteria in response to the chemical substrate concentration, respectively. $p(c)$ represents the rate of consumption of the chemical substrate by the bacteria. It has been shown that chemotaxis must be sufficiently strong and sufficiently singular for the system to admit travelling bands solutions, i.e. $\chi(c) = \delta c^{-1}$. It has later been shown that, using a velocity jump model, it is possible to obtain travelling wave solutions without the singularity in the chemotactic sensitivity and without explicit growth terms, or the introduction of additional attractant [143].

In model (2.6), the concentration of the chemical substrate is fixed to start with and there is no production of the chemical, only consumption by the bacteria. Motivated by this work, a different group of researchers has used a slightly different model to account for chemical production [138]:

$$\begin{cases} \dfrac{\partial n}{\partial c} = D\dfrac{\partial^2 n}{\partial x^2} - \dfrac{\partial}{\partial x}\left(\chi\dfrac{n}{c}\dfrac{\partial c}{\partial x}\right), \\ \dfrac{\partial c}{\partial t} = \epsilon\dfrac{\partial^2 c}{\partial x^2} + hv - p(c)n, \end{cases} \tag{2.7}$$

where ϵ is the diffusion rate of the chemical substrate and h is its production rate. In this case, it has been shown using proof by contradiction that the system does not admit travelling waves as solution. Other work has considered bacterial kinetics such as reproduction and death and by introducing logistic bacterial growth rate, it has been shown that system:

$$\begin{cases} \dfrac{\partial n}{\partial c} = D\dfrac{\partial^2 n}{\partial x^2} - \dfrac{\partial}{\partial x}\left(\chi(c)n\dfrac{\partial c}{\partial x}\right) + rn(1-n), \\ \dfrac{\partial c}{\partial t} = \epsilon\dfrac{\partial^2 c}{\partial x^2} + hv - p(c)n, \end{cases} \tag{2.8}$$

admits travelling waves as solution without the requirement that $\chi(c)$ needs to be singular. In addition, they have proven the existence of a minimum wave speed

for which the model exhibits non-negative travelling wave solutions in order to desribe the spreading or receding of the bacteria and chemical over the spatial medium [11, 72].

It is clear that, commonly, researchers have focused their attention on cases where the chemical substrate is consumed by the bacteria. In this chapter, the one-species model we consider investigates the existence of travelling wave solutions when the chemical agent is produced by the bacteria. In addition, the system includes both bacterial and chemical diffusion, bacterial kinetics such as reproduction and death, and the chemotactic response of the bacteria to changes in the concentration field of the chemical. When bacteria produce their own chemotactic agent [17, 16, 59], we show that the system admits travelling wavefronts as solutions. However, depending on the strength of the chemotactic agent and whether it acts as an attractant or repellent, Turing patterns can also form behind the travelling front. If chemorepulsion is strong enough, the speed of the fronts increases as the strength of chemorepulsion also increases, and exact speeds have been calculated under the assumption that the diffusion and reproduction of the bacteria are sufficiently small. On the other hand, if chemoattraction is strong enough, chemotactic sensitivity does not have a significant effect on the speed of the front.

The second part of this chapter focuses on the existence of travelling wave solutions in a two-species system. The Lotka-Volterra model is the simplest way to describe the interactions between two competing populations [76, 135]. This is a system of two partial differential equations used to describe the changes in the population density of two species of microorganisms that can diffuse, reproduce, die, and compete for resources:

$$\begin{cases} \dfrac{\partial n}{\partial t} = \dfrac{\partial^2 n}{\partial x^2} + n(1 - n - b_1 v), \\ \dfrac{\partial v}{\partial t} = D\dfrac{\partial^2 v}{\partial x^2} + v(r - v - b_2 n), \end{cases} \tag{2.9}$$

where n and v represent two populations, r the intrinsic growth rate, b_1 represents the competitive effect of species v on n and similarly, b_2 represents the competitive effect of species n on v. The main types of interactions in this system have been well studied: predator-prey, competition and symbiosis [28, 31, 86, 87, 99] and travelling wave solutions in these situations are well understood. Similar to the Fisher-Kolmogorov equation, methods of linear analysis can be used to find minimum travelling wavespeed between unstable and stable steady states when travelling wavefronts are admitted as solutions [86, 87]. One of the most important cases in this system is considered to be when one of the species survives while the other becomes extinct, depending on initial data. In this case, the

direct tanh method has been used to find the exact speed of the travelling front between $(N,\ V)(-\infty) = (0,\ r)$ and $(N,\ V)(\infty) = (1,\ 0)$. By using the ansatz that $\dfrac{dN}{dz} = F(N)$ and and $V = G(N)$, where:

$$\begin{cases} F(N) = \sum_{i=0}^{m} a_i N^i, \\ G(N) = \sum_{i=0}^{n} b_i N^i, \end{cases} \tag{2.10}$$

where m and n are such that $2m = n + 2$. Substituting into system (2.9) and equating all coefficients of powers of N to zero, for the obvious case that $m = n = 2$, one can obtain parameters such that:

$$D = \frac{1}{3b_1},\ b_2 = 2 + \frac{5r}{3} - rb_1,\ s = \frac{-2 + rb_1}{\sqrt{2rb_1}},$$

which give an exact monotone travelling wave solution:

$$\begin{cases} N(z) = \dfrac{1}{2}\left[1 + \tanh\left(\dfrac{\sqrt{2rb_1}}{4}z\right)\right], \\ V(z) = \dfrac{r}{4}\left[1 - \tanh\left(\dfrac{\sqrt{2rb_1}}{4}z\right)\right]^2, \end{cases} \tag{2.11}$$

as explained in detail in [106]. This is not as powerful as finding minimum wavespeed by methods of linear analysis, since solution is found for specific parameter conditions, in which parameters depend on one another. Similarly, researchers have looked into finding exact travelling wavefront solutions for systems transitioning from coexistence to extinction, however mistakes in expansion and analysis have been found when using the hyperbolic function ansatz [52]. We believe that when analysing travelling wavefront solutions belonging to Lotka-Volterra-type systems, linear analysis is more powerful than nonlinear analysis, as nonlinear analysis provides exact solutions only for specific parameter regimes, while linear analysis provides a minimum wavespeed requirement with no parameter dependence on one another.

More recently, researchers have focused their attention on the effects of chemotaxis in a two species system to understand the long-time behaviour of species in response to chemical agents. Lin and Wang have considered a two species model in which both species chemotactically react to a chemical agent degraded

by themselves [73]:

$$\begin{cases} \dfrac{\partial n}{\partial t} = \dfrac{\partial^2 n}{\partial x^2} - \dfrac{\partial}{\partial x}\left(\chi_1 n \dfrac{\partial \phi(c)}{\partial x} - \beta n \dfrac{\partial \phi(v)}{\partial x}\right), \\ \dfrac{\partial v}{\partial t} = \dfrac{\partial^2 v}{\partial x^2} - \dfrac{\partial}{\partial x}\left(\chi_2 v \dfrac{\partial \phi(c)}{\partial x} - \beta v \dfrac{\partial \phi(u)}{\partial x}\right), \\ \dfrac{\partial c}{\partial t} = \epsilon \dfrac{\partial^2 c}{\partial x^2} - u - v, \end{cases} \tag{2.12}$$

where $\chi_1,\ \chi_2,\ \beta$ represent the chemotactic strengths and ϕ the chemotactic sensitivity function. In this case, the chemotactic sensitivity is considered to be logarithmic, $\phi(c) = \ln c$ and if $\beta = 0$, then n and v have no mutual chemotactic effects. The main results of the paper have shown that regions in which the system admits travelling waves as solution depend on the chemotactic strengths $(\chi_1,\ \chi_2)$ for different β regimes. In particular, if $\beta = 1$, travelling wave solutions exist if $\chi_1 = \chi_2 \geq 2$. In other models, the species are assumed to exhibit Lotka-Volterra competitive kinetics and produce the same chemical agent [53, 69, 123]:

$$\begin{cases} \dfrac{\partial n}{\partial t} = D_1 \dfrac{\partial^2 n}{\partial x^2} - \chi_1 \dfrac{\partial}{\partial x}\left(n \dfrac{\partial c}{\partial x}\right) + r_1 n(1 - n - b_1 v), \\ \dfrac{\partial v}{\partial t} = D_2 \dfrac{\partial^2 v}{\partial x^2} - \chi_2 \dfrac{\partial}{\partial x}\left(v \dfrac{\partial c}{\partial x}\right) + r_2 v(1 - v - b_2 n), \\ \dfrac{\partial c}{\partial t} = D_3 \dfrac{\partial^2 c}{\partial x^2} + h_1 u + h_2 v - pc, \end{cases} \tag{2.13}$$

where h_1 and h_2 represent the production rates of c by n and v, respectively and p represents the degradation rate of c. In [69] the existence of travelling wavefronts and heteroclinic solutions has been established by the perturbation method and computational simulations have been used to show existence of travelling wavefronts numerically. By assuming that the concentration of the chemical does not change over time, i.e:

$$0 = D_3 \frac{\partial^2 c}{\partial x^2} + h_1 u + h_2 v - pc,$$

$0 << b_1,\ b_2 << 1$ and $D_1,\ D_2,\ D_3 > 0$, system (2.13) has been proven to have a spatially homogeneous equilibrium point, which is asympotically stable in an nonempty range of r_1 and r_2 in [123]. Moreover, under further assumptions that $D_1 = 1$ and $r_1 = 1$ and that the chemotaxis strength is sufficiently small, $\chi_1 < \dfrac{1}{h_1}$ and $\chi_2 < \dfrac{r_2}{h_2}$, the existence of travelling wave solutions connecting two spatially homogeneous equilibrium points with wave speed greater than a critical number $s^* = 2\sqrt{(1 - b_1)}$ has been proven in [53].

To understand the long-term behaviour of two competing species, we examine the existence of travelling wave solutions both in the absence and presence of a chemotactic agent. In the first instance, the classical Lotka-Volterra model [49, 76, 135] is considered to demonstrate the formation of travelling waves between the four steady states and to obtain the minimal travelling wave speed, which is compared against speeds obtained numerically. An interesting result is that, in certain cases, the waves can travel at different speeds, and we provide an explanation as to why this occurs. Additionally, a novel result presented in this chapter is the existence and minimum wavespeed of travelling wavefronts moving away from the unstable coexistence steady state to one of the stable extinction states. The two-species chemotaxis model considered here consists of two bacterial species with Lotka-Volterra kinetics, where one of the species produces a chemical agent that affects the other species. In this case, the effects of chemotaxis on the formation of travelling wave solutions and its impact on the minimal wave speed are analysed through computational simulations. Results show that, due to chemotaxis, as time tends to infinity, all three travelling wavefronts move at the same speed as the leading wavefront, and the distance between the two species as they travel across the medium remains constant after a certain time point.

2.1 Travelling wave solutions in a one species system

In the first part of this chapter, the existence of travelling wave solutions in a system of one bacterial species producing a chemical is investigated. Initially, the concentration of the chemical agent does not affect the bacterial species, which means the system behaves like the Fisher-Kolmogorov equation [33, 62]. However, we investigate the effects of model parameters, such as the diffusion and reproduction of bacteria, on the shape of the travelling front. In the second scenario, the chemical affects the bacteria by either acting as an attractant or repellent. We are interested in how chemotaxis affects the speed of the travelling wavefronts, which indicates how fast the bacteria and chemical spread across the medium. In the case of small bacterial diffusion and reproduction, we obtain a formula for the speed of the travelling wave in response to chemorepulsion. Analytical results are supported by computational simulations.

2.1.1 Travelling waves in a system without chemotaxis

Travelling waves are important solutions to reaction-diffusion systems, and they help in understanding the long-term behaviour of such systems. Analysing the minimum wave speed of travelling wave solutions aids in understanding the spread of populations, or in our case, the spread of bacteria in response to a chemical agent it produces.

One of the simplest ways to describe a diffusive microorganism producing a chemical agent is to model the density of the bacteria according to the Fisher-Kolmogorov equation, and the concentration of the chemical changes according to diffusion, its production by the bacteria, and its decay:

$$\begin{cases} \dfrac{\partial n}{\partial t} = D\dfrac{\partial^2 n}{\partial x^2} + rn(1-n), \\ \dfrac{\partial c}{\partial t} = \dfrac{\partial^2 c}{\partial x^2} + n - c, \end{cases} \tag{2.14}$$

where n and c represent the density of bacteria and the concentration of the chemical, respectively. Since the first equation is decoupled from the second and the concentration of the chemical agent does not affect the bacterial density, the system behaves like the Fisher-Kolmogorov equation and admits travelling wavefronts as solutions, making the transition from the unstable steady state $(n,\ c) = (0,\ 0)$ to the stable steady state $(n,\ c) = (1,\ 1)$ with minimal wave speed $s_{min} \geq 2\sqrt{Dr}$.

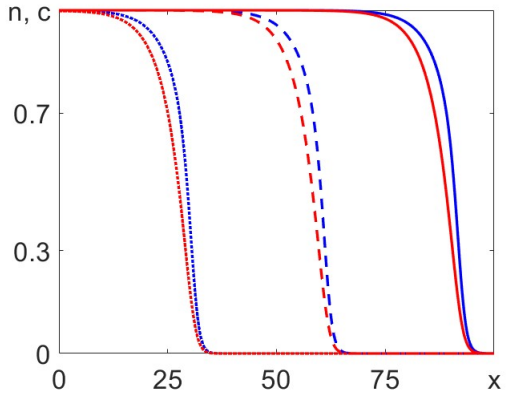

Figure 2.1: ***Numerical simulation of travelling fronts in system (2.14).*** *Initial conditions such as* $(n,\ c)(x,\ 0) = (1,\ 1)$ *if* $x < 10$ *and* $(n,\ c)(x,\ 0) = (0,\ 0)$ *if* $x \geq 10$. *Blue represents the density of bacteria and red the concentration of the chemical. Dotted, dashed and solid lines represent the profiles at time* $t = 10$, $t = 25$ *and* $t = 40$, *respectively. Model parameters:* $D = r = 1$ *and speed:* $s \approx 2$.

Figure 2.1 shows numerically that system (2.14) admits travelling wavefronts as solutions. It is clear that wavefront c, corresponding to the concentration of

the chemical, follows closely behind wavefront n, corresponding to the density of bacteria. However, they both travel at the same speed, as the gap between the two fronts remains unchanged over time. An interesting question in this case is whether model parameters, such as bacterial diffusivity and reproduction, affect the shape of the profiles and, consequently, the gap between them. By fixing the medium length $L = 1000$ and running simulations for time $T = 250$, with $dt = 6.9 \times 10^{-3}$ and $dx = 1.67$, the difference between the two fronts is investigated, such that $\Delta a(i) = n(i) - c(i)$, where i represents each mesh point from $i = 1 : 6000$. Numerical results for $\Delta a(i)$ are shown in Figure 2.2.

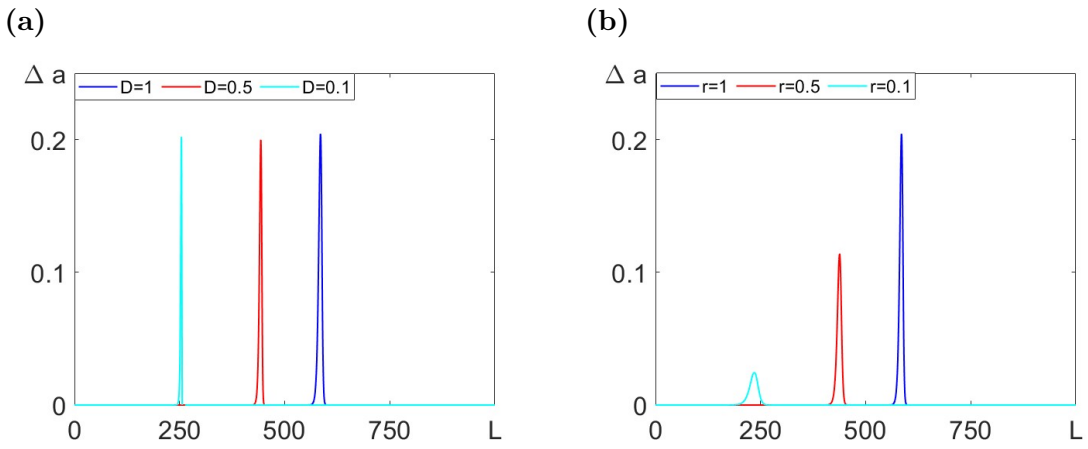

Figure 2.2: ***Numerical comparison between the profiles of the two wavefronts of system*** (2.14)***, as parameters vary.*** ***(a)****: The effects of bacterial diffusion on the speed and shape of the numerical profiles. Fixed parameter* $r = 1$. ***(b)****: The effects of bacterial reproduction on the numerical profiles. Fixed parameter* $D = 1$.

Figure 2.2 describes characteristics of the travelling wavefronts, such as shape, speed, and the distance between the wavefront of n and that of c. In each panel, the amplitude of the spikes is related to the distance between the two wavefronts, the width of the spikes is related to the shape of the profiles, and the positioning of the spikes is related to the speed of the wavefront, or how far along the medium they have travelled. Both panels show that increasing either diffusion or reproduction results in faster travelling fronts, which is expected from the minimum wave speed condition. Interestingly, in Figure 2.2 a, the amplitude of the spikes is approximately the same, which shows that the distance between the two wavefronts does not change as the diffusion parameter increases. However, the width of the spikes increases, meaning that the shape of the profiles changes, and wavefront n becomes smoother with an increase in diffusion. On the other hand, in Figure 2.2 b, the amplitude of the spikes increases with an increase in reproduction, indicating that the distance between the two fronts increases. The

width of the spikes gets smaller, meaning that wavefront n becomes sharper as reproduction increases. Results related to the shape of wavefront n can be seen graphically in Figure 2.3.

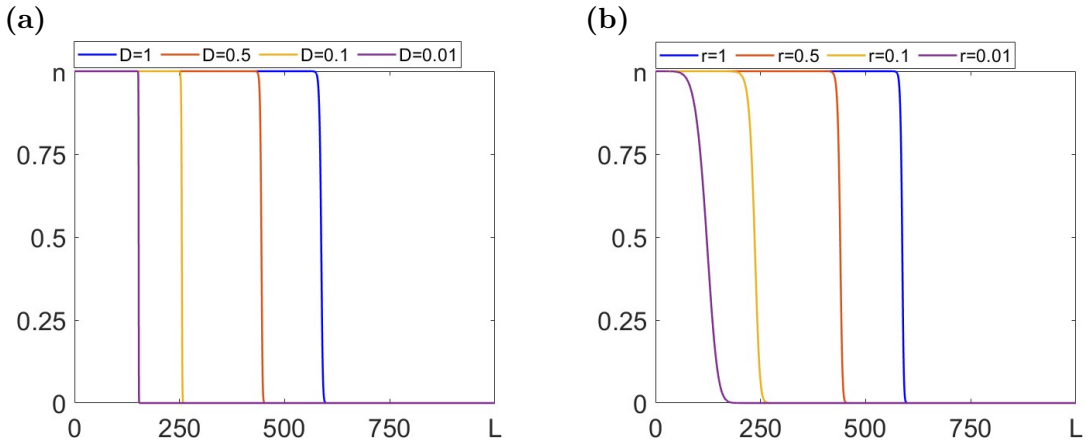

Figure 2.3: ***Travelling wavefronts*** n ***in system (2.14)*** . ***(a)****: As the diffusion parameter,* D*, is increased, the wavefront becomes smoother. Fixed parameter* $r = 1$*.* ***(b)****: As the reproduction parameter,* r*, is increased, the wavefront becomes sharper. Fixed parameter* $D = 1$*. Initial conditions:* $n(x,\ 0) = 1$ *if* $x < 50$ *and* $n(x,\ 0) = 0$ *if* $x \geq 50$*.*

Figure 2.3 shows a graphical representation of the numerical solution to system (2.14) corresponding to the wavefront n. In Figure 2.3 a, as the diffusion coefficient is increased up to $D = 1$, the shape of the profile becomes smoother compared to the shallow shape corresponding to very small diffusion, $D = 0.01$. On the other hand, in Figure 2.3 b, it is clear that a very small reproduction coefficient, $r = 0.01$, results in a smoother profile shape compared to the shallower shape given by a larger $r = 1$. A suitable conclusion from this analysis would be to state that $n \approx c$ if $D << 1$ to ensure the profiles have similar shapes (see Figure 2.2 a) and $r < 1$ to ensure the distance between the fronts is very small (see Figure 2.2 b).

In this section, the existence of travelling wave solutions in a one-species system without chemotaxis is investigated. In addition, we have examined the effects of model parameters, such as diffusion and reproduction, on the shape and the distance between the two fronts corresponding to the density of bacteria and the concentration of the chemical. The key result is that system (2.14) behaves like the Fisher-Kolmogorov equation, admitting travelling wavefronts as solutions, and that the characteristics of the solutions, such as shape and distance between the profiles, are affected by model parameters. In the next section, attention focuses on the existence of travelling wave solutions in a system with chemotaxis, meaning that gradients in the concentration field of the chemical will affect the

spatial spread of bacteria.

2.1.2 Travelling waves in a system with chemotaxis

In this section, chemotactic activity is considered, which implies the directed motion of bacteria in response to gradients in the concentration field of the chemical. The chemical gradient affects the spread of bacteria by acting either as an attractant or a repellent. This can be modelled mathematically by introducing the advection term $\chi\frac{\partial}{\partial x}\left(f(n,c)\frac{\partial c}{\partial x}\right)$, where χ represents the chemotaxis strength and its sign indicates whether it is attraction or repulsion. The simplest assumption is that chemotaxis strongly depends on bacterial density, i.e. $f(n,c) = n$, and model (2.14) becomes:

$$\begin{cases} \dfrac{\partial n}{\partial t} = D\dfrac{\partial^2 n}{\partial x^2} - \chi\dfrac{\partial}{\partial x}\left(n\dfrac{\partial c}{\partial x}\right) + rn(1-n), \\ \dfrac{\partial c}{\partial t} = \dfrac{\partial^2 c}{\partial x^2} + n - c, \end{cases} \tag{2.15}$$

where, as before, c is a chemical agent produced by the bacterial species n. In order to check analytically if the system admits travelling waves as solutions, the ansatz $n(x,\ t) = N(z)$, $c(x,\ t) = C(z)$, where $z = x - st$ is substituted into (2.15), which becomes,

$$\begin{cases} N' = U, \\ U' = \dfrac{1}{D}\left(-sU + \chi(UW - sNW - N^2 + NC) + rN(N-1)\right), \\ C' = W, \\ W' = -sW - N + C. \end{cases} \tag{2.16}$$

This system has two steady states, $(N,U,C,W) = (0,0,0,0)$ and $(1,0,1,0)$. By evaluating the Jacobian of (2.16) at the first steady state, we find that this is unstable when $s \geq 2\sqrt{Dr}$; however, evaluating the Jacobian at the second steady state is more complicated, as an analytical expression for its corresponding eigenvalues cannot be obtained. As discussed, if $\chi = 0$, the chemical agent does not affect the spatial spread of bacterial density, and the system behaves like the Fisher-Kolmogorov equation, allowing the formation of travelling waves between the two steady states. Intuitively, we expect that travelling waves also appear if the chemotaxis strength is small enough, $|\chi| << 1$, since this would not significantly impact the solutions admitted by the system. By fixing model parameters and running numerical simulations, we investigate the effect of chemotaxis on the existence of travelling waves and their speed, both when the chemical agent acts as an attractant or repellent, with no constraint on the strength of chemotaxis.

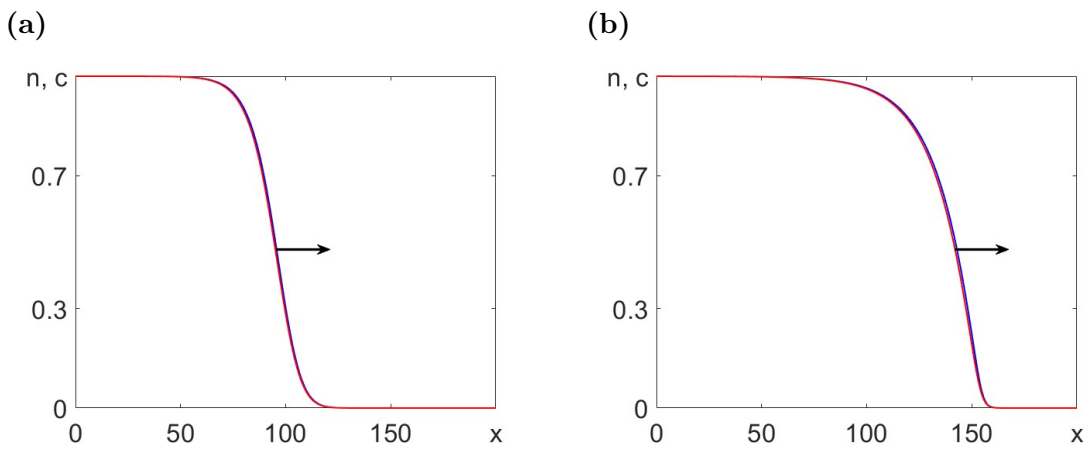

Figure 2.4: ***Travelling wave solutions to system (2.15) obtained in numerical simulations.*** ***(a)****: Travelling wave solutions in the case of no chemotaxis,* $\chi = 0$. ***(b)****: Travelling wave solutions when the chemical agent acts as a strong repeller,* $\chi = -10$. *Fixed parameters:* $D = 1$, $r = 0.1$ *and time*=150. *Initial conditions:* $(n,\ c) = (1,\ 1)$ *if* $x < 20$ *and* $(n,\ c) = (0,\ 0)$ *if* $x \geq 20$.

Figure 2.4 shows travelling waves admitted as solutions to system (2.15). In Figure 2.4 a, there is no chemotaxis, meaning the chemical agent c does not affect the bacterial species n and $\chi = 0$. In Figure 2.4 b, the chemical agent acts as a strong repeller, $\chi = -10$, and clearly, the waves have travelled faster and further along the medium in this case, compared to the case of no chemotaxis. This shows numerically that chemorepulsion affects the speed of the travelling waves.

Typically, the speed of the travelling wavefront can be determined analytically by requiring that the steady state $(N, U, C, W) = (0, 0, 0, 0)$ of system (2.16) is an unstable node, rather than a spiral, to avoid negative concentrations. Mathematically, this means that all eigenvalues corresponding to this steady state must be real, and this constraint provides the minimal speed of the travelling wavefront, $s \geq 2\sqrt{Dr}$. Clearly, this speed depends only on diffusion and reproduction, not chemotaxis, and it does not align with the results seen in the numerical simulations presented in Figure 2.4. One way to understand how model parameters, including chemotaxis, affect the speed of the travelling wavefronts admitted as solutions to system (2.15) is to run computational simulations and calculate the speed s numerically. Numerical results are presented graphically in Figure 2.5.

Figure 2.5 shows how the speed of the travelling wavefronts, admitted as solutions to system (2.15), changes with chemotaxis for different model parameters. In Figure 2.5 a, the reproduction coefficient is fixed such that $r = 1$, and the diffusion coefficient is varied such that $D < 1$, since $D = \dfrac{D_n}{D_c}$ and the chemical agent is expected to diffuse faster than the bacteria. Three different diffusion values are considered, and in all cases, it is clear that the speed of the front

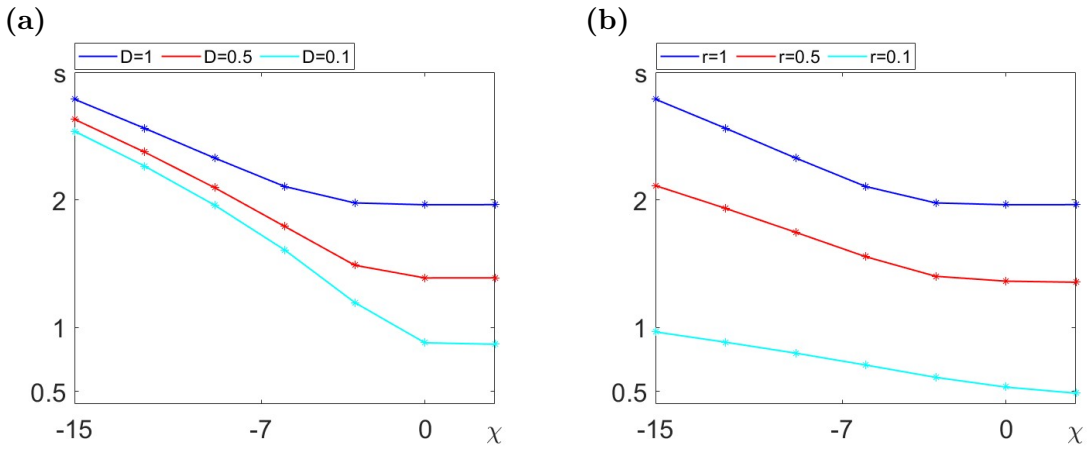

Figure 2.5: ***Numerical speed of the travelling wavefront solutions to system (2.15) as chemotaxis changes. (a)****: The effect of chemotaxis on the speed of the front for different diffusion rates:* $D = 1$ *(navy line),* $D = 0.5$ *(red line),* $D = 0.1$ *(blue line) and fixed* $r = 1$*.* ***(b)****: The effect of chemotaxis on the speed of the front for different reproduction rates:* $r = 1$ *(navy line),* $r = 0.5$ *(red line),* $r = 0.1$ *(blue line) and fixed* $D = 1$*.*

increases significantly as the strength of chemorepulsion increases. Similarly, in Figure 2.5 b, the diffusion coefficient is fixed such that $D = 1$, and three different reproduction rates are considered. Again, in all three cases, the speed of the travelling wavefront increases as chemorepulsion gets stronger. On the other hand, it is evident that chemoattraction does not significantly impact the speed of the front, though Figure 2.4 shows that if chemoattraction is strong enough, Turing patterns can appear behind the travelling front.

Computational simulations provide great insight into how the speed of travelling wavefront solutions is affected by the presence of a chemical agent that chemotactically influences the spatial distribution of the bacterial species producing it. However, numerical results do not offer a quantitative measure of how much a model parameter affects how fast bacteria spread or recede across the medium. Since the linear analysis of system (2.15) around the trivial equilibrium point provides a minimum wave speed formula that depends only on diffusion and reproduction, this motivates our next work: using observations from numerical simulations to analytically derive a wave speed formula that depends on all three model parameters.

As seen in the previous section, in Figure 2.2 a, the width of the spikes is smaller for smaller diffusion coefficients, meaning the difference between the two profiles of n and c is also reduced. Additionally, in Figure 2.2 b, the amplitude of the spikes is smaller for lower reproduction coefficients, which indicates that the distance between the two profiles is also smaller. Combining these results,

for small diffusion and reproduction, the distance between the two profiles (n, c) is minimal, and the shape of the profiles is similar. Under the assumption that $D, r << 1$, we can use the approximation $n \approx c$ to transform the system of two partial differential equations (2.15) into one partial differential equation:

$$\frac{\partial n}{\partial t} = D\frac{\partial^2 n}{\partial x^2} - \chi\frac{\partial}{\partial x}\left(n\frac{\partial n}{\partial x}\right) + rn(1-n), \tag{2.17}$$

which using the ansatz $n(x,t) = N(z)$, where $z = x - st$, can be transformed into the nonlinear ordinary differential equation:

$$Dn'' - \chi nn'' - \chi(n')^2 + sn' + rn - rn^2 = 0, \tag{2.18}$$

that can be solved for s to obtain the speed of the travelling front.

Now, we seek travelling wave solutions between the unstable state $n(\infty) = 0$ and the stable state $n(-\infty) = 1$. For the specific ansatz:

$$n(z) = \frac{1}{1 + a\exp(\alpha z)}, \quad \text{such that } \begin{cases} n \to 0 \text{ as } z \to \infty, \\ n \to 1 \text{ as } z \to -\infty, \end{cases} \tag{2.19}$$

one can approximate:

$$\begin{cases} n \approx a\exp(-\alpha z) \text{ as } z \to \infty, \\ n \approx 1 - a\exp(\alpha z) \text{ as } z \to -\infty. \end{cases} \tag{2.20}$$

To solve equation (2.18), we assume that the density of bacteria takes the form $n = 1 - a\exp(\alpha z)$, where a is the coefficient responsible for the amplitude of the wave and α is the wavenumber. Substituting into the ode, we get:

$$e^{\alpha z}(D\alpha^2 - \chi\alpha^2 a + s\alpha a - ra) + e^{2\alpha z}(-2\chi\alpha^2 a^2 - ra^2) = 0, \tag{2.21}$$

which holds for all z if and only if the coefficients of the exponential terms are equal to zero:

$$\begin{cases} D\alpha^2 a - \chi\alpha^2 a + s\alpha a - ra = 0, \\ -2\chi\alpha^2 a^2 - ra^2 = 0, \end{cases} \tag{2.22}$$

which gives:

$$\begin{cases} \alpha^2 = -\dfrac{r}{2\chi}, \\ s = -D\sqrt{-\dfrac{r}{2\chi}} + \sqrt{-\dfrac{r\chi}{2}} + \sqrt{-2\chi r}. \end{cases} \tag{2.23}$$

Note that we are interested in the case of chemorepulsion, for which $\chi < 0$, so the formula gives a real number for the speed value. In addition, this formula only holds for cases when the solution of n takes the form (2.19). Next step is to

check this formula against numerical results and see if the speed of the front is captured accurately for $D, r << 1$.

Figure 2.6 shows a graphical comparison between the wavefront speeds obtained analytically according to (2.23) and the speeds obtained from numerical simulations for four different pairs of model parameters, with $D, r << 1$. In Figure 2.6 a, $D = r = 0.05$, the smallest values considered, and it is evident that there is good correlation between numerical and analytical results, indicating that formula (2.23) accurately captures the effects of chemorepulsion on the speed of the front. In Figure 2.6 b, diffusion remains the same, but bacterial reproduction is increased to $r = 0.2$, and it is clear that, in this case, the analytical formula perfectly captures the speed of the front. This result is due to the fact that, for larger reproduction rates, the shape of the profile of n becomes sharper, and the difference between the shapes of the two profiles becomes smaller, which is an important factor when assuming $n \approx c$. In Figure 2.6 c and d, reproduction is fixed at $r = 0.2$, and diffusion is increased to $D = 0.15$ (panel c) and $D = 0.3$ (panel d). Clearly, as bacterial diffusivity increases, the discrepancy between numerical and analytical results also increases, and (2.23) provides a lower bound for the speed of the travelling wavefront. These results are also related to observations about the shape of the profiles of n and c, as presented in Figure 2.2. As diffusion increases, the difference between the two profile shapes grows, while conversely, as reproduction increases, the difference between the shapes of the profiles decreases.

The minimum wave speed of the travelling wavefronts, admitted as solutions to (2.15), is an important characteristic to understand, as it describes how fast bacteria spread over a spatial medium in response to chemical agents. It has been shown that chemorepulsion strongly affects the speed of the front, and since the minimum wave speed formula obtained from linear analysis depends only on diffusion and reproduction, it does not represent an accurate approximation. By assuming that $D, r << 1$, such that $n \approx c$, we have been able to derive a minimum wave speed formula given by (2.23) that considers the effects of all model parameters, i.e., diffusion, reproduction, and chemorepulsion. We believe this is a novel result and a step forward in understanding how chemorepulsion affects the speed at which bacteria spread over a given medium.

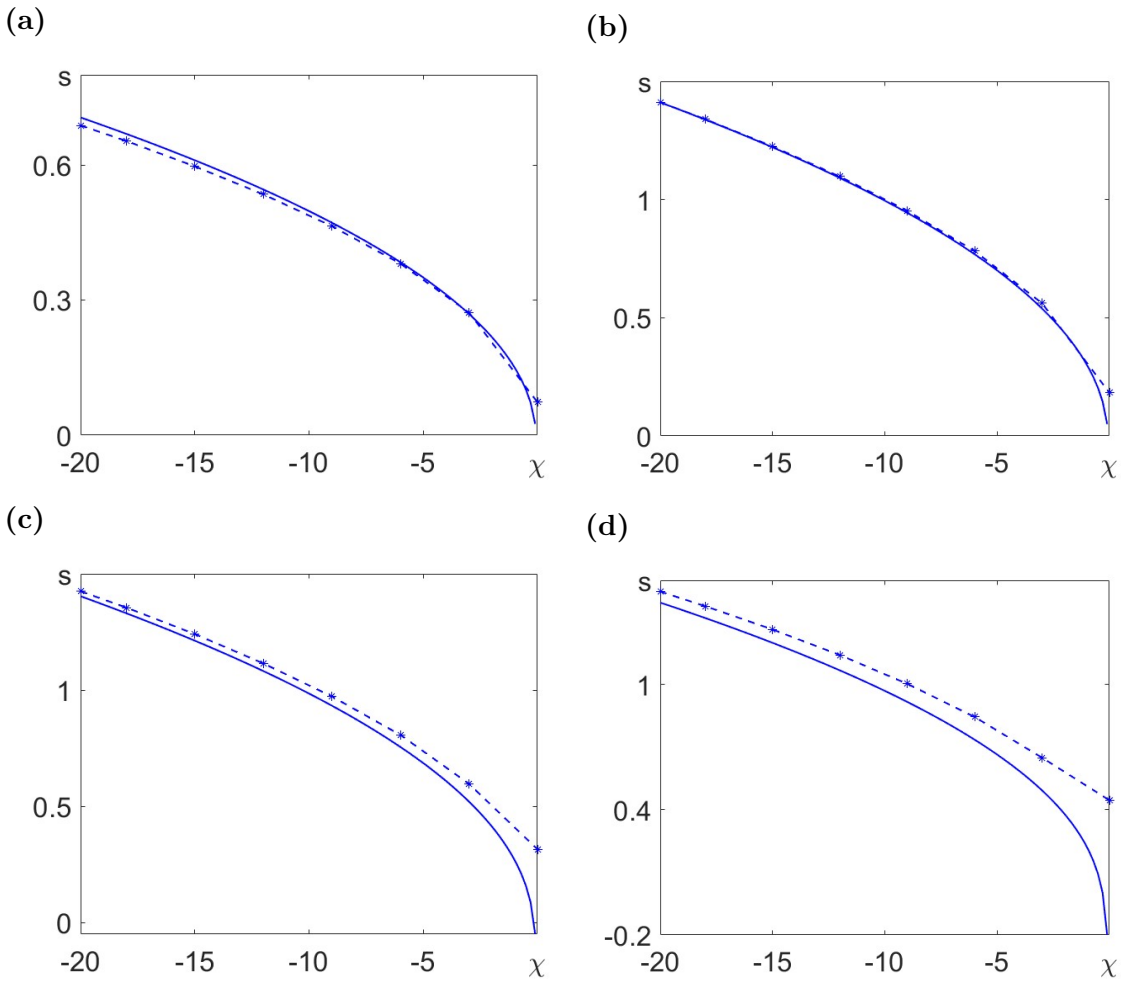

Figure 2.6: ***Analytical speeds of the travelling wavefront solutions to system (2.15) as given by (2.23) compared against speeds obtained from numerical simulations as strength of chemorepulsion varies.*** *Solid curves represent analytical speeds given by (2.23) and dotted curves represent speeds from numerical simulations.* ***(a)****:* $D = r = 0.05$. ***(b)****:* $D = 0.05,\ r = 0.2$. ***(c)****:* $D = 0.15,\ r = 0.2$. ***(d)****:* $D = 0.3,\ r = 0.2$.

In the first part of this chapter, the existence of travelling wavefront solutions in a system with one bacterial species producing a chemical has been investigated. It has been shown that in the absence of chemotaxis, the system behaves like the Fisher-Kolmogorov equation, and travelling wavefronts are admitted as solutions that transition from the unstable trivial steady state to the stable non-trivial state. When the chemical agent affects the distribution of bacteria, either by chemoattraction or chemorepulsion, travelling wavefronts appear, and when chemoattraction is strong enough, Turing patterns also form behind the front. One of the most important characteristics of such fronts is that their speed significantly increases with an increase in chemorepulsion strength. To quantify this increase, we have derived a minimum wave speed formula that accounts for the

effects of all model parameters, such as diffusion, reproduction, and chemorepulsion. In the next part, we investigate the existence of travelling wave solutions in a two-species system, with and without chemotaxis.

2.2 Travelling wave solutions in a two species system

In the second part of this chapter, the existence of travelling wave solutions in a two-species system, where one of the species produces a chemical agent, is investigated. Initially, the concentration of the chemical agent does not affect the population density, and the formation of travelling wavefronts in a system of three partial differential equations with Lotka-Volterra kinetics is studied, along with their respective minimum wave speeds. In the second part, the density of the species is influenced by changes in the concentration field of the chemical. The effects of chemotaxis on the existence of travelling wavefronts, as well as its impact on the minimum wave speed, are investigated both analytically and numerically through computational simulations. The aim of this section is to provide an in-depth understanding of the spatial spread of interacting populations and how the speed of colonisation is influenced by chemotaxis.

2.2.1 Travelling waves in a two species system without chemotaxis

The aim of this section is to provide a better understanding of the interactions between two species and how these are affected by the presence of a chemical agent. The existence of travelling wavefronts in such a system is important, as it provides information about how quickly interspecific competition can lead to colonisation or extinction. Mathematically, this can be modelled by a non-dimensional system of three partial differential equations, in which the bacterial species exhibit Lotka-Volterra kinetics:

$$\begin{cases} \dfrac{\partial u}{\partial t} = D_1 \dfrac{\partial^2 u}{\partial x^2} + r_1 u(1 - u - b_1 v), \\ \dfrac{\partial v}{\partial t} = D_2 \dfrac{\partial^2 v}{\partial x^2} + r_2 v(1 - v - b_2 n), \\ \dfrac{\partial c}{\partial t} = \dfrac{\partial^2 c}{\partial x^2} + v - c, \end{cases} \tag{2.24}$$

where u and v represent two bacterial species and c is the chemical agent produced by the latter. Since the third partial differential equation is decoupled, the system behaves like the Lotka-Volterra model [76, 135], in which D_1 and D_2 represent

the diffusion coefficients and r_1 and r_2 represent the reproduction coefficients of u and v, respectively.

The aim of this section is to investigate how the minimum wavespeed of the travelling wavefronts admitted as solutions to system (2.24) depends on model parameters. It is clear that the system has four steady states, such that:

$$(u,\ v,\ c) = \left\{(0,\ 0,\ 0),\ (1,\ 0,\ 0),\ (0,\ 1,\ 1),\ \left(\frac{b_1-1}{b_1b_2-1},\ \frac{b_2-1}{b_1b_2-1},\ \frac{b_2-1}{b_1b_2-1}\right)\right\}. \tag{2.25}$$

In the well-mixed system, the trivial steady state is always unstable and the stability of the other steady states depends on the interspecific competititon rates b_1 and b_2, as presented in Figure 2.7 .

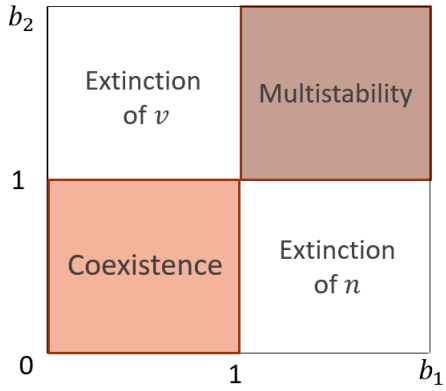

Figure 2.7: ***Domains in the parameter plane*** $(b_1,\ b_2)$ *corresponding to stability of the equilibria of system (2.24). Modified version of Figure 1 in [24].*

Since travelling wavefronts make the transition from an unstable steady state to a stable one, there is a wide range of travelling wavefronts that can be admitted as solutions to system (2.24), and it is important to consider their minimum wave speed requirements. To simplify the mathematical analysis, only the first two partial differential equations of the system are considered, with the characteristic that wavefront c follows wavefront v at the same speed. System (2.24) is now reduced to a system of two partial differential equations, and using the ansatz $u(x,\ t) = U(z)$ and $v(x,\ t) = V(z)$, where $z = x - st$, this becomes:

$$\begin{cases} -sU' = D_1U'' + r_1U(1 - U - b_1V), \\ -sV' = D_2V'' + r_2V(1 - V - b_2U), \end{cases} \tag{2.26}$$

and by letting $U' = N$ and $V' = W$, the Jacobian of the system ca be obtained

such that:

$$J(U,\ N,\ V,\ W) = \begin{pmatrix} 0 & 1 & 0 & 0 \\ \frac{r_1}{D_1}(-1+2U+b_1V) & -\frac{s}{D_1} & \frac{r_1 b_1 U}{D_1} & 0 \\ 0 & 0 & 0 & 1 \\ \frac{r_2 b_2 V}{D_2} & 0 & \frac{r_2}{D_2}(-1+2V+b_2U) & -\frac{s}{D_2} \end{pmatrix}. \tag{2.27}$$

By evaluating the Jacobian (2.27) at $(n,\ v) = \{(0,\ 0),\ (1,\ 0),\ (0,\ 1)\}$, and finding its corresponding eigenvalues while requiring that they are real, such that oscillations around 0, and hence negative densities, are avoided, the minimum wave speed requirements can be determined and are presented in Table 2.1. On the other hand, the eigenvalues of the Jacobian evaluated at the coexistence steady state do not need to be real, as in this case, oscillations around coexistence would not result in negative densities.

Unstable steady state	$(0,\ 0,\ 0)$	$(1,\ 0,\ 0)$	$(0,\ 1,\ 1)$
Minimum wavespeed	$s_u \geq 2\sqrt{D_1 r_1}$ $s_{v,c} \geq 2\sqrt{D_2 r_2}$	$s \geq 2\sqrt{D_2 r_2(1-b_2)}$	$s \geq 2\sqrt{D_1 r_1(1-b_1)}$

Table 2.1: ***Minimum wavespeed requirement for travelling wavefronts to be admitted as solutions to system (2.24), making the transition from specific unstable steady states.***

Next, with the aid of computational simulations, we show the different wavefront transitions that system (2.24) admits as solutions, including waves moving at different speeds when transitioning from the trivial steady state. In addition, the analytical speed of the wavefronts, as given in Table 2.1, is compared against the speeds obtained from numerical simulations.

Wavefronts transitioning from the trivial steady state $(0,\ 0,\ 0)$

The trivial steady state $(u,\ v,\ c) = (0,\ 0,\ 0)$ is always unstable, meaning that, depending on the interspecific competition rates b_1 and b_2, system (2.24) can transition from the trivial state to any other stable state with speeds given by $s_u \geq 2\sqrt{D_1 r_1}$ and $s_{v,c} \geq 2\sqrt{D_2 r_2}$. Clearly, if $D_1 r_1 = D_2 r_2$, all three wavefronts move at the same speed. However, if $D_1 r_1 \neq D_2 r_2$, wavefront u moves at a different speed compared to wavefronts v and c, which move at the same speed.

Figure 2.8 shows the different wavefronts that can be admitted as solutions to system (2.24), transitioning from the unstable trivial steady state $(u,\ v,\ c) = (0,\ 0,\ 0)$ to the final stable state $(u,\ v,\ c) = \left(\frac{b_1 - 1}{b_1 b_2 - 1},\ \frac{b_2 - 1}{b_1 b_2 - 1},\ \frac{b_2 - 1}{b_1 b_2 - 1}\right)$. In Figure 2.8 a and b, $D_1 r_1 = D_2 r_2$, and the wavefronts move at the same speed $s \approx 0.6$. The difference between the profiles of the wavefronts is caused by the interspecific competition rates, which results in all three wavefronts having the same profile when the two species have the same competitive effect (Figure 2.8 a), and different profiles when one species is more competitive than the other (Figure 2.8 b). In Figure 2.8 c, $D_1 r_1 \neq D_2 r_2$, and species v has a higher diffusivity rate than species u, with $D_1 = 0.5 < D_2 = 1$. In this case, wavefront u moves slower, transitioning from the steady state $(u,\ v,\ c) = (0,\ 1,\ 1)$ to coexistence with speed $s_u \approx 0.3$, while wavefronts v and c first transition from the trivial steady state to $(u,\ v,\ c) = (0,\ 1,\ 1)$ with speed $s \approx 0.4$. Similarly, in Figure 2.8 d, $D_1 r_1 \neq D_2 r_2$, and species u has a higher proliferation rate than species v, with $r_1 = 0.15 > r_2 = 0.1$. This results in species u moving at a higher speed, $s \approx 0.7$, from the trivial steady state to $(u,\ v,\ c) = (1,\ 0,\ 0)$, while species v and the chemical c transition from $(u,\ v,\ c) = (1,\ 0,\ 0)$ to coexistence with speed $s \approx 0.4$.

Figure 2.9 shows a comparison between the numerical and analytical wave speeds corresponding to the transitions seen in Figure 2.8 c and d. In Figure 2.9, parameters are chosen such that $D_1 r_1 \neq D_2 r_2$. In Figure 2.9 a, the diffusivity of species u varies such that $D_1 \in [0.2,\ 1.4]$. When $D_1 < 1$, the system transitions from the trivial state to $(u,\ v,\ c) = (0,\ 1,\ 1)$ to coexistence. In this case, wavefronts v and c move with speed $s_{v,c} = 2\sqrt{D_2 r_2}$, while wavefront u moves with speed $s \geq 2\sqrt{D_1 r_1 (1 - b_1)}$. For $D_1 = 1$, where $D_1 r_1 = D_2 r_2$, both wavefronts move at the same speed $s_{u,v,c} = 2\sqrt{D_1 r_1} = 2\sqrt{D_2 r_2}$. When $D_1 > 1$, the system transitions from the trivial state to $(u,\ v,\ c) = (1,\ 0,\ 0)$, and in this case, wavefront u moves with speed $s = 2\sqrt{D_1 r_1}$, while wavefronts v and c move with speed $s_{v,c} \geq 2\sqrt{D_2 r_2 (1 - b_2)}$. In Figure 2.9 b, the wavefront transitions and minimal speeds work in a similar way. However, in this case, the proliferation rate of the first species varies, such that $r_1 \in [0.05,\ 0.35]$.

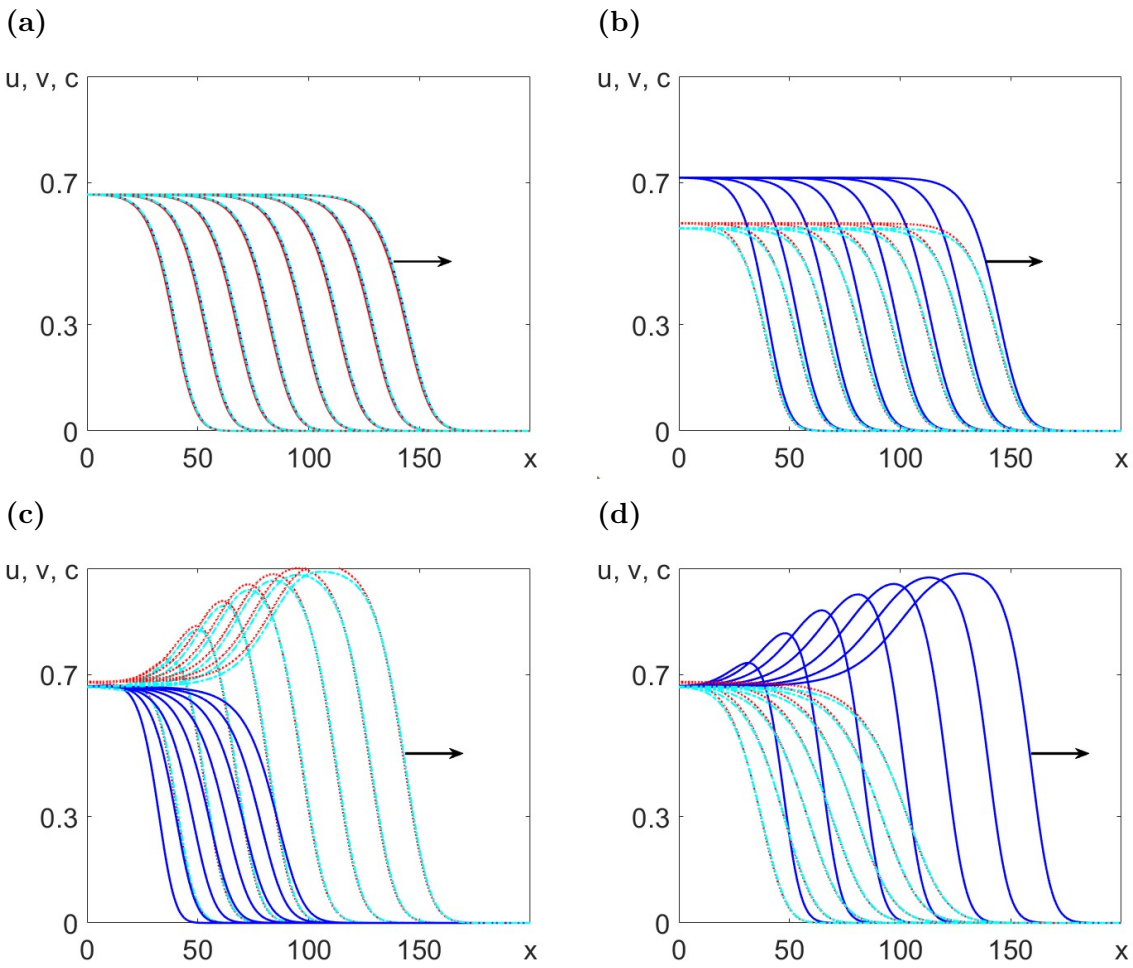

Figure 2.8: ***Travelling wavefront solutions to system (2.24), making the transition from the trivial unstable steady state to the stable coexistence steady state.*** *Solid blue and dash-dotted cyan lines represent the densities of populations u and v, respectively, and dotted red line represents the concentration of the chemical, c.* ***(a)****: $D_1 = D_2 = 1,\ r_1 = r_2 = 0.1,\ b_1 = b_2 = 0.5$;* ***(b)****: $D_1 = D_2 = 1,\ r_1 = r_2 = 0.1,\ b_1 = 0.5,\ b_2 = 0.6$;* ***(c)****: $D_1 = 0.5,\ D_2 = 1,\ r_1 = r_2 = 0.1,\ b_1 = b_2 = 0.5$;* ***(d)****: $D_1 = D_2 = 1,\ r_1 = 0.15,\ r_2 = 0.1,\ b_1 = b_2 = 0.5$. Initial conditions such that $(u,\ v,\ c)(x,\ 0)$ is at coexistence if $x < 20$ and $(u,\ v,\ c)(x,\ 0) = (0,\ 0,\ 0)$ if $x \geq 20$.*

Under appropriate conditions on the interspecific competition rates b_1 and b_2, system (2.24) can also transition from the steady state $(u,\ v,\ c) = (0,\ 0,\ 0)$ to the extinction steady state $(u,\ v,\ c) = (1,\ 0,\ 0)$, if $b_2 > 1$. However, in this case, there is no density of the second species v or the chemical agent c, so only travelling wavefronts corresponding to u are admitted as solutions. Similarly, the system can also transition from the trivial steady state to the other extinction state $(u,\ v,\ c) = (0,\ 1,\ 1)$, if $b_1 > 1$. In this case, there is no density of the first species u, so only wavefronts corresponding to species v and the chemical agent c

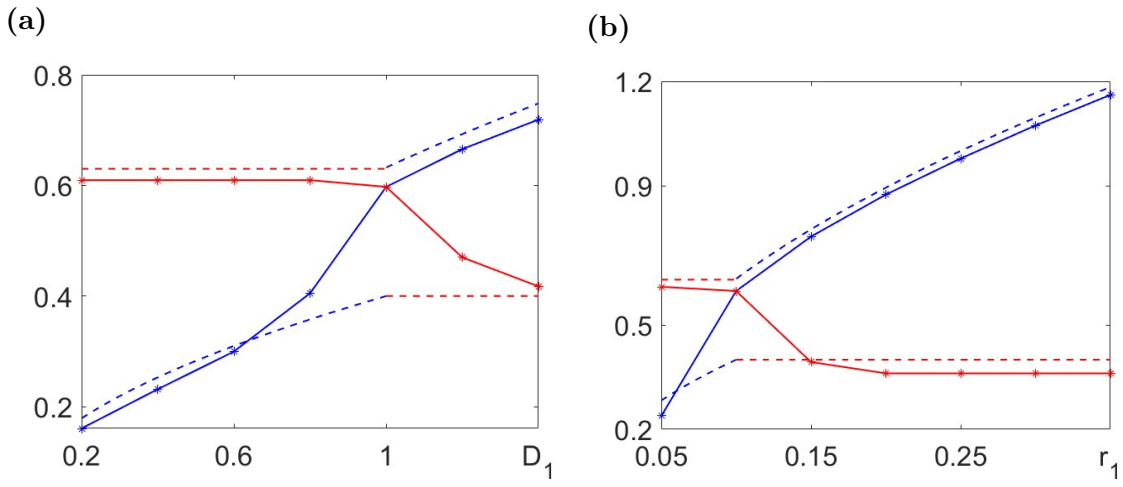

Figure 2.9: ***Comparison between numerical and analytical speeds for wavefronts that transition from*** $(u,\ v,\ c) = (0,\ 0,\ 0)$ ***when*** $D_1 r_1 \neq D_2 r_2$***. Blue and red represent the speeds of wavefronts*** u ***and*** v, c***, respectively, with solid lines representing numerical results and dashed lines analytical results according to Table 2.1. (a):*** $D_1 \in [0.2,\ 1.4]$, $D_2 = 1,\ r_1 = r_2 = 0.1,\ b_1 = b_2 = 0.6$***; (b):*** $D_1 = D_2 = 1,\ r_1 \in [0.05,\ 0.35]$, $r_2 = 0.1,\ b_1 = b_2 = 0.6$.

appear as solutions. Since these wavefronts transition from the origin, the speeds of such wavefronts are $s_u \geq 2\sqrt{D_1 r_1}$ and $s_{v,c} \geq 2\sqrt{D_2 r_2}$.

This section has shown all the possible travelling wavefronts that system (2.24) admits as solutions when transitioning from the trivial steady state $(u,\ v,\ c) = (0,\ 0,\ 0)$, as well as the minimum speed of such wavefronts. An interesting characteristic of these wavefronts is that if $D_1 r_1 \neq D_2 r_2$, the system exhibits waves moving at different speeds. We have shown, both analytically and numerically, how these minimum speeds depend on model parameters. Next, wavefronts transitioning from the extinction steady states are investigated.

Wavefronts transitioning from the extinction steady states

Travelling wave solutions are highly dependent on the interspecific competition rates between the two species considered. When considering system (2.24), it has been shown that coexistence is always stable if $b_1,\ b_2 < 1$. If $b_1 < 1$, then the steady state $(u,\ v,\ c) = (0,\ 1,\ 1)$ is unstable, and similarly, if $b_2 < 1$, the steady state $(u,\ v,\ c) = (1,\ 0,\ 0)$ is unstable. This means that species can transition from one of these extinction steady states to coexistence, with minimum wave speed requirements as given in Table 2.1.

Figure 2.10 graphically illustrates the transition from the extinction steady states to coexistence, aided by numerical simulations. In Figure 2.10 a, since

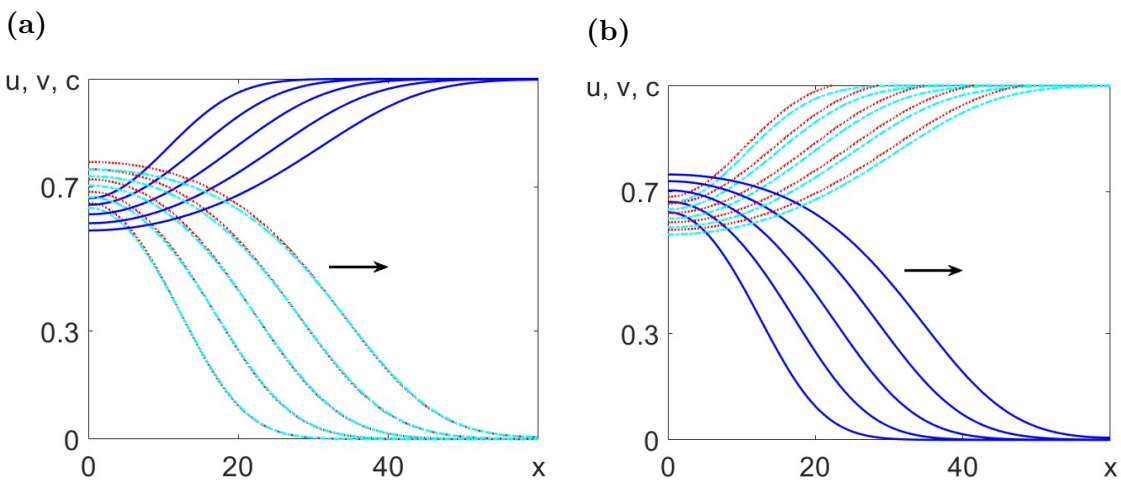

Figure 2.10: ***Travelling wavefront solutions to system (2.24) making the transition from the two extinction steady states to coexistence.*** ***(a)****: System moves from the unstable steady state* $(n,\ v,\ c) = (1,\ 0,\ 0)$ *to coexistence, with competition rates:* $b_1 = 0.6$ *and* $b_2 = 0.4$*. Initially,* $(u,\ v,\ c)(x,\ 0)$ *is at coexistence if* $x < 10$ *and* $(u,\ v,\ c)(x,\ 0) = (1,\ 0,\ 0)$ *if* $x \geq 10$*.* ***(b)****: System moves from the unstable steady state* $(n,\ v,\ c) = (0,\ 1,\ 1)$ *to coexistence, with competition rates:* $b_1 = 0.4$ *and* $b_2 = 0.6$*. Initially,* $(u,\ v,\ c)(x,\ 0)$ *is at coexistence if* $x < 10$ *and* $(u,\ v,\ c)(x,\ 0) = (0,\ 1,\ 1)$ *if* $x \geq 10$*. Solid blue lines represent the density of* n*, while dotted red and dash-dotted cyan lines the concencentration of* c *and* v*, respectively. Fixed parameters:* $D_1 = D_2 = 1,\ r_1 = r_2 = 0.1$*.*

$b_2 < 1$, the steady state $(u,\ v,\ c) = (1,\ 0,\ 0)$ is unstable, and the system moves from this state to the stable coexistence state, with all three wavefronts moving at speed $s = 2\sqrt{D_2 r_2(1 - b_2)}$. Similarly, in Figure 2.10 b, $b_1 < 1$, and the steady state $(u,\ v,\ c) = (0,\ 1,\ 1)$ is unstable. The system once again transitions to the stable coexistence state, with all three wavefronts moving at speed $s = 2\sqrt{D_1 r_1(1 - b_1)}$. Clearly, the speeds of these wavefronts depend significantly on the diffusivity of each species, as well as their reproduction and competition rates. If the reproduction or diffusion rates increase, the minimum wave speed also increases. Conversely, if the competition rate increases, the minimum wave speed decreases.

With the aid of computational simulations, this section has shown the types of wavefronts that can appear as solutions to system (2.24) when the extinction steady states are unstable, and coexistence is stable. In the next section, the opposite case is considered, where $b_1,\ b_2 > 1$, making coexistence unstable and the extinction states stable. The case in which one of the competition rates is greater than one and the other is less than one cannot be considered, as this would result in negative coexistence, and negative densities are not feasible or relevant to our research.

Wavefronts transitioning from the coexistence steady state

Travelling wavefronts admitted as solutions to system (2.24) from the coexistence steady state are less studied, and we believe this to be the most interesting case. As seen from linear analysis, the coexistence steady state $(u,\ v,\ c) = \left(\frac{b_1-1}{b_1b_2-1}, \frac{b_2-1}{b_1b_2-1}, \frac{b_2-1}{b_1b_2-1}\right)$ is stable if $b_1,\ b_2 < 1$ and unstable if at least one of the competition rates is greater than one. If one of the competition rates is positive and the other negative, then at least one of the concentrations $u,\ v,\ c$ would be negative, making the scenario biologically irrelevant. Therefore, the only biologically relevant case is when both competition rates are greater than one, i.e., $b_1,\ b_2 > 1$. In this case, coexistence is unstable, and both extinction states: $(u,\ v,\ c) = (1,\ 0,\ 0)$ and $(u,\ v,\ c) = (0,\ 1,\ 1)$ are stable, meaning travelling wavefronts can transition from coexistence to either state, depending on initial conditions. Figure 2.11 graphically shows the two types of travelling wavefronts with the aid of computational simulations.

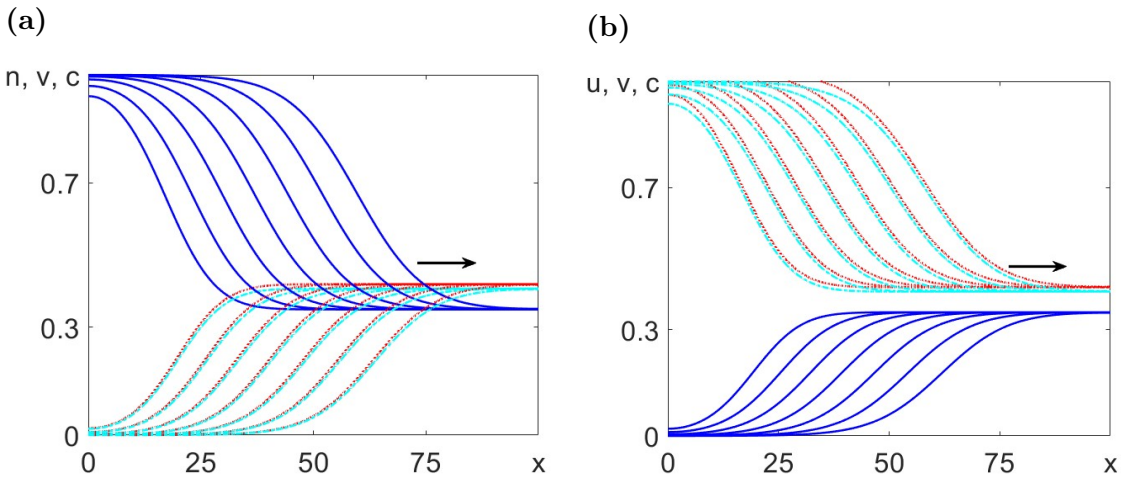

Figure 2.11: ***Travelling wavefront solutions to system (2.24) making the transition from the unstable coexistence state to the two stable extinction steady states.*** ***(a)****: Initial conditions such as:* $(u,\ v,\ c) = (1,\ 0,\ 0)$ *if* $x < 10$ *and coexistence otherwise.* ***(b)****:Initial conditions such as:* $(u,\ v,\ c) = (0,\ 1\ 1)$ *if* $x < 10$ *and coexistence otherwise. Fixed parameters:* $D_1 = D_2 = 1,\ r_1 = r_2 = 0.1,\ b_1 = 1.6,\ b_2 = 1.7$.

Understanding the speed of travelling wavefronts moving from coexistence is more challenging to approach analytically, as oscillations around coexistence do not result in negative concentrations. Therefore, this steady state can behave either as a node or a spiral. In this case, linear analysis is not an effective method for determining the speed of the travelling wavefront, so nonlinear analysis may be more appropriate. Methods of nonlinear analysis, such as the direct tanh

method based on Mimura's work [106], have previously been attempted to describe the speeds of travelling wavefronts moving from coexistence. However, we have identified errors in the expansion of the solution, expressed as a sum of hyperbolic functions [52]. In this work, system (2.24) is reduced to a system of two equations for $(u,\ v)$, as wavefront c closely follows wavefront v at the same speed. The general form of the solution is taken to be:

$$\begin{cases} u(z) = \dfrac{1+u^*}{2} + \dfrac{-1+u^*}{2}\tanh(z), \\ v(z) = \dfrac{v^*}{4}(1+\tanh(z))^2, \end{cases} \tag{2.28}$$

where $(u^*,\ v^*)$ represents the coexistence state and the solution satisfies boundary conditions such that $(u,\ v)(-\infty) = (1,\ 0)$ and $(u,\ v)(\infty) = (u^*,\ v^*) = \left(\dfrac{b_1-1}{b_1b_2-1},\ \dfrac{b_2-1}{b_1b_2-1}\right)$. By substiting this into system (2.26), we get a system of 9 simultaneous equations which need to be solved to find the speed, s. This is an overdetermined system and to overcome this, researchers have solved this type of problem by considering model parameters such as $D,\ r,\ b_1$ as unknowns and they have obtained solutions for this model parameters depending on b_2 [52, 106]. By fixing the errors found in [52], we have not been able to find any exact solutions using (2.28).

Methods of solving for nonlinear partial differential equations most often involve sums of hyperbolic functions [52, 64, 106, 121] such as:

$$\begin{cases} u(z) = \displaystyle\sum_{i=0}^{m} a_i \tanh^i(\beta z), \\ v(z) = \displaystyle\sum_{i=0}^{n} g_i \tanh^i(\beta z), \end{cases} \tag{2.29}$$

where m and n are obtained by balancing the highest order derivative terms with the highest nonlinear terms. In our case, for system (2.26), we get $2m = n+2$ and the most obvious choice is $m = n = 2$. This means that if, for example, we are looking for travelling wavefronts from coexistence to the extinction steady state $(u,\ v) = (0,\ 1)$, we seek solutions of the form:

$$\begin{cases} u(z) = a_0 + a_1\tanh(\beta z) + a_2\tanh^2(\beta z), \\ v(z) = g_0 + g_1\tanh(\beta z) + a_2\tanh^2(\beta z), \end{cases} \tag{2.30}$$

to system:

$$\begin{cases} 0 = D_1u'' + su' + r_1u(1-u-b_1v), \\ 0 = D_2v'' + sv' + r_2v(1-v-b_2u), \end{cases} \tag{2.31}$$

with boundary conditions:

$$\begin{cases} (u,\ v)(-\infty) = (0,\ 1), \\ (u,\ v)(\infty) = \left(\dfrac{b_1 - 1}{b_1 b_2 - 1},\ \dfrac{b_2 - 1}{b_1 b_2 - 1} \right). \end{cases} \tag{2.32}$$

Substituting (2.30) into (2.31) and (2.32) and equating coefficients of powers of tanh to 0, we get a system of 14 simultaneous equations which needs to be solved for 8 unknowns: $a_0,\ a_1,\ a_2,\ g_0,\ g_1,\ g_2,\ s,\ \beta$:

$$\begin{cases} a_0 + a_1 + a_2 - \dfrac{b_1 - 1}{b_1 b_2 - 1} = 0, \\ a_0 - a_1 + a_2 = 0, \\ g_0 - g_1 + g_2 - 1 = 0, \\ g_0 + g_1 + g_2 - \dfrac{b_2 - 1}{b_1 b_2 - 1} = 0, \\ 2D_1 a_2 \beta^2 + s a_1 \beta + r_1 a_0 - r_1 a_0^2 - r_1 b_1 a_0 g_0 = 0, \\ -2D_1 a_1 \beta^2 + 2s a_2 \beta + r_1 a_1 - 2r_1 a_0 a_1 - r_1 b_1 a_0 g_1 - r_1 b_1 a_1 g_0 = 0, \\ -8D_1 a_2 \beta^2 - s a_1 \beta + r_1 a_2 - r_1 a_1^2 - 2r_1 a_0 a_2 - r_1 b_1 a_0 g_2 - r_1 b_1 a_1 g_1 - r_1 b_1 a_2 g_0 = 0, \\ 2D_1 a_1 \beta^2 - 2s a_2 \beta - 2r_1 a_1 a_2 - r_1 b_1 a_1 g_2 - r_1 b_1 a_2 g_1 = 0, \\ 6D_1 a_2 \beta^2 - r_1 a_2^2 - r_1 b_1 a_2 g_2 = 0, \\ 2D_2 g_2 \beta^2 + s g_1 \beta + r_2 g_0 - r_2 g_0^2 - r_2 b_2 a_0 g_0 = 0, \\ -2D_2 g_1 \beta^2 + 2s g_2 \beta + r_2 g_1 - 2r_2 g_0 g_1 - r_2 b_2 a_0 g_1 - r_2 b_2 a_1 g_0 = 0, \\ -8D_2 g_2 \beta^2 - s g_1 \beta + r_2 g_2 - r_2 g_1^2 - 2r_2 g_0 g_2 - r_2 b_2 a_0 g_2 - r_2 b_2 a_1 g_1 - r_2 b_2 a_2 g_0 = 0, \\ 2D_2 g_1 \beta^2 - 2s g_2 \beta - 2r_2 g_1 g_2 - r_2 b_2 a_1 g_2 - r_2 b_2 a_2 g_1 = 0, \\ 6D_2 g_2 \beta^2 - r_2 g_2^2 - r_2 b_2 a_2 g_2 = 0, \end{cases} \tag{2.33}$$

which clearly is an overdetermined system. They only way to solve this is to use Maple and treat model parameters: $D_1,\ D_2,\ r_1,\ r_2,\ b_1$ and b_2 as unknowns in order to have 14 equations for 14 unknowns. The solution obtained:

$$a_0 = a_1 = 4.95,\ a_2 = 0,\ g_0 = 1,\ g_1 = g_2 = 0,\ \beta = 2.85,\ s = 0.61,\ D_1 = D_2 = 0,$$

$$r_1 = -0.35,\ r_2 = 0,\ b_1 = -8.9,\ b_2 = 0,$$

is clearly not satisfactory and biologically relevant for a number of reasons, such as negative model parameters and $b_1,\ b_2 \not> 1$.

A more useful method of finding the speed of the travelling wavefronts moving from coexistence to one of the two extinction steady states is to express the densities of the two bacterial species as:

$$\begin{cases} u \approx u_0 + \alpha_1 \exp(-\beta z), \\ v \approx v_0 + \alpha_2 \exp(-\beta z), \end{cases} \tag{2.34}$$

as $z \longrightarrow \infty$, where $(u_0,\ v_0)$ represents the coexistence state, $\alpha_1,\ \alpha_2$ are the coefficients responsible for amplitude and β is the wavenumber. It is important to investigate the behaviour of the initial data at infinity, as this is crucial for describing the long-time behaviour of the system [67]. Note that wavefront c is assumed to follow closely behind wavefront v, so using $c \approx v$ allows us to reduce a system of three partial differential equations to a system of two partial differential equations for simplicity. Substituting (2.34) into system (2.26) results in a system of two simultaneous equations for four unknowns: $\alpha_1,\ \alpha_2,\ \beta,\ s$:

$$\begin{cases} D_1\alpha_1\beta^2 - s\alpha_1\beta + r_1\alpha_1 - 2r_1u_0\alpha_1 - r_1b_1u_0\alpha_2 - r_1b_1v_0\alpha_1 = 0, \\ D_2\alpha_2\beta_2 - s\alpha_2\beta + r_2\alpha_2 - 2r_2v_0\alpha_2 - r_2b_2u_0\alpha_2 - r_2b_2v_0\alpha_1 = 0. \end{cases} \tag{2.35}$$

Using the second equation of system (2.35), an expression for α_2 in terms of α_1 can be obtained, such as:

$$\alpha_2 = \frac{r_2b_2v_0\alpha_1}{D_2\beta^2 - s\beta + r_2 - 2r_2v_0 - r_2b_2u_0}, \tag{2.36}$$

which can be substituted into the first equation of the system to obtain an implicit equation for s and β:

$$D_1\beta^2 - s\beta + r_1 - 2r_1u_0 - r_1b_1v_0 - \frac{r_1r_2b_1b_2u_0v_0}{D_2\beta^2 - s\beta + r_2 - 2r_2v_0 - r_2b_2u_0} = 0. \tag{2.37}$$

Clearly, equation (2.37) is a quadratic equation for the speed, s, as depending on the wavenumber, β:

$$\begin{aligned} s^2\beta^2 + s(2\beta r_1u_0 + 2\beta r_2v_0 + \beta r_1b_1v_0 + \beta r_2b_2u_0 - D_1\beta^2 - D_2\beta^3 - \beta r_1 - \beta r_2) + (D_1D_2\beta^4 + \\ D_1\beta^2r_2 + D_2\beta^2r_1 - 2D_1\beta^2r_2v_0 - 2D_2\beta^2r_1u_0 - D_1\beta^2r_2b_2u_0 - D_2\beta^2r_1b_1v_0 + r_1r_2 - 2r_1r_2u_0 - \\ 2r_1r_2v_0 - r_1r_2b_2u_0 - r_1r_2b_1v_0 + 4r_1r_2u_0v_0 + 2r_1r_2b_2u_0^2 + 2r_1r_2b_1v_0^2). \end{aligned} \tag{2.38}$$

Solutions to equation (2.38) are difficult to obtain analytically, however we can investigate them graphically by looking at solutions in the positive quadrant since we are looking for wavefronts moving from left to right such that $s \geq 0$. Figure 2.12 shows the dispersion curve for speed as a function of the wavenumber β for fixed model parameters.

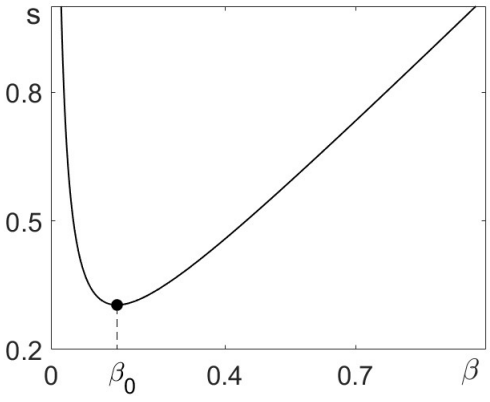

Figure 2.12: ***Dispersion curve*** (2.38) ***for speed as a function of wavenumber for wavefronts transitioning from the unstable coexistence steady state.*** *β_0 represents the minimum of the curve. Fixed model parameters: $D_1 = D_2 = 1$, $r_1 = r_2 = 0.1$ and $b_1 = b_2 = 1.6$.*

From the dispersion curve in Figure 2.12, one can see that the dot represents $s_{min} = 0.3038$ for $\beta_0 = 0.1519$. For $\beta < \beta_0$, the waves move with speed s_{min} and for $\beta > \beta_0$, the speed is given by the dispersion curve. This method has first been introduced for Fisher type equations by McKean [84] and Larson [67] in the 1970's, proved numerically by Manoranjan [81] and adapted by Murray in [86]. This method can be used to analytically obtain the speed of the travelling wavefronts transitioning from coexistence, however it is important to know the magnitude of the wavenumber β and whether $\beta \lessgtr \beta_0$. By using numerical simulations for fixed model parameters: $D_1 = D_2 = 1$, $r_1 = r_2 = 0.1$ and $b_1 = b_2 = 1.6$ and waves transitioning from coexistence to obtain and fit data to an exponential curve, one can show that the densities of the species $(n,\ v)$ at infinity follow the distribution:

$$\begin{cases} u \approx n_0 + 0.0036\exp(-0.024z), \\ v \approx v_0 + 0.0688\exp(-0.024z), \end{cases} \tag{2.39}$$

as $z \longrightarrow \infty$, where clearly $\beta = 0.024 < \beta_0$, meaning that waves move with $s = s_{min}$, as given by the dispersion curve in Figure 2.12. This is a powerful method of obtaining the analytical speeds of travelling wavefronts moving from the unstable coexistence steady state admitted as solutions to system (2.24), irrespective of the stable steady state they are transitioning to. To show that the speeds obtained via this method are in line with speeds obtained from numerical simulations, the effect of model parameters on speed has been investigated and shown in Figure 2.13.

Figure 2.13 shows the effect of model parameters on the speed of the travelling wavefronts when system (2.24) transitions from coexistence. In the numerical simulations, the system transitions to the stable extinction steady state

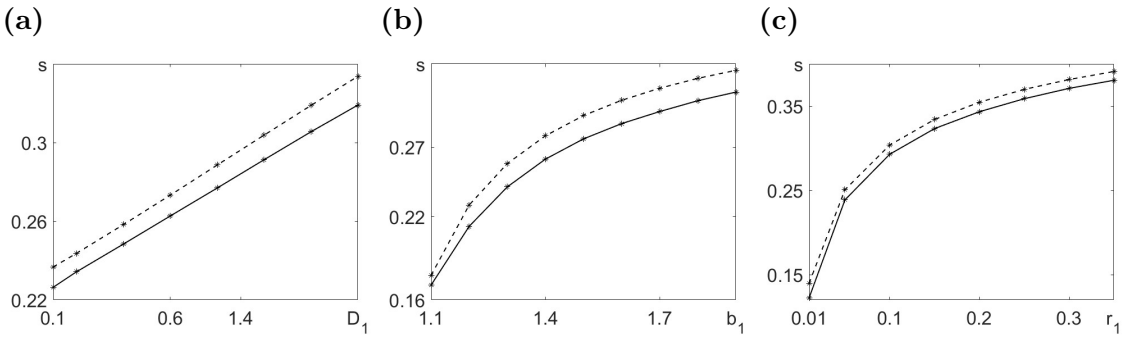

Figure 2.13: ***Speed of travelling wavefronts transitioning from unstable coexistence admitted as solutions to system*** (2.24)***.*** *Numerical speeds (solid lines) are obtained from simulations and analytical speeds (dashed lines) are given by the minimum of the dispersion curve as given by solutions to equation* (2.38)*. Fixed parameters:* $D_1 = D_2 = 1$*,* $r_1 = r_2 = 0.1$ *and* $b_1 = b_2 = 1.6$*.*

$(u,\ v,\ c) = (1,\ 0,\ 0)$. However, the speed of the waves is influenced only by the long-term behaviour of the system at $+\infty$, not by its behaviour at $-\infty$ [67]. The minimum of the dispersion curve given by (2.38) clearly captures the effect of diffusion, competition, and reproduction, with the difference between numerical and analytical speeds being less than 5%, likely due to numerical error. As the diffusion and reproduction rates of the first species increase, the speed of the wavefronts also increases. Similarly, as the competition of the second species, v, on the first species, u, increases, the speed also increases. Changing the parameters corresponding to species v: D_2, b_2, and r_2, has the same effects on the speeds of the travelling wavefronts as altering D_1, b_1, and r_1.

This section has focused on illustrating the different types of travelling wavefronts that can arise as solutions in a system of two bacterial species and a chemical, which behaves similarly to the Lotka-Volterra competition model, as the chemical does not affect the spatial distribution of the bacterial species. The speed of the fronts has been determined through both analytical methods and computational simulations, allowing us to analytically calculate the speed of the travelling wavefronts when the system transitions from the unstable coexistence steady state. In the next section, we will consider the chemotactic effect of the chemical produced by the second species on the first species, and we will investigate the existence and speed of the resulting travelling wavefronts.

2.2.2 Travelling waves in a two species system with chemotaxis

In this section, the chemical agent c produced by species v in system (2.24) is considered to have a chemotactic effect on the spatial distribution of species u.

We consider this to be of high biological relevance, as it investigates a slightly modified Lotka-Volterra competition model in which two species compete for resources, but only one of them produces a chemical agent that affects the density of the other species. It is important to understand whether chemotaxis impacts species survival or wave speed, and its effects on colonisation. Chemotaxis is mathematically modelled by the introduction of an advection term, such that system (2.24) becomes:

$$\begin{cases} \dfrac{\partial u}{\partial t} = D_1 \dfrac{\partial^2 u}{\partial x^2} - \chi \dfrac{\partial}{\partial x}\left(u \dfrac{\partial c}{\partial x}\right) + r_1 u(1 - u - b_1 v), \\ \dfrac{\partial v}{\partial t} = D_2 \dfrac{\partial^2 v}{\partial x^2} + r_2 v(1 - v - b_2 u), \\ \dfrac{\partial c}{\partial t} = \dfrac{\partial^2 c}{\partial x^2} + v - c, \end{cases} \tag{2.40}$$

where χ represents the chemotactic strength of c on u and its sign whether its chemoattraction (χ positivie) or chemorepulsion (χ negative). Clearly, this system has the same steady states as system (2.24):

$$(u,\ v,\ c) = \left\{ (0,\ 0,\ 0),\ (1,\ 0,\ 0),\ (0,\ 1,\ 1),\ \left(\frac{b_1 - 1}{b_1 b_2 - 1},\ \frac{b_2 - 1}{b_1 b_2 - 1},\ \frac{b_2 - 1}{b_1 b_2 - 1} \right) \right\}, \tag{2.41}$$

with stabilities as shown in Figure 2.7. The aim of this section is to understand the types of travelling wavefronts admitted as solutions to system (2.40) and how chemotaxis affects the wave speed of such fronts. It has been shown in the previous section that, under specific conditions, all four steady states of system (2.24) can be unstable, and travelling wavefronts can emerge to make the transition from any unstable steady state to a stable one. In addition, using methods of linear analysis, the minimum travelling wave speed has been obtained, and these analytical results have been compared against numerical wave speeds obtained through computational simulations.

One of the most interesting features of travelling wavefronts in a system of two species is the appearance of wavefronts moving at different speeds when the system transitions from the unstable trivial steady state and $D_1 r_1 \neq D_2 r_2$. It has been shown that if $D_1 r_1 > D_2 r_2$, the system transitions from the steady state $(u,\ v,\ c) = (0,\ 0,\ 0)$ to the steady state $(u,\ v,\ c) = (1,\ 0,\ 0)$ to coexistence. In this case, wavefront u moves with speed $s_{min,u} = 2\sqrt{D_1 r_1}$, and wavefronts v and c move with speed $s_{min,v,c} = 2\sqrt{D_2 r_2 (1 - b_2)}$. Similarly, when $D_2 r_2 > D_1 r_1$, the system transitions from the steady state $(u,\ v,\ c) = (0,\ 0,\ 0)$ to the steady state $(u,\ v,\ c) = (0,\ 1,\ 1)$ to coexistence. In this case, wavefront u moves with speed $s_{min,u} = 2\sqrt{D_1 r_1 (1 - b_1)}$, and wavefronts v and c move with speed $s_{min,v,c} =$

$2\sqrt{D_2 r_2}$. In this section, with the aid of computational simulations, we study the long-time behaviour of such wavefronts and show that, due to chemotaxis, all three wavefronts eventually move at the same speed.

One of the simplest travelling wavefronts that can be admitted as a solution to system (2.24) is a wavefront making the transition from the trivial steady state to coexistence, moving at the same speed when $D_1 r_1 = D_2 r_2$. In this case, it is important to understand how chemotaxis affects both the formation of the wavefronts and their speed. Using computational simulations, Figure 2.14 shows the effects of chemorepulsion (Figure 2.14 (a)) and chemoattraction (Figure 2.14 (b)) on the shape and speed of the travelling wavefronts.

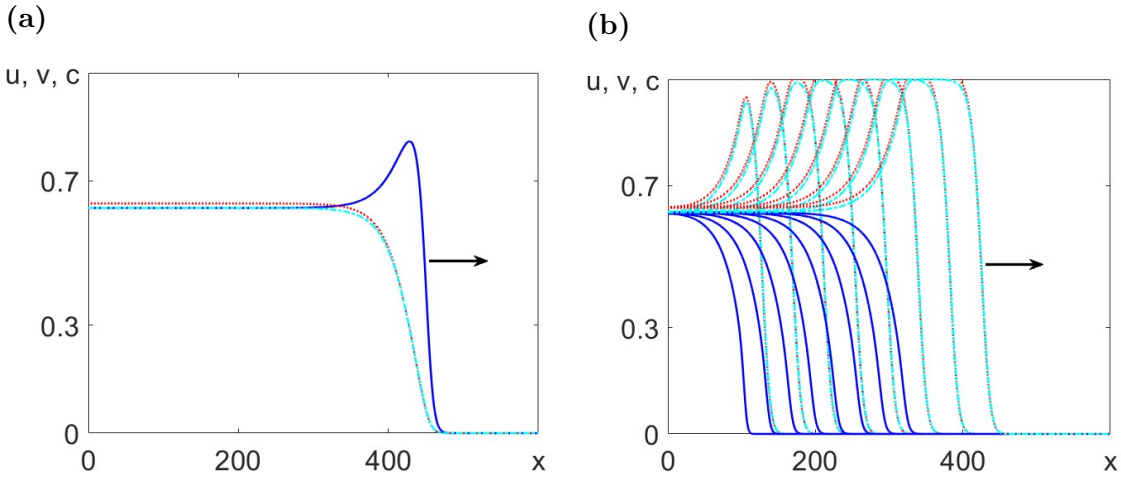

Figure 2.14: ***Travelling wavefront solutions to system (2.40) making the transition from the trivial steady state to coexistence.*** ***(a)****: System moves from the trivial steady state to coexistence, in the case of chemorepulsion,* $\chi = -5$. ***(b)****: System moves from the trivial steady state to* $(u,\ v,\ c) = (0,\ 1,\ 1)$ *to coexistence, in the case of chemoattraction,* $\chi = 20$. *Solid blue line represents the density of* u *and dotted red and dash-dotted cyan lines represent the concentration of* c *and* v*, respectively. Fixed parameters:* $D_1 = D_2 = 1$, $r_1 = r_2 = 0.1$, $b_1 = b_2 = 0.6$. *Initial conditions such as:* $(u,\ v,\ c)(x,\ 0)$ *is at coexistence if* $x < 100$ *and* $(u,\ v,\ c)(x,\ 0) = (0,\ 0,\ 0)$ *if* $x \geq 100$.

Figure 2.14 shows the effects of chemotaxis on the speed and shape of the travelling wavefronts admitted as solutions to system (2.40) for fixed parameters: $D_1 = D_2 = 1$, $r_1 = r_2 = 0.1$, and $b_1 = b_2 = 0.6$. Since in this case $D_1 r_1 = D_2 r_2$, in the absence of chemotaxis ($\chi = 0$), the system transitions from $(u,\ v,\ c) = (0,\ 0,\ 0)$ to coexistence, with the wavefronts moving at the same speed $s_{min} = 2\sqrt{D_1 r_1} = 2\sqrt{D_2 r_2}$. This also holds for the case of chemorepulsion, as seen in Figure 2.14 a. However, in the case of chemoattraction, Figure 2.14 b, the system transitions from the trivial steady state to $(u,\ v,\ c) = (0,\ 1,\ 1)$, and then to coexistence. In this case, initially, the wavefronts move at different

speeds, as shown in Figure 2.8, where the chemical agent has no effect on the two species. However, due to the chemotactic effect of c on n, in the long run, the wavefronts will move at the same speed as the leading wavefront. It is important to understand the time-dependent behaviour of the wavefront speeds, as well as how the distance between them changes over time. This has been investigated with the aid of computational simulations for fixed parameters, and the results are presented in Figure 2.15.

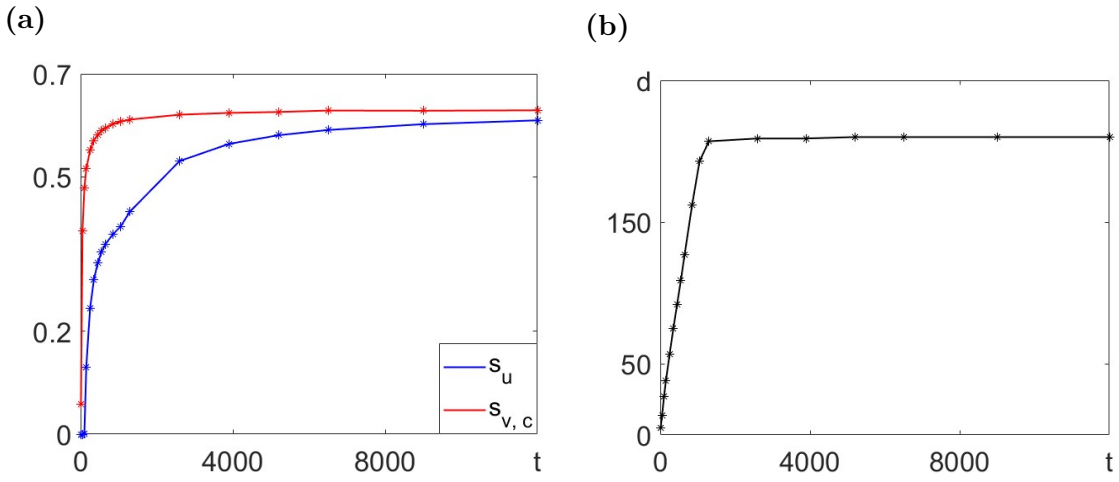

Figure 2.15: ***Effect of chemotaxis on the wavespeed of the wavefronts admitted as solution to system*** (2.40) ***and the distance between the two species.*** ***(a)****: The long-time behaviour of the speed of wavefronts due to chemoattraction.* ***(b)****: The effect of chemoattraction on the distance between the species as time increases, represented by* d*. Fixed parameters:* $D_1 = D_2 = 1,\ r_1 = r_2 = 0.1,\ b_1 = b_2 = 0.6$ *and* $\chi = 20$.

Figure 2.15 examines the effect of chemoattraction on the speed of the wavefronts and the distance between the two species as time $t \longrightarrow \infty$. As seen in Figure 2.14 b, when the steady state $(u,\ v,\ c) = (0,\ 0,\ 0)$ is unstable and coexistence is stable, system (2.40) transitions from the unstable trivial steady state to $(u,\ v,\ c) = (0,\ 1,\ 1)$ and then to coexistence. In the absence of chemotaxis, wavefronts v and c move with a speed $s_{min,v,c} \geq 2\sqrt{D_2 r_2}$, while wavefront u moves with a speed $s_{min,u} \geq 2\sqrt{D_1 r_1(1-b_1)}$. However, in the presence of chemotaxis, as shown in Figure 2.15 a, the speed of wavefront u increases over time, and eventually, all wavefronts move at the same speed, $s_{min} \geq 2\sqrt{D_2 r_2}$. Additionally, Figure 2.15 b, shows that initially, as time increases, the distance between the two species increases rapidly, as wavefront v travels significantly faster than wavefront u. However, in the long run, the distance between the two wavefronts converges to approximately $d \approx 210$, due to the wavefronts eventually moving at the same speed as $t \longrightarrow \infty$. Similarly, in the case of chemorepulsion, as seen in Figure 2.14

a, the speed of wavefront v also increases over time, until all wavefronts move with speed $s_{min} \geq 2\sqrt{D_1 r_1}$. This indicates that the long-time behaviour of the wavefronts is influenced by chemotaxis, such that as time tends to infinity, both species, as well as the chemical agent, move at the speed of the leading wavefront. However, it is important to note that the speed of the leading wavefront is not affected by the chemotactic strength of the chemical agent.

In the absence of chemotaxis, system (2.24) also allows transitions from the two extinction steady states $(u,\ v,\ c) = (1,\ 0,\ 0),\ (0,\ 1,\ 1)$, and in these cases, the wavefronts transition at the same speed, as given by the analytical expressions obtained in the previous section. In the presence of chemotaxis, our numerical analysis has shown that chemotaxis does not affect the speed of the travelling wavefronts, and it remains the same as when the chemical agent has no effect on the spatial distribution of species u. This means that regardless of the chemotaxis strength, the wavefronts move at the speeds given in Table 2.1.

On the other hand, if $b_1,\ b_2 > 1$, coexistence becomes unstable, and in this case, chemotaxis impacts the speed of the travelling wavefronts that make the transition from the unstable coexistence state to one of the stable extinction states in system (2.40). To analytically find conditions for the wavefront speed, we seek travelling wavefront solutions to the system:

$$\begin{cases} 0 = D_1 u'' + s u' - \chi(u'c' + uc'') + r_1 u(1 - u - b_1 v), \\ 0 = D_2 v'' + s v' + r_2 v(1 - v - b_2 u), \\ 0 = c'' + s c' + v - c. \end{cases} \tag{2.42}$$

The difficulty in solving this nonlinear system of three simultaneous partial differential equations, leads us to making the simplification that $v \approx c$ if $D_2,\ r_2 << 1$, as shown in the first section of this chapter. This allows us to work with the simplified system:

$$\begin{cases} 0 = D_1 u'' + s u' - \chi(u'v' + uv'') + r_1 u(1 - u - b_1 v), \\ 0 = D_2 v'' + s v' + r_2 v(1 - v - b_2 u), \end{cases} \tag{2.43}$$

for which we seek solutions of the form (2.34), as in the no chemotaxis case. By substituting (2.34) into (2.43) and solving the set of two simultaneous equations, one can obtain the dispersion curve for speed and the wavenumber β:

$$D_1\beta^2 - s\beta + r_1 - 2r_1u_0 - r_1b_1v_0 - \frac{r_1r_2b_1b_2u_0v_0}{D_2\beta^2 - s\beta + r_2 - 2r_2v_0 - r_2b_2u_0} - \frac{\chi\beta^2u_0v_0r_2b_2}{D_2\beta^2 - s\beta + r_2 - 2r_2v_0 - r_2b_2u_0} = 0. \tag{2.44}$$

Clearly, an analytical expression for speed as a function of the wavenumber is difficult to obtain, however solutions can be investigated graphically by plotting equation (2.44) in the positive quadrant and looking for its minimum point, as seen in Figure 2.16 a.

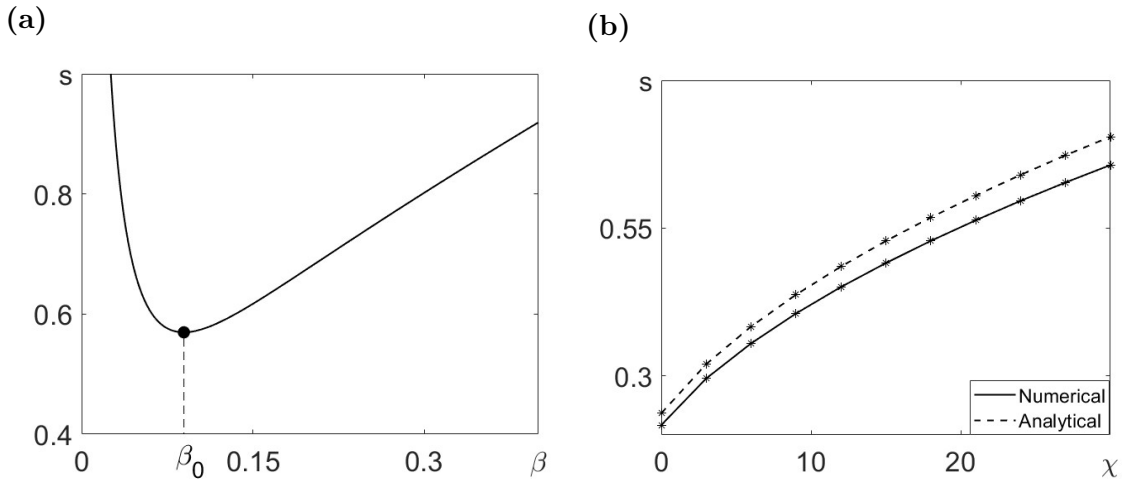

Figure 2.16: ***Use of dispersion curve*** (2.44) ***to investigate the effects of chemotaxis in a system of two species transitioning from the unstable coexistence steady state. (a)****: The dispersion curve of system* (2.43) *representing speed as function of the wavenumber for fixed chemotaxis strength* $\chi = 15$. ***(b)****: The effect of chemoattraction on the speed of the travelling wavefronts when coexistence is unstable. Fixed parameters:* $D_1 = 1,\ D_2 = 0.1,\ r_1 = r_2 = 0.1,\ b_1 = b_2 = 1.6$.

It has been discussed in the case of no chemotaxis that if the wavenumber β is smaller than β_0, then wavefronts travel at the minimum speed as given by the dispersion curve (2.44) in Figure 2.16 a. By fixing model parameters such that $D_1 = 1,\ D_2 = 0.1,\ r_1 = r_2 = 0.1,\ b_1 = b_2 = 1.6$, and $\chi = 15$, numerical simulations have been used to find the wavenumber β for travelling wavefront solutions to system (2.42). By fitting numerical data to an exponential curve, it can be seen that the two species, u and v, and the chemical c follow the distributions:

$$\begin{cases} u \approx 0.0007 \exp(-0.014z), \\ v \approx 0.0006 \exp(-0.018z), \\ c \approx 0.0005 \exp(-0.018z), \end{cases} \tag{2.45}$$

as $z \longrightarrow \infty$. Since $\beta_0 = 0.089$, it can be seen that $\beta < \beta_0$, which means that the travelling wavefronts transition with speed $s = s_{min}$, as given by (2.44). The next step in verifying the accuracy of the method is to compare the analytical speeds, provided by the minimum of the dispersion curve, against the speeds obtained

from numerical simulations for different chemoattraction strengths. A graphical comparison of the results is presented in Figure 2.16 b. Clearly, chemotaxis has a significant impact on the speed of the wavefronts, and as the strength of chemoattraction increases, the wave speed also increases. This means that the two competing species and the chemical travel across the medium significantly faster when the chemotactic effect of the chemical is stronger. This shows that using the dispersion curve is a powerful method for obtaining the speed of wavefronts in a nonlinear system of PDEs.

In conclusion, our investigation into the effects of chemotaxis in a two-species system transitioning from either the trivial state or one of the unstable extinction states has shown that chemotaxis does not affect the speed of the leading wavefront, and due to chemotaxis, all wavefronts move at the same speed as time tends to infinity. Additionally, the distance between the two species stabilises after a certain time point. On the other hand, we have shown that the speed of the travelling wavefronts transitioning from the unstable coexistence steady state is highly impacted by the strength of chemoattraction. Moreover, we have obtained the dispersion curve for such a system and demonstrated that it can successfully predict the minimum wave speed of the two bacterial species, as well as the chemical, as they travel across the medium.

Discussion

In this chapter, we study a particular class of partial differential equations that exhibit the formation of travelling wavefronts in reaction-diffusion systems, as well as reaction-diffusion-advection systems. In the first section, we consider the case of one bacterial species producing a chemical agent, both in the absence and presence of chemotaxis. In the second section, we explore two bacterial species, one of which produces a chemical agent that may or may not affect the spatial distribution of the other species. In both sections, to address the complexity of solving nonlinear partial differential equations, we employ various analytical and numerical methods to demonstrate the existence of travelling wavefronts and determine their minimum wave speeds.

The simplest case involves one bacterial species producing a chemical that does not affect the spatial distribution of the bacteria. In this scenario, the bacteria's kinetics follow logistic growth, resembling the Fisher-Kolmogorov equation [33, 62], with the chemical agent following closely behind. This is mathematically represented by a system of two decoupled partial differential equations, where both travel across the medium with speed $s \geq 2\sqrt{Dr}$. Since both model parameters, diffusion and reproduction, influence the speed of the wavefronts,

we have also investigated their effects on the shape of the wavefront. It has been shown that increasing diffusion makes the wavefront corresponding to the bacterial species smoother, while increasing reproduction makes it sharper.

The more interesting case in the one-species model arises when the chemotactic agent affects the distribution of the bacterial species, with chemotaxis being introduced via an advection term in the system of PDEs. Numerical computations have shown that travelling wavefronts exist whether the chemical agent acts as an attractant or a repellent. Investigating the effects of chemotaxis on the speed of the front is crucial to understanding the dynamics of such a system. Under the assumption that both diffusion and reproduction are very small, $D,\ r << 1$, we have derived a formula for the minimum wave speed that depends on all three model parameters: diffusion, reproduction, and chemorepulsion. These analytical speeds have been compared against those from numerical simulations, showing a strong correlation between the two methods.

In the second section of this chapter, a two-species model is considered in which one of the species produces a chemical agent, and both species compete for resources following Lotka-Volterra kinetics [76, 135]. The mathematical model corresponding to this scenario consists of three partial differential equations and has four steady states. It has been shown that, under specific conditions, all steady states can be unstable, and the system admits travelling wavefronts that transition from any unstable steady state to a stable one. One important characteristic of waves transitioning from the unstable trivial steady state is that, depending on model parameters, wavefronts can move at different speeds if $D_1 r_1 \neq D_2 r_2$. Conditions for the minimum wave speed of fronts transitioning from the unstable trivial steady state or any of the unstable extinction states have been obtained through linear analysis, requiring that the steady state is an unstable node rather than a spiral, to avoid negative species densities, which are biologically irrelevant.

Another novel result in this section is that if both competition rates, $b_1,\ b_2 > 1$, then the coexistence steady state is unstable, and the system can transition from coexistence to one of the stable extinction states. In this case, the dispersal curve of the system provides valuable information about the minimum wave speed, which strongly correlates with results from numerical simulations. In the two-species system with chemotaxis, it has been shown that, due to attraction or repulsion, the long-time behaviour of travelling wavefronts transitioning from the trivial steady state or one of the extinction states is such that they all move at the same speed as the leading wavefront, and the distance between the two species stabilises after a specific time point. While chemotaxis does not greatly impact the speed of the leading wavefront, it does cause both species, as well as

the chemical, to move at the same speed in the long run, as time tends to infinity. More interestingly, in the case of wavefronts transitioning from the unstable coexistence state to one of the stable extinction states, it has been shown that chemoattraction significantly increases the wave speed of the fronts. By examining the dispersion curve of the system when D_2, $r_2 << 1$, such that $v \approx c$, we have been able to analytically describe the increase in speed with increasing chemotaxis strength. It has also been shown that this is in accordance with the wave speeds obtained from numerical simulations.

In conclusion, the aim of this chapter was to thoroughly investigate the existence of travelling wavefronts in a system of one or two interacting bacterial populations and to understand how their speed is affected by model parameters, particularly how chemotaxis influences the dynamics of the system. This is of high biological relevance, as it helps understand how quickly bacteria and chemicals can spread across a medium and sheds light on the early stages of colonisation in species competing for resources.

Chapter 3

Modelling pattern formation in a single species system

Biological pattern formation is one of the most fascinating phenomena in nature. The simplest examples of such patterns are travelling waves and stationary periodic patterns, which emerge during various biological processes, including morphogenesis and population dynamics. The formation of these patterns in populations of motile microorganisms, such as *Dictyostelium discoideum* and *E. coli*, has been demonstrated in numerous experimental studies.

The conditions under which various types of patterns form are typically explored in mathematical studies of dynamical systems that include diffusive and advection terms. In this work, we perform a mathematical study of spatio-temporal patterns arising in a growing population of chemotactically active bacteria. Specifically, we use linear analysis to determine the conditions for the formation of stationary periodic patterns and nonlinear (Fourier) analysis to identify key characteristics, such as the amplitude and wavelength of these patterns.

The novel contributions of this chapter centre around approximating the most unstable wavelength in a reaction-diffusion-advection system. In particular, we demonstrate that using an implicit equation to identify the largest positive eigenvalue of the characteristic matrix is a significantly more effective method for determining the most unstable mode compared to classical linear analysis. This is especially evident when studying the effects of reproduction, where the results from the two approaches are qualitatively different. Additionally, we show that Fourier analysis is a more effective method for estimating the amplitude of Turing patterns, as it is both simpler and computationally more efficient compared to other approaches in the literature.

The methods employed in this chapter to study pattern formation and its characteristics have previously been introduced for reaction-diffusion and activator-inhibitor systems. However, we address gaps in the literature by extending these

methods to reaction-diffusion-advection systems, which are less commonly studied than other classical systems. Throughout the chapter, we validate our analytical results through numerical simulations.

3.1 Introduction

Pattern formation is a widely observed phenomenon in nature and is one of the key outcomes of biological self-organization. It manifests in well-known patterns, such as animal markings, and processes like embryogenesis. Growing bacterial communities form patterns that significantly impact biofilm formation [56]. Non-biological examples include the formation of dunes in deserts [**?**], temperature hot spots in autocatalytic chemical systems [41] and various other processes in physical [116], chemical [146] and social [96] systems.

The most representative examples of spatio-temporal patterns are travelling waves and stationary periodic patterns. The formation of travelling waves in biological populations has been studied for many decades using the Kolmogorov-Fisher equation [33, 62] and its modifications [1, 32]. A key future of these models is the inclusion of an advection term, which accounts for the directional motion of biological species in response to chemical signals (chemotaxis) [11, 37, 49, 58, 137]. Studies of the mechanism for stationary periodic pattern formation in chemical and biological systems have been launched by Alan Turing in his fundamental work [128]. Turing considered a system of differential equations that describe the dynamics of two interacting substances, or morphogens. Typically, in a well-mixed system (or in the absence of diffusion), the system maintains a stable homogeneous solution. However, for certain types of interactions between the morphogens, specifically in what is known as an "activator-inhibitor" system, the homogeneous state becomes unstable when the diffusion rate of one morphogen (the inhibitor) is significantly higher than that of the other (the activator). In this scenario, non-homogeneous patterns, such as stripes or spots, emerge [17, 59, 39]. This pattern formation mechanism has been termed "diffusion driven instability" and, in the context of activator-inhibitor systems, is often described as "local self-enhancement and long-range inhibition" [39, 144].

Stationary periodic patterns are frequently observed in populations of chemotactically active microorganisms, which tend to aggregate and form regularly spaced clusters. Chemotactic activity refers to the movement of microorganisms either along or against chemical gradients, which may be produced externally or by the microorganisms themselves. Numerous theoretical studies have investigated the mechanisms underlying pattern formation in growing populations of such microorganisms, including bacteria and amoebae [59, 46]. The general form

of these models is given as

$$\begin{cases} \dfrac{\partial n}{\partial t} = D_n \nabla^2 n - \nabla \left(\chi(n,c) \nabla c \right) + f(n,c), \\ \dfrac{\partial c}{\partial t} = D_c \nabla^2 c + g(n,c), \end{cases} \tag{3.1}$$

where the variable n represents the density of microorganisms, while the variable c denotes the concentration of the chemotactic agent. The parameter D_n is the diffusion coefficient describing the random motion of cells, and D_c - the diffusion constant of the chemotactic agent. The function $\chi(n,c)$ describes the chemotactic response of the microorganisms, while the functions $f(n,c)$ and $g(n,c)$ represent the microbial and chemical kinetics, respectively.

If $\chi(n,c) = 0$ (indicating no chemotaxis) the system (3.1) reduces to a reaction-diffusion model similar to the classical Lotka-Volterra model (as presented in Chapters 1 and 2 of [87]). However, if $\chi(n,c) \neq 0$ an advection term appears in the first equation transforming the system (3.1) into a reaction-diffusion-advection model. Furthermore, if $f(n,c) = 0$, the system simplifies to the well-known Keller-Segel model [59]. The Keller-Segel model, introduced in 1970, was designed to describe the aggregation of *Dictyosteium discoideum* amoebae, mediated by a chemotactic agent (cAMP, known at the time as acrasin) produced by the amoebae themselves [59]. The original model consisted of four equations, but by applying the quasi-steady-state assumption (i.e. replacing 'fast' differential equations with algebraic relationships) it was reduced to a system of two reaction-diffusion-advection equations. The analysis conducted on the simplest version of the model, where the following assumptions were made: (a) the the chemotactic sensitivity is constant ($\chi(n,c) = \chi_0$), (b) the amoebae do not die or reproduce, ($f(n,c) = 0$), and (c) the chemical agent is produced by the amoebae and degrades at a constant rate, $g(n,c) = hn - pc$, where h represents the production rate per amoeba, and p is the degradation rate. Under these assumptions, the model (3.1) is represented by the following system:

$$\begin{cases} \dfrac{\partial n}{\partial t} = D \nabla^2 n - \chi_0 \nabla^2 c, \\ \dfrac{\partial c}{\partial t} = \nabla^2 c + hn - pc, \end{cases}$$

where $D = D_n / D_c$ is the ratio of the diffusion constants of the amoebae and the chemical, and the spatial variable is rescaled so that the diffusion of the chemical c is normalised to one. In the absence of chemotaxis ($\chi_0 = 0$) the system evolves towards the stable steady state $(n,c) = (n_0, c_0)$, which is determined by the initial amount of amoebae, where n_0 represents the average initial density of the

amoebae and $c_0 = n_0 * h/p$. It was shown in [59] that in the presence of chemotaxis the homogeneous state (n_0, c_0) becomes unstable if

$$\frac{\chi_0 p}{Dh} + \frac{n_0 h}{p} > 1.$$

This condition implies that an increase in the chemotactic activity χ disrupts the stability of the homogeneous state, causing the amoebae to aggregate into clusters and form stationary periodic patterns. Since the instability in this system arises from spatial coupling, though due to the advection rather than the diffusion term, it has been suggested to consider such a system as a Turing system [90], where Turing instability - a term broader than diffusion-driven instability - occurs.

An assumption made in [59] that the chemotactic response is independent of both the density of cells and the concentration of the chemotactic agent (i.e., $\chi(n, c) = \chi_0$), simplifies the mathematical analysis but leads to unbounded solutions. It is more reasonable to assume that the chemotactic response is proportional to the density of cells and that it decreases with increasing concentration of the chemotactic agent [77]. Several modifications of the Keller-Segel model, incorporating different forms of the chemotactic term and/or variations in bacterial and chemical kinetics, have been explored by researchers, with some listed in [46]. Notably, models describing patterns in growing *E. coli* colonies [6, 97]have been developed, as E. coli is another species exhibiting chemotactic activity. One such model, known as the 'liquid model,' is designed to reproduce patterns formed by bacteria in a liquid environment [130]. This model, similar to the Keller-Segel model, is represented by a variant of the system (3.1). In this model cell death and proliferation is again neglected ($f(n, c) = 0$) and the chemotactic sensitivity is given by $\chi(n, c) = \chi_0 \frac{n}{1 + c^2}$, meaning it is proportional to the cell density and decreases with the concentration of the chemotactic agent. While the decay of the chemical is neglected, its production is modelled using the Hill function $g(n, c) = \omega \frac{n^2}{\nu + n^2}$. Analysis of this model in [130] showed that for sufficiently large χ_0, the homogeneous state becomes unstable, leading to the formation of periodic patterns. However, these patterns were found to be non-stationary, with their spatial periodicity changing over time. Subsequent research demonstrated the formation of stationary periodic patterns within larger systems of differential equations modeling E. coli populations [6, 75, 97]. Conversely, other models of the type (3.1) have shown non-stationary patterns resulting from Turing instability [147, 105].

While the mechanisms and conditions for periodic pattern formation have been extensively studied [128, 59, 86], the properties of these patterns, such as wavelength and amplitude, have been explored to a lesser extent. The estimation of the wavelength of patterns is typically based on linear stability analysis and

is often given by the wave number of the most unstable mode (see Chapter 2 of [87]). The amplitude of periodic patterns is generally estimated through weakly nonlinear analysis. In this approach, the solution of (3.1) is approximated in the form:

$$\begin{cases} n(x,t) = n_0 + \alpha(\epsilon,t)\cos(kx), \\ c(x,t) = c_0 + \beta(\epsilon,t)\cos(kx), \end{cases} \tag{3.2}$$

where the point (n_0, c_0) represents the homogeneous steady state of the system. k is the wave number of the first unstable mode which occurs after a Turing bifurcation and is found through linear stability analysis. $\alpha(\epsilon,t)$ and $\beta(\epsilon,t)$ represent the amplitudes of n- and c-profiles in the emerging periodic pattern. The parameter ϵ indicates the distance from the bifurcation point; for instance, if the homogeneous state becomes unstable when $\chi_0 = \chi^*$, then $\epsilon = \chi_0 - \chi^*$. ϵ should be small enough so that there is only one unstable mode as it appears in the equation (3.2). The amplitude equation is a differential equation for $\alpha(\epsilon,t)$ (or $\beta(\epsilon,t)$), i.e. $\dot{a} = F(\epsilon,a)$, which should be derived for a system under consideration.

For the linear system, $\dot{a} \approx \lambda a$, where λ is the largest eigenvalue of the system, which for an unstable mode leads to infinite growth in the amplitude of the pattern. In the vicinity of the Turing bifurcation, the amplitude equation gives a slow evolution along the centre manifold, $\dot{a} \approx \epsilon a$. In the case of a nonlinear system the amplitude equation also becomes nonlinear:

$$\frac{da}{dt} = \epsilon a h(\epsilon,a).$$

First- and second-order approximations of the function $h(\epsilon,a)$ (under the assumption that $\epsilon \ll 1$) has been found for a set of nonlinear systems and boundary conditions [30, 137, 142]. It has been shown that the amplitude equation, derived for the model with no flux boundary condition, has a cubic (rather than quadratic) nonlinearity: $h(\epsilon,a) = h'_\epsilon \epsilon + 0.5 h''_{aa} a^2$, which points to a supercritical pitchfork bifurcation associated with Turing instability [30, 142]. In this case, the loss of stability of homogeneous state is accompanied by the formation of two stable stationary periodic patterns of opposite phase and equal amplitude:

$$a = \left| \frac{2h'_\epsilon}{h''_{aa}} \right| \sqrt{\epsilon}. \tag{3.3}$$

Derivation of the function $h(\epsilon,a)$ for systems of differential equations (such as (3.1)) is associated with tedious algebra and any technique that reduces the time and effort required to address the problem would be greatly appreciated. Most recently, an alternative approach to estimate the amplitude of Turing patterns, forming in a class of two-variable reaction-diffusion models with kinetics terms given by polynomial functions, was presented in [19]. The amplitude was also

estimated based of weakly nonlinear analysis, but by setting the amplitudes $\alpha(\epsilon t)$ and $\beta(\epsilon t)$ in (3.2) to be constants. Consequently, the amplitudes were found as the roots of algebraic equations. It was also shown that the amplitude obtained analytically matched the numerical results reasonably well [19]. However, it is evident that other techniques, which would allow for accurate estimation of the wavelength and amplitude of periodic patterns and are not limited to the vicinity to bifurcation point, would be of great value.

In this chapter, we introduce a prototype model of a growing population of chemotactically active cells, which is relatively simple, biologically justifiable, and reproduces the formation of stationary periodic patterns. We use Fourier series for the analysis of patterns obtained from numerical simulations, as well as for the analytical estimation of the amplitude and wavelength of stationary periodic patterns emerging in the model. For greater accuracy, we perform our analytical studies on a small domain that can contain only half (or one) spike. We demonstrate that the use of Fourier series is a good alternative to deriving the amplitude equation, as it provides a more accurate estimation of the pattern's amplitude and is not limited to the vicinity of the bifurcation point. We also study how the amplitude and wavelength of periodic patterns depend on the values of the model parameters.

3.2 Model

In this section, we introduce the model of growing population of motile bacteria which we will analyse throughout this chapter. This model is represented by a system of two partial-differential equations which include diffusion, reaction and advection terms. It is known that such systems allow formation of travelling wavefronts [37, 72] as well as Turing patterns [46, 86, 87].

We look for Turing patterns forming in one-dimensional domain (of size L) under no-flux boundary conditions. We have performed preliminary numerical simulations using various models of type (3.1) and based on the results of these simulations we have chosen the following system:

$$\begin{cases} \dfrac{\partial n}{\partial t} = D_n \dfrac{\partial^2 n}{\partial x^2} - \tilde{\chi} \dfrac{\partial}{\partial x}\left(n \dfrac{\partial c}{\partial x}\right) + r_0 n \left(1 - \dfrac{n}{k}\right), \\ \dfrac{\partial c}{\partial t} = D_c \dfrac{\partial^2 c}{\partial x^2} + hn - pc, \end{cases}$$

This system is a version of the system (3.1) and describes the dynamics of population of bacteria, whose density is given by n, which respond chemotactically to a chemical agent of concentration c, produced by bacteria themselves. Here the chemotactic sensitivity of cells is assumed to be proportional to n and takes the

form $\chi(n,c) = \tilde{\chi}n$. Also, cells reproduce according to logistic law with growth rate r_0 and carrying capacity k: $f(n,c) = r(1-r/k)$. The kinetics of chemical is assumed to be linear , $g(n,c) = hn - pc$ (like in Keller-Segel model [59]), that is, it is being produced by cells with rate h and decays with rate p. This system can be nondimensionalised using the substitutions $\tilde{t} = tp$, $\tilde{x} = x\sqrt{\dfrac{p}{D_c}}$, $\tilde{n} = \dfrac{n}{k}$, $\tilde{c} = \dfrac{cp}{hk}$. This gives (after dropping the tildes):

$$\begin{cases} \dfrac{\partial n}{\partial t} = D\dfrac{\partial^2 n}{\partial x^2} - \chi_0 \dfrac{\partial}{\partial x}\left(n\dfrac{\partial c}{\partial x}\right) + rn(1-n), \\ \dfrac{\partial c}{\partial t} = \dfrac{\partial^2 c}{\partial x^2} + n - c, \end{cases} \tag{3.4}$$

with new constants $D = \dfrac{D_n}{D_c}$, $\chi_0 = \dfrac{\tilde{\chi}hk}{D_c p}$ and $r = \dfrac{r_0 k}{p}$ While the parameters D and r are essentially non-negative, χ can be positive (chemoattraction) or negative (chemorepulsion).

In the absence of diffusion and chemotaxis, the system is said to be well-mixed, meaning that both variables, n and c, don't depend on the spatial variable x. In this case, the first equation is detached from the second and describes the logistic growth of population of bacteria. The system has two steady states $(n,c) = (0,0)$ and $(1,1)$, which are unstable and stable respectively [86]. After putting back the diffusion term ($D \neq 0$, $\chi_0 = 0$) the first equation transfers into Kolmogorov-Fisher equation which is known for travelling front solutions [62, 33]. The system now allows the formation of travelling wavefronts between the steady states $(n,c) = (0,0)$ and $(n,c) = (1,1)$, which are now stable and unstable, respectively [86].

When the system includes the flow of cells due to chemotaxis ($\chi_0 \neq 0$) then the two equations in (3.4) are coupled and the known solutions of this system include stationary periodic, or Turing, patterns [86], when the chemotactic flow is strong enough. That is, if the value of χ_0 is above certain value, then the formation of stationary periodic patterns given by periodic functions, $n(x)$ and $c(x)$, can be observed in Figure 3.1.

3.3 Conditions for formation of Turing patterns

Our numerical simulations, illustrated in Figure 3.1, have indicated that Turing patterns can appear only if the chemotactic sensitivity, χ_0, is above some threshold value. This threshold value can be found analytically by applying the standard linear analysis technique, which is well known from the literature [59, 87]. It is known that Turing patterns form due to so-called Turing instability when a

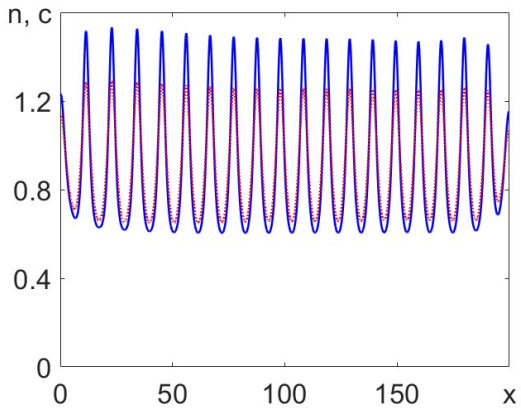

Figure 3.1: ***Numerical simulation of the Turing pattern formed in system (3.4).*** *Profiles of cell density, n, (solid blue line) and concentration of chemotactic agent, c, (dotted red line) are shown. Solutions are obtained in the domain $0 \leq x \leq 200$, $t \geq 0$. Initial conditions: $n(x,0) = 0$ if $x > 2$ and $n(x,0) = 1$ if $0 \leq x \leq 2$; $c(x) = 0$ $\forall x$. Model parameters: $D = 1$, $\chi = 1.9$, $r = 0.1$ and time $T = 800$.*

steady state, which is stable in the well-mixed system, becomes unstable in the full reaction-diffusion-advection system. This means that the equilibrium point $(n_0, c_0) = (1, 1)$ in system (3.4), which is stable if $D = \chi_0 = 0$, should become unstable for some non-zero values of D and χ_0.

Investigation of stability of steady state (n_0, c_0) involves linearisation of the system (3.4) at this state and checking the dynamics of perturbations, which are given in the form $e^{\lambda t}\cos(kx)$. Parameter k represents a perturbation mode and can have any value from the set, given as $k = i\pi/L$, with i taking any integer value so that the perturbation satisfies no-flux boundary conditions. It appears that these perturbations represent solutions of the linearised system provided that λ is an eigenvalue of the characteristic matrix, which is, for the system (3.4) at the steady state $(1, 1)$, given as

$$M = \begin{pmatrix} -Dk^2 - r & \chi_0 k^2 \\ 1 & -k^2 - 1 \end{pmatrix}. \tag{3.5}$$

The steady state $(1, 1)$ is stable if both eigenvalues of this matrix are negative, which is known to require $\det M > 0$ and $rmTrM < 0$ [87]. We can see that TrM $= -Dk^2 - r - k^2 - 1$ is always negative, so for the system to be driven unstable by perturbation, we require $\det M < 0$, which leads to the following condition for Turing instability,

$$\det M = Dk^4 + k^2(D + r - \chi_0) + r < 0.$$

From this, a necessary but not sufficient condition is

$$D + r - \chi_0 < 0 \tag{3.6}$$

since if $D + r - \chi_0 > 0$ then $\det M > 0$ for any k.The second necessary condition for initiation of Turing patterns comes from the fact that the equation $\det M = 0$ should have real roots, so that $\det M < 0$ between these two roots. Clearly, the roots are given as

$$k^2_{1,2} = \frac{-(D + r - \chi_0) \pm \sqrt{(D + r - \chi_0)^2 - 4Dr}}{2D}, \tag{3.7}$$

and therefore we require

$$(D + r - \chi_0)^2 - 4Dr > 0.$$

Taking into account (3.6) we get

$$\chi_0 - D - r > 2\sqrt{Dr}.$$

After rearranging terms in this inequality and, by introducing new notation R_T, we can state the condition for Turing instability in the form:

$$R_T = \frac{\chi_0}{D + r + 2\sqrt{Dr}} > 1. \tag{3.8}$$

Looking again at Figure 3.1, the factor of instability is $R_T = 1.1 > 1$, confirming that if equation (3.8) holds, then infinitesimal perturbances of system (3.4) result in formation of stationary periodic patterns.

Using the above technique we have performed stability analysis for a number of models, which are represented by system (3.1) but differ by functions $\chi(n, c)$ and $f(n, c)$. Following [59] we assumed that the chemical kinetics is linear and didn't alter it across models, i.e. $g(n, c) = n - c$ in all models. List of the analysed models together with the obtained formulas for instability factor, R_T, is shown in Table 3.1. Note that travelling wave solutions form if $R_T < 1$ (and $f(n, c) \neq 0$), while if $R_T > 1$ then formation of Turing patterns should be observed.

Most of the models listed in Table 3.1 have been introduced earlier (see [46]), however, the conditions for Turing instability for most of these models have not been stated so far. These conditions are qualitatively similar for all considered models and this is illustrated by domains where these conditions satisfied (in parameter planes for models $M3$ and $M7$) in Fig. 3.2. We see from this figure that for Turing instability to take place the chemotactic sensitivity, χ_0 should be strong enough, while the diffusion of chemotactic agent, D and reproduction rate r are small enough.

We have reproduced numerically Turing patterns forming in all models given in Table 3.1 aiming to find the simplest model, which allows formation of Turing patterns, such that its shape is within physical constrains. Here is a summary of our numerical results:

	$\chi(n,c)$	$f(n,c)$	R_T
M_1	χ_0	0	$\frac{\chi_0}{D}$
M_2	$\chi_0 n$	0	$\frac{\chi_0 n_0}{D}$
M_3	$\chi_0 n$	$rn(1-n)$	$\frac{\chi_0}{D+r+2\sqrt{Dr}}$
M_4	$\chi_0 \frac{1}{c}$	0	$\frac{\chi_0}{Dn_0}$
M_5	$\chi_0 \frac{1}{c}$	$rn(1-n)$	$\frac{\chi_0}{D+r+2\sqrt{Dr}}$
M_6	$\chi_0 \frac{n}{c}$	$rn(1-n)$	$\frac{\chi_0}{D+r+2\sqrt{Dr}}$
M_7	$\chi_0 \frac{n}{c+\nu}$	$rn(1-n)$	$\frac{\chi_0}{(\nu+1)(D+r+2\sqrt{Dr})}$
M_8	$\chi_0 \frac{n}{(c+\nu)^2}$	$rn(1-n)$	$\frac{\chi_0}{(\nu+1)^2(D+r+2\sqrt{Dr})}$
M_9	$\chi_0 \frac{n+\nu_1}{c+\nu_2}$	$rn(1-n)$	$\frac{\chi_0(1+\nu_1)}{(\nu_2+1)(D+r+2\sqrt{Dr})}$

Table 3.1: ***Results of Turing instability analysis for nine models represented by system*** (3.1). *Model notations are given in the first column. Functions $\chi(n,c)$ and $f(n,c)$ corresponding to each model are given in columns 2 and 3. Calculated formula for instability factor, R_T, is given in column 4. In models M2 and M4, where $f(n,c)=0$, the instability factor, R_T, depends on n_0, which is an average value of n in the domain and determined by the initial conditions.*

- M_1 is the simplest model where the chemotactic sensitivity is assumed to be constant, and no cell death/proliferation takes place [59]. Numerical simulations show that Turing patterns in this model evolve towards infinite amplitude and involve negative values for density of cells and concentration of chemical (see Figure 3.3 a), which is physically impossible. So, we can conclude, that $\chi(n,c)$ has to depend on at least one of the two variables, n and c.

- In M_2 the chemotactic sensitivity is assumed to be proportional to the concentration of cells, $\chi(n,c)=\chi_0 n$, but there is still no cell death/proliferation taking place. When the instability condition is met we observe only one sharp spike forming in response to stimulus (see Figure 3.3 b). Thus, no Turing pattern can be observed in this model.

- M_3 is M_2 with added logistic growth of cells, $f(n,c)=rn(1-n)$. In this model Turing patterns of finite amplitude and non-negative values of n and

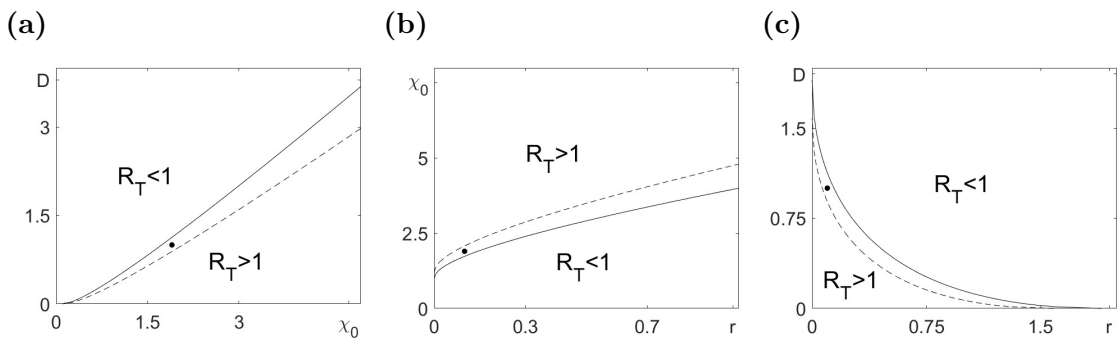

Figure 3.2: ***Domains*** $R_T > 1$ ***(where Turing instability takes place) in parameter planes for models*** **M3** ***(solid) and*** **M7** ***(dashed).*** *Plots* $R_T = 1$ *are drown according to the formulas for* R_T *given in Table 3.1 in an assumption that one of parameters has a fixed (default) value, which are* $D = 1$, $\chi_0 = 1.9$, $r = 0.1$. *Dashed line is plotted for* $\nu = 0.2$ *(model M7). The dot indicates position of the point with coordinates given by default values of parameters.*

c are observed. Thus, this is a simplest model which allows reproduction of Turing pattern of physically justifiable shape.

- In M_4 the chemotactic sensitivity is inversely proportional to the concentration of cells and there is no cell proliferation. Here numerical simulations end up with division by zero and abruptly stop after short period of time.

- M_5 is M_4 with added logistic growth of cells. Simulations can be ran for longer periods of time, however division by zero is still taking place.

- In M_6 $\chi(n, c)$ is proportional to n and inversely proportional to c. Eventually, division by zero is not taking place here and we obtain appropriately shaped Turing patterns.

- The main feature of models $M_{7,8,9}$ is that $\chi(n, c)$ is proportional to linear function of n and inverse proportional to linear function, or a square of linear function of c. The latter property lets us to safely avoid division by zero (see [46, 130]). In all these cases, we get reasonably shaped Turing patterns, which can be sharper or smoother for particular models (i.e. M_7, M_8 or M_9).

Our main conclusion after analysis and numerical simulations presented in this chapter that model M_3 is the simplest model where periodic stationary patterns, which do not violate any physical constrains, are observed. Model M_3 (which is given by the system (3.4)) will be used in the rest of this paper for analysis of properties of Turing patterns such as their amplitude and wavelength.

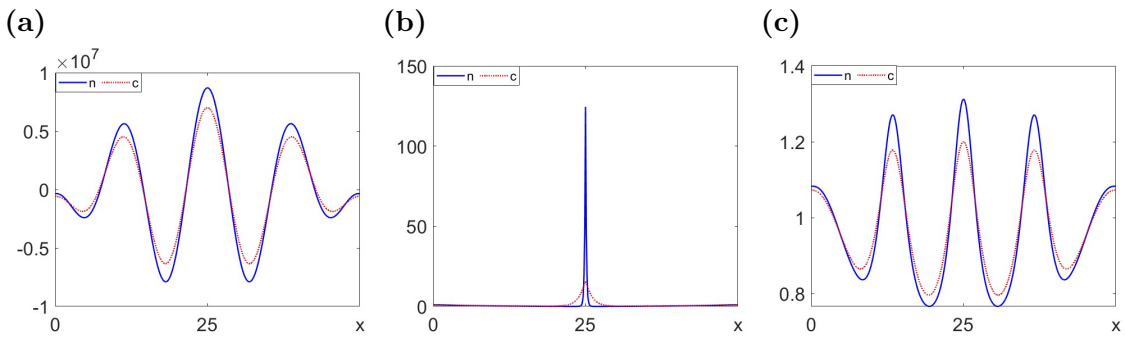

Figure 3.3: ***Numerical simulations of patterns forming in models*** M_1 ***(panel a),*** M_2 ***(panel b) and*** M_3 ***(panel c).*** *Profiles of cell density,* n*, (blue line) and concentration of chemotactic agent,* c*, (dotted red line) at time* $T = 500$ *in the domain of size* $L = 50$ *shown in all three panels. Initial condition* $n = c = 0$ *in panels a and c, and* $n = 1$ *and* $c = 0$ *in b. Patterns were initiated using stimulus applied to the centre of the domain:* $n = 1.1$ *for* $24 < x < 26$ *at time* $t = 0$*. Model parameters:* $D = 1$*,* $\chi_0 = 1.8$ *and* $r = 0.1$ *(in* M_3*).*

3.4 Estimation of the wavelength of Turing patterns

In the previous section, we identified the conditions for the formation of stationary periodic patterns in the model (3.4), as given by equation (3.6), and presented numerical simulations (see Figure 3.1) to illustrate the validity of this estimation. Our next task is to analyse the properties of these patterns, specifically their wavelength and amplitude. The amplitude is defined as the difference between the maximal and minimal values of cell density, n, in the pattern, while the wavelength is the distance representing the spatial periodicity of the pattern. As an alternative to the wavelength, we will also consider a characteristic length, which is the distance between consecutive maxima and minima and is half the wavelength.

In this section, we consider the wavelength of the periodic pattern and will estimate it based on the linear stability analysis presented in the previous section. A periodic pattern forming under no-flux boundary conditions can be represented as a sum of cosinusoidal profiles, each given as $a(k)\cos(kx)$, where $k = i\pi/L$, i is an integer, and L is the domain size. The integer i should be such that k belongs to the interval $k \in (k_1, k_2)$, where k_1 and k_2 are given by equation (3.7). Wavenumbers k in this interval correspond to unstable modes, each having a wavelength $\omega = 2\pi/k$. It is reasonable to assume that the periodic pattern is predominantly defined by the most unstable mode. A popular way to choose this mode is to take the one corresponding to the arithmetic average of k_1^2 and k_2^2, as

given by equation (3.7) [87, 19], which is:

$$k_{av}^2 = \frac{\chi_0 - D - r}{2D}.$$

The wavelength corresponding to this mode is given as:

$$\omega = 2\pi\sqrt{\frac{2D}{\chi_0 - D - r}}. \tag{3.9}$$

A more accurate way to estimate the most unstable mode is to find the mode for which the characteristic matrix (3.5) has the largest positive eigenvalue. In terms of the trace and determinant, the two eigenvalues of the characteristic matrix, M, are

$$\lambda_{1,2} = \frac{trM \pm \sqrt{trM^2 - 4\det M}}{2},$$

which gives

$$\lambda_{1,2} = \frac{-Dk^2 - k^2 - r - 1}{2} \pm \frac{\sqrt{k^4(D^2 - 2D + 1) + k^2(2D(r-1) + 4\chi_0 - 2r + 2) + 1 - 2r}}{2}. \tag{3.10}$$

Clearly, $\lambda_1 < 0$ always, so we are interested in the value of k^2 that corresponds to the largest value of λ_2. Similar analysis has been used previously to determine the most unstable mode in a system in which pattern formation is diffusion driven, rather than as a result of chemotaxis [87]. This means we are looking for the value of k^2 at which the derivative of λ_2 with respect to k^2 is zero:

$$\frac{d\lambda_2}{dk^2} = \frac{-D-1}{2} + \frac{\tau(1-D)^2 + (2\chi_0 + Dr - D - r + 1)}{2\sqrt{\tau^2(1-D)^2 + 2\tau(2\chi_0 + Dr - D - r + 1) - 2r + 1}} = 0. \tag{3.11}$$

Numerically, we found the value of k^2 (for fixed values of the parameters D, χ_0, and r) that satisfies the above equation, and subsequently calculated the corresponding wavelength, $\omega = 2\pi/k$.

To complete the presented linear analysis, we checked the dependence of the wavelength, ω, on the values of the model parameters for the system (3.4), according to formula (3.9) and the implicit formula (3.11). The corresponding plots are shown in Figure 3.4. It can be seen that, according to both formulas, the wavelength is a monotonically increasing function of diffusion, D (Figure 3.4 a), and a decreasing function of chemotactic sensitivity, χ_0 (Figure 3.4 b). The vertical asymptotes in these panels confirm that periodic patterns cannot be observed when diffusion is too fast or chemotactic sensitivity is too weak (see the condition given by equation (3.8) and the domains for Turing instability in

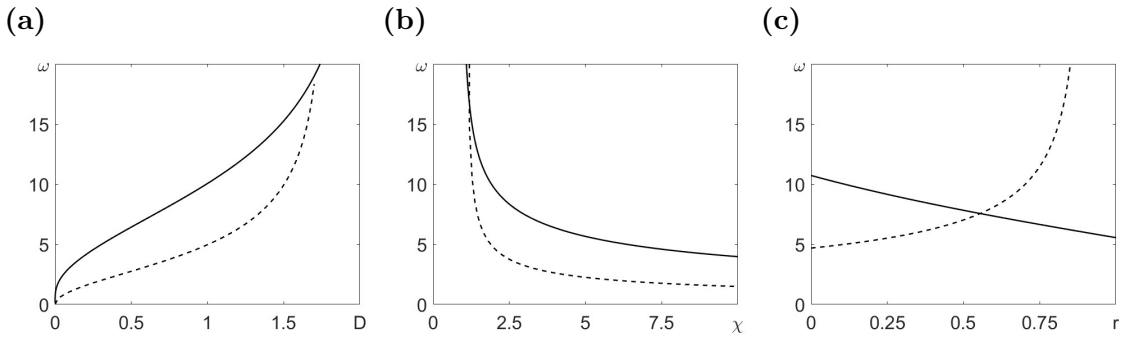

Figure 3.4: ***Dependence of the wavelength of the periodic pattern,*** ω***, on the parameters of model*** (3.4) ***as found according to the equation*** (3.9) ***(dashed) and the implicit formula*** (3.11) ***(solid).*** *Default values of the model parameters:* $D = 1$*,* $\chi_0 = 1.9$ *and* $r = 0.1$*.*

Figure 3.2). While certain quantitative differences between the plots in Figure 3.4 a and Figure 3.4 b are observed, the plots in Figure 3.4 c differ qualitatively: the wavelength of the most unstable mode in the periodic pattern is a decreasing function of the growth rate, r, according to formula (3.11), and an increasing function according to formula (3.9). Our numerical simulations (shown in Section 7) indicate that the dependence given by formula (3.11) is not only correct qualitatively but also quite accurate quantitatively.

We note that equations (3.9) and (3.11) provide only approximations of the wavelength for the periodic pattern, based on the linear analysis of the system (3.4). These approximations will later be compared with results obtained through nonlinear analysis and numerical simulations.

3.5 Fourier series for numerically simulated profiles

Numerically simulated profiles are given by stationary periodic patterns and can naturally be represented as Fourier series. A pattern forming in a domain of size L under no-flux boundary conditions is given as a superposition of cosines. In the case of the system (3.4), we have:

$$\begin{cases} n(x) = \sum_{i=0}^{M} \alpha_i \cos \dfrac{i\pi x}{L}, \\ c(x) = \sum_{i=0}^{M} \beta_i \cos \dfrac{i\pi x}{L}. \end{cases} \tag{3.12}$$

The coefficients α_i and β_i define the amplitudes of mode i for the variables n and c (with the amplitudes given as $2\alpha_i$ and $2\beta_i$). For smooth profiles, these

coefficients quickly tend to zero as i increases, allowing us to truncate the series by considering only the first M terms, where M should be carefully chosen. For a known profile, $n(x)$, a spectral Fourier decomposition can be performed, by breaking down the pattern into cosine functions with different frequencies. The lowest ferquency mode represents the homogeneous state of the system, while the highest frequency mode is responsible for the amplitude and the most unstable wavelength of the system. The coefficients of the Fourier series can be found by integrating the numerical profile $n(x)$ according to the formulas:

$$\alpha_0 = \frac{1}{L}\int_0^L n(x)dx,$$

and for $i > 0$

$$\alpha_i = \frac{2}{L}\int_0^L n(x)\cos\frac{i\pi x}{L}dx. \tag{3.13}$$

In the rest of this chapter, we will focus on profiles $n(x)$ (and coefficients α_i), keeping in mind that the analysis of the profile $c(x)$ is done in the same way.

Figure 3.5 shows patterns obtained in numerical simulations of system (3.4) corresponding to species n for different medium lengths. Figure 3.5 a shows a pattern of nine and a half spikes for which we expect α_{19} to be the most unstable mode following Fourier decomposition. Since investigating a large number of modes would result in a tedious analysis, the medium length has been reduced to obtain a half spike (Figure 3.5 b) and a full spike (Figure 3.5 c) for which the most unstable modes would be α_1 and α_2. A numerical investigation of how these most unstable modes change for different medium lengths is presented in Figure 3.6.

Formulas (3.13) can be used for the spectral decomposition of patterns obtained numerically. A typical stationary profile for cell density, n, obtained from numerical simulations of the system (3.4) is shown in Figure 3.5 a. Spectral decomposition of this profile reveals that only four modes have reasonably high coefficients: $\alpha_0 = 0.8979$, $\alpha_{19} = 0.3945$, $\alpha_{38} = 0.1293$, and $\alpha_{57} = 0.0345$, while all other coefficients are considerably smaller (less than 0.1). α_0 represents the average level of n for the entire pattern, α_{19} defines the amplitude of the mode with a characteristic length of 1/19th of the domain size, which corresponds to the 9.5 spikes seen in Figure 3.5 a. Finally, α_{38} and α_{57} correspond to the second and third harmonics of the main harmonic given by α_{19}. Thus, the amplitude of the pattern shown in Figure 3.5 a can be estimated as $2\alpha_{19}$. Varying the size of the domain will change the number of observed spikes but will not affect their amplitude or spatial periodicity. This is illustrated by the patterns shown in Figure 3.5 b and Figure 3.5 c, which are obtained by changing the medium size of the simulation in Figure 3.5 a, such that half a spike and full spike patterns are obtained. These profiles are generally easier to consider analytically, since they

require a smaller number of simultaneous equations, such as those in (3.15), to be solved for Fourier coefficients α_i.

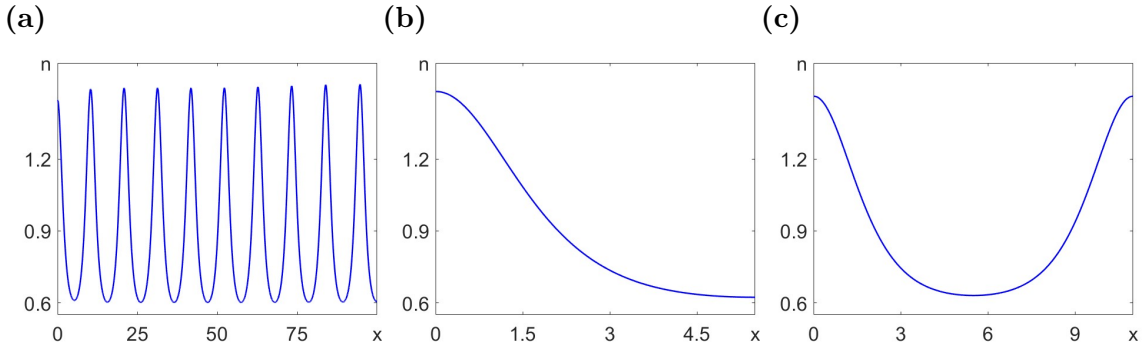

Figure 3.5: ***Profiles of cell density,*** $n(x)$***, for patterns in the system*** (3.4) ***obtained numerically****. Domain size:* $L = 100$ *in* ***(a)****,* $L = 5.5$ *in* ***(b)****, and* $L = 11$ *in* ***(c)****. Model parameters are* $D = 1$*,* $\chi_0 = 1.9$ *and* $r = 0.1$*. Initial conditions such that* $n(x,\ 0) = 1$ *if* $x < 20$ *(in a) and* $n(x,\ 0) = 1$ *if* $x < 2$ *(in b and c), and* $n(x,\ 0) = 0$ *otherwise.*

Patterns occurring in a small domain (like those shown in Figure 3.5 b and c) are of particular interest, as the corresponding Fourier series can be truncated at a reasonably low value of M (see equation (3.12)). Using Fourier decomposition of numerically obtained patterns, we investigated how the coefficients of Fourier modes depend on the domain size. In Figure 3.6, we show how the numerical values of α_i for $i = \{0, 1, 2, 3, 4, 6, 8, 9, 12\}$ change with increase in the domain size, L, which varies from 0 to 25. To obtain these values we have ran numerical simulations for $L \in [0,\ 25]$ with step 0.5 and have numerically integrated the profiles according to formula (3.13) to obtain the corresponding Fourier series coefficients. We observe that while α_0 does not vary much (staying in the range between 0.9 and 1) and the omitted α-coefficients are always negligibly small, the displayed coefficients vary significantly. For $L < 4$, $\alpha_0 = 1$ and all other coefficients are zero, indicating that the system is in a homogeneous state with no spikes formed. For $4 < L < 7.5$, the first coefficient, α_1, is larger than any subsequent coefficient ($\alpha_1 > \alpha_i, \forall i > 1$), reflecting the fact that only half of a spike can form in a simulation with domain length in this range. Within this range of domain sizes, the value of α_1 increases from zero, reaches a maximum value $\alpha_1 (= \alpha_{\max}) = 0.385$ at $L = 5.5$, and then decreases to zero. This domain size, which corresponds to the maximal value of α_1, will be considered the characteristic length (or half-wavelength) of the periodic pattern and will be denoted as Λ_0, i.e., $\Lambda_0 = 5.5$ for the system (3.4) with the model parameters used in simulations to produce Figure 3.6.

In Figure 3.6, we observe that for $L \approx 8$, $\alpha_0 = 1$ and all other coefiicients

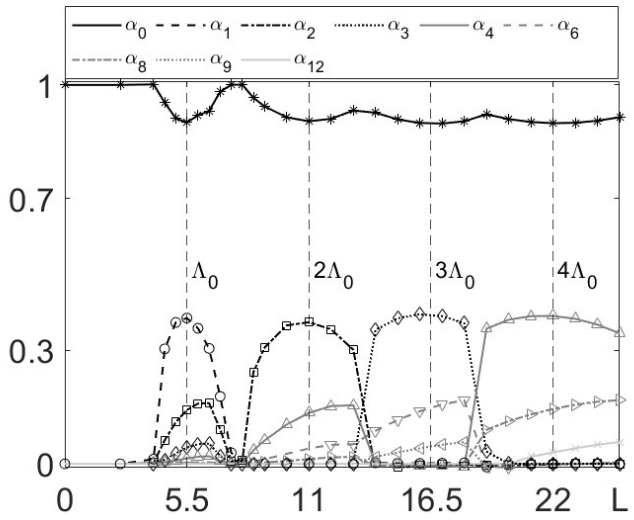

Figure 3.6: ***Dependence of coefficients*** α_i ***for*** $i = \{0, 1, 2, 3, 4, 6, 8, 9, 12\}$ ***on domain size,*** L**.** *The values for the coefficients* α_i *are obtained by integrating numerical profiles according to the formula* (3.13)*. Model parameters are* $D = 1$*,* $\chi_0 = 1.9$*, and* $r = 0.1$*. Vertical dashed lines represent the most unstable wavelengths for patterns of half a spike* (Λ_0)*, one full spike* $(2\Lambda_0)$*, spike and a half* $(3\Lambda_0)$ *and two full spikes* $(4\Lambda_0)$*.*

are 0, which means the half spike pattern dissapears and we get a homogeneous steady state before a full spike is observed for $L > 8.5$. The pattern - no pattern - pattern behaviour is due to the fact that there are no unstable modes for $L \in [7.5,\ 8.5]$ to result in patten formation when system (3.4) is perturbed. In essence, there are no eigenvalues (3.10) with positive real part. This phenomenon is also explained in Chapter 2 of [87] for a system driven unstable by diffusion, rather than chemotaxis. With a further increase in domain size ($L > 8.5$), the coefficient α_2 increases and then decreases, and a similar pattern is seen with the coefficients α_3 and α_4, each reaching a maximum of $\alpha_{\max} = 0.385$ when the domain size is such that $L = i \cdot \Lambda_0$ for α_i (where $i = 2$, 3, and 4), as indicated by the vertical dashed lines. From these observations, we conclude that the periodic patterns observed in the system (3.4) with the model parameters used to obtain the Fourier coefficients in Figure 3.6 have a characteristic length $\Lambda_0 = 5.5$ (size of half a spike) and an amplitude $A = 2\alpha_{\max} = 0.77$. Another conclusion we can draw from the coefficients in Figure 3.6 is that the shape of the observed periodic patterns are defined by four coefficients: α_0, the main mode α_i with i given by the integer closest to the ratio L/Λ_0, and its second (α_{2i}) and third (α_{3i}) modes.

In this section, we have performed Fourier decomposition of patterns obtained from numerical simulations. Our next task is to find the Fourier coefficients describing patterns forming in the system (3.4) analytically. This will allow us to compare the analytical results with the numerical ones and to predict the

dependence of the most unstable half wavelength, Λ_0, and amplitude, A, of the periodic patterns on the model parameters in (3.4).

3.6 Nonlinear analysis of stationary periodic patterns

Stationary solutions of the system (3.4), represented by their Fourier series, satisfy the system (3.4) where the partial derivatives with respect to time are set to zero, and the variables n and c are replaced by their Fourier series (3.12). This results in the following equations for the coefficients of the Fourier series, α_i and β_i:

$$\begin{cases} -D\sum_{i=0}^{M}(i\kappa)^2\alpha_i\cos(i\kappa x)+\chi_0\dfrac{\partial}{\partial x}\left(\sum_{i=0}^{M}\alpha_i\cos(i\kappa x)\sum_{i=0}^{M}i\kappa\beta_i\sin(i\kappa x)\right)+ \\ \qquad\qquad r\sum_{i=0}^{M}\alpha_i\cos(i\kappa x)\left(1-\sum_{i=0}^{M}\alpha_i\cos(i\kappa x)\right)=0, \\ -\sum_{i=0}^{M}(i\kappa)^2\beta_i\cos(i\kappa x)+\sum_{i=0}^{M}\alpha_i\cos(i\kappa x)-\sum_{i=0}^{M}\beta_i\cos(i\kappa x)=0, \end{cases} \tag{3.14}$$

where $\kappa=\pi/L$. We will begin the analysis of this system by finding the homogeneous solutions, or the solutions for which $\alpha_i=\beta_i=0$ when $i>0$. This means that, in order to find the homogeneous solution, we truncate the above system at $M=0$ and obtain:

$$\begin{cases} \alpha_0-\alpha_0^2=0, \\ \alpha_0-\beta_0=0. \end{cases}$$

Roots of this system correspond to two homogeneous solutions: $\alpha_0=\beta_0=1$ (meaning that $n(x,t)=c(x,t)=1$, $\forall x,t$) and $\alpha_0=\beta_0=0$ (meaning that $n(x,t)=c(x,t)=0$, $\forall x,t$).

To derive the equations for α_i and β_i when we truncate the system (3.14) at an arbitrary M, we use trigonometric identities to replace the product of cosines with cosines of sums. By equating the terms containing $\cos(ikx)$ for each i, we break the first equation in the system (3.14) into the following $M+1$ equations:

$$\begin{cases} \alpha_0 - \alpha_0^2 - \sum\limits_{i=1}^{M} \dfrac{\alpha_i^2}{2} = 0, \\ -D\alpha_1 k^2 + \chi_0 k^2 \left(\alpha_0\beta_1 + \sum\limits_{i\geq 1}^{M} \dfrac{i+1}{2}\alpha_i\beta_{i+1} - \sum\limits_{i\geq 2}^{M} \dfrac{i-1}{2}\alpha_i\beta_{i-1} \right) + \\ \qquad\qquad r\left(\alpha_1 - 2\alpha_0\alpha_1 - \sum\limits_{i\geq 1}^{M} \alpha_i\alpha_{i+1} \right) = 0, \\ -4D\alpha_2 k^2 + \chi_0 k^2 \left(4\alpha_0\beta_2 + \alpha_1\beta_1 + \sum\limits_{i\geq 1}^{M} (i+2)\alpha_i\beta_{i+2} - \sum\limits_{i\geq 3}^{M} (i-2)\alpha_i\beta_{i-2} \right) + \\ \qquad\qquad r\left(-\dfrac{\alpha_1^2}{2} + \alpha_2 - 2\alpha_0\alpha_2 - \sum\limits_{i\geq 1}^{M} \alpha_i\alpha_{i+2} \right) = 0, \\ -9D\alpha_3 k^2 + \chi_0 k^2 \left(9\alpha_0\beta_3 + 3\alpha_1\beta_2 + \dfrac{3}{2}\alpha_2\beta_1 + \sum\limits_{i\geq 1}^{M} \dfrac{3(i+3)}{2}\alpha_i\beta_{i+3} - \sum\limits_{i\geq 4}^{M} \dfrac{3(i-3)}{2}\alpha_i\beta_{i-3} \right) + \\ \qquad\qquad r\left(\alpha_3 - 2\alpha_0\alpha_3 - \alpha_1\alpha_2 - \sum\limits_{i\geq 1}^{M} \alpha_i\alpha_{i+3} \right) = 0, \\ .... \end{cases} \tag{3.15}$$

The first equation is constructed as an identity for the coefficients of $\cos(0)$, the second equation for $\cos(kx)$, and the i-th equation for $\cos(ikx)$. Since the second equation in (3.14) is linear, it breaks into $M+1$ identical equations:

$$-\beta_i(ik)^2 + \alpha_i - \beta_i = 0.$$

This gives $\beta_i = \dfrac{\alpha_i}{1+(ik)^2}$, so the coefficients β_i can be eliminated from the system (3.15), resulting in a system of $M+1$ equations for $M+1$ unknowns.

By truncating the system (3.15) at $M=1$ and using the formula $\beta_1 = \dfrac{\alpha_1}{1+k^2}$, we obtain the following system for finding the coefficients α_0 and α_1:

$$\begin{cases} \alpha_0 - \alpha_0^2 - \dfrac{\alpha_1^2}{2} = 0, \\ -Dk^2\alpha_1 + k^2\chi_0\alpha_0\dfrac{\alpha_1}{1+k^2} + r(-2\alpha_0\alpha_1 + \alpha_1) = 0. \end{cases} \tag{3.16}$$

This system has four solutions of which two, namely $(0,0)$ and $(1,0)$, correspond to homogeneous solutions of the system (3.4), and the two others,

$$\alpha_0 = \frac{(Dk^2 - r)(1+k^2)}{\chi_0 k^2 - 2r(1+k^2)} \text{ and } \alpha_1 = \pm\sqrt{2\alpha_0(1-\alpha_0)} \tag{3.17}$$

- to the spatial periodic patterns (in opposite phase) forming in (3.4). The roots associated with the homogeneous solutions were found earlier by truncating the

system (3.15) at $M = 0$, while the solutions (3.17) correspond to the first mode of the spectral decomposition of the periodic pattern. Thus, equations (3.17) provide the dependence of α_0 and α_1 on the model parameters and can be compared with the results obtained numerically, as shown in Figure 3.6.

Truncation of the system (3.15) at $M = 2$ gives three equations for three unknowns, α_0, α_1 and α_2:

$$\begin{cases} \alpha_0 - \alpha_0^2 - \dfrac{\alpha_1^2}{2} - \dfrac{\alpha_2^2}{2} = 0, \\ -D\alpha_1 k^2 + \chi_0 k^2 \left(\alpha_0\beta_1 + \alpha_1\beta_2 - \dfrac{1}{2}\alpha_2\beta_1 \right) + r(\alpha_1 - 2\alpha_0\alpha_1 - \alpha_1\alpha_2) = 0, \\ -4D\alpha_2 k^2 + \chi_0 k^2 (4\alpha_0\beta_2 + \alpha_1\beta_1) + r \left(\alpha_2 - \dfrac{\alpha_1^2}{2} - 2\alpha_0\alpha 2 \right) = 0. \end{cases}$$

Similarly, systems of equations for 4 and 5 unknowns, when the system (3.15) is truncated at $M = 3$ or $M = 4$, can be derived. Although the roots of these systems cannot be expressed explicitly, their values (for a given set of model parameters) can be found numerically. Using numerical methods, we have found solutions to the system (3.15) truncated up to $M = 4$. These solutions for the model (3.4), with the model parameter values $D = 1$, $\chi_0 = 1.9$, and $r = 0.1$ (see Figures 3.5 and 3.6), and a domain size of $L = 5.5$, are shown in Table 3.2. For comparison, we have also shown in this table the coefficients α_i obtained by the spectral decomposition of the numerically simulated pattern (shown in Figure 3.5 b). As we can see from this table, the solutions obtained are consistent across different truncations and fairly comparable with the results of the spectral decomposition of the simulated pattern. Additionally, the coefficients α_3 and α_4 are considerably small, which indicates that truncating the system (3.15) at $M = 4$ should provide a fairly accurate solution for the model (3.4) when the domain size is reasonably small (in the presented case, $L = \Lambda_0$).

To check the accuracy of the truncated solutions presented in Table 3.2, we have reproduced the corresponding profiles (for $M = 1$, 2, and 3) and compared them with the profile obtained from numerical simulations. All these profiles are shown in Figure 3.7 a. Visually, it is evident that the solution of (3.15) truncated at $M = 2$ fits the profiles obtained from numerical simulations better than the one truncated at $M = 1$. Furthermore, the profile corresponding to the solution truncated at $M = 3$ is almost indistinguishable from the simulated profile. As a numerical measure of the discrepancy between the profiles, $n_i(x)$ and $n_0(x)$, one can use the integral:

$$I = \int_0^L [n_i(x) - n_0(x)]^2 dx,$$

where $n_i(x)$ correspond to one of the solutions of (3.15) (truncated at $M = i$, $i > 0$), while $n_0(x)$ - to the profile obtained in numerical simulations. The value

	α_0	α_1	α_2	α_3	α_4
Simulation	0.9009	0.3849	0.1423	0.0428	0.0143
$M = 1$	0.8462	0.5103	0	0	0
$M = 2$	0.8868	0.4153	0.1680	0	0
$M = 3$	0.8938	0.4035	0.1563	0.0508	0
$M = 4$	0.8941	0.4033	0.1550	0.0496	0.0155

Table 3.2: ***Coefficients of Fourier series,*** α_i***, for the first five modes of the pattern represented by a half-spike.*** *First row: coefficients are obtained using eq.* (4.13) *for the profile shown in Figure 3.5 b. Following four rows: coefficients are obtained by truncating the system* (3.15) *at* $M = 1$*,* 2*,* 3 *and* 4 *for the model parameters used in Figure 3.5 b.*

of this integral for the solutions truncated at $M = 1$ is $I = 0.1353$, at $M = 2$ - $I = 0.0114$ and at $M = 3$ - $I = 0.0026$. Thus, the discrepancy between the solution, truncated at $M = 3$, and the one obtained numerically is less than 1%. Additionally, the numerical discrepancy for $M = 4$ is $I = 0.0020$ and fairly the same as for $M = 3$.

The amplitude of the profile for the variable n in a small domain (when $L \approx \Lambda_0$) is predominantly defined by the coefficient α_1, while its average value is defined by α_0. Figure 3.7 b shows the dependence of these two coefficients on the size of the domain, L, obtained from the spectral decomposition of the simulated profile and according to the equation (3.14) truncated at $M = 1$ and $M = 3$. We observe that, while all three plots are qualitatively similar, the plots for the simulated profile and for the solution of equation (3.14) truncated at $M = 3$ also show good quantitative agreement.

In this section, we have focused on finding the analytical solutions of the system (3.4), represented by truncated Fourier series. Numerically, we were able to find solutions truncated up to $M = 4$, and have shown that these solutions (at $M \geq 3$) are fairly accurate if the modelled domain is small. Throughout this section, we have fixed the model parameters: $D = 1$, $\chi_0 = 1.9$, and $r = 0.1$. In the next section, we will examine how the characteristics of periodic patterns, obtained numerically and given by the analytical solutions of (3.14), depend on the model parameters.

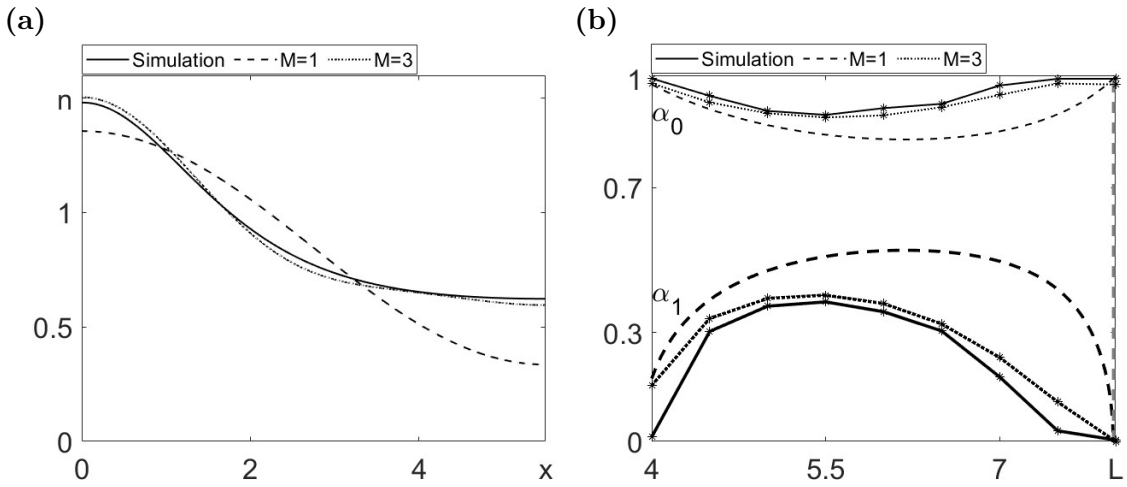

Figure 3.7: ***Comparison of analytical and numerical solutions.*** ***A****: Profiles of solutions to* (3.15) *truncated at* $M = 1$ *(dashed) and* $M = 3$ *(dotted) as compared to numerically simulated profile (solid, same as in Figure 3.5 b).* ***B****: Dependence of the coefficients* α_0 *(thin lines) and* α_1 *(thick lines) on the domain size* L *found by spectral decomposition of profiles obtained in simulations (solid) and from* (3.15) *truncated at* $M = 1$ *(dashed) and* $M = 3$ *(dotted). Values of model parameters are the same as in Figure 3.5.*

3.7 Impact of model parameters on characteristics of stationary periodic pattern

Based on the linear analysis of pattern formation presented in Section 3, we were able to predict the dependence of the pattern's wavelength on model parameters (see equations (3.9), (3.11), and Figure 3.4). However, linear analysis did not allow us to make any predictions concerning the amplitude of the periodic pattern. In this section, we will make such predictions using the nonlinear analysis presented in the previous section and compare them with the results of numerical simulations. The outcome of this study is presented in Fig. 3.8. Since D represents the ratio of the rate of random motion of cells to the diffusion coefficient of the chemotactic agent, it is essentially smaller than one; therefore, $D < 1$ in our plots. Additionally, the ranges of values for χ_0 and r were chosen such that the condition for Turing instability given by equation (3.8) (and illustrated in Figure 3.2) is satisfied, and therefore $\chi_0 \geq 1.9$ or $r \leq 0.14$ in all presented plots.

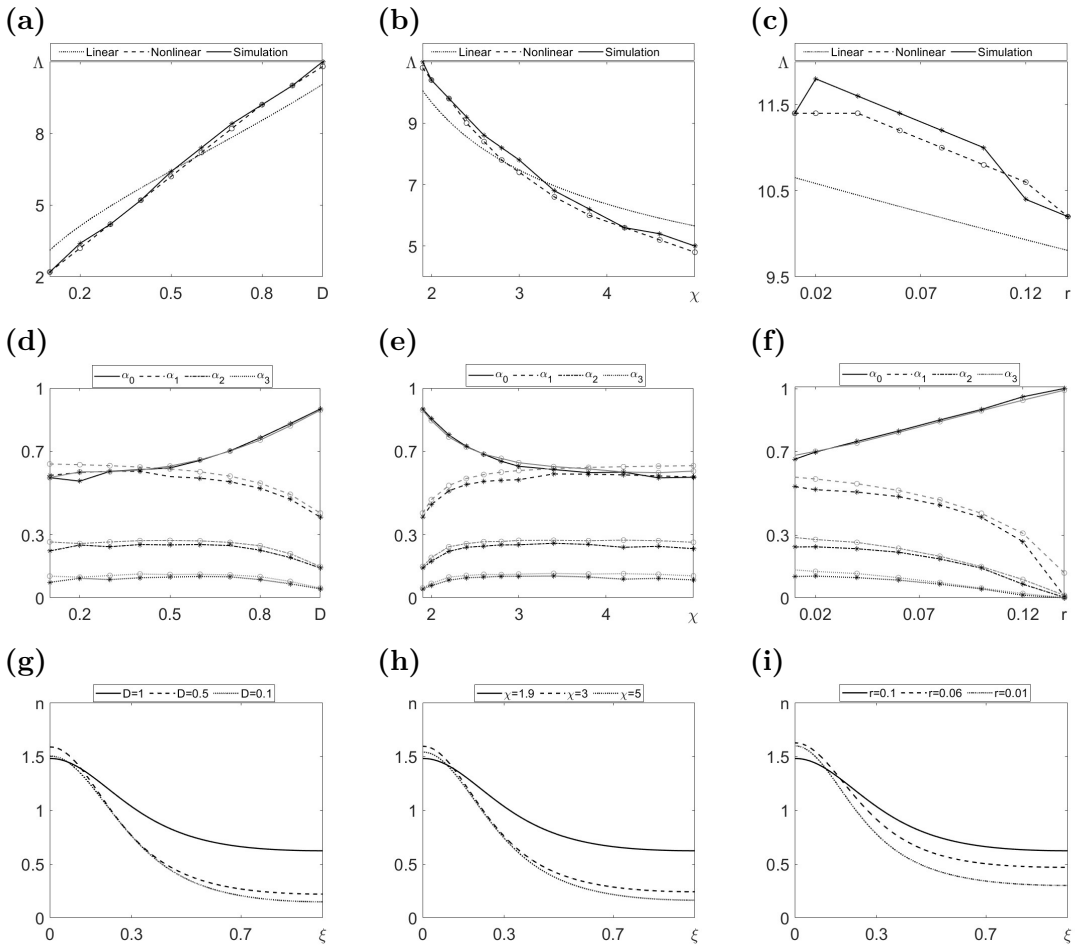

Figure 3.8: ***Dependence of the characteristics of stationary periodic pattern on model parameters.*** ***(a)-(c)*** *Dependence of the wavelength on the diffusion coefficient, D, (panel* ***(a)****), chemotactic coefficient, χ_0, (panel* ***(b)****), and reproduction rate, r, (panel* ***(c)****): dotted lines - from linear analysis (same as solid line in Fig. 3.4), dashed lines - from Fourier series truncated at $M = 3$, and solid lines - from simulations.* ***(d)-(f)*** *Coefficients of Fourier series versus the diffusion coefficient, D, (panel* ***(d)****), chemotactic coefficient, χ_0, (panel* ***(e)****), and reproduction rate, r, (panel* ***(f)****) found after spectral decomposition of numerically simulated profile (black lines) and found analytically from eq.* (3.15) *with $M = 3$ (grey lines).* ***(g)-(i)*** *Profiles of cell density obtained numerically for different values of the diffusion coefficient, D, (panel* ***(g)****), chemotactic coefficient, χ_0, (panel* ***(h)****), and reproduction rate, r, (panel* ***(i)****). Each profile obtained in the domain of size of characteristic length, $L = \Lambda_0$ (for given set of parameter values) and presented versus scaled spatial variable $\xi = x/\Lambda_0$.*

The dependence of the pattern's wavelength on model parameters, as predicted by linear analysis (equation (3.11)), nonlinear analysis (equation (3.15)), and found numerically, is shown in Figure 3.8 a-c. The wavelength in numerical simulations was determined as the length of the domain for which the Fourier

decomposition of the obtained profile gave the maximal value of α_2 (or $2\Lambda_0$ according to Figure 3.6). Similarly, using equation (3.15) truncated at $M = 4$, we found the value of k for which the value of α_2 is maximal, and the wavelength was calculated as the length of the domain corresponding to this value of k, namely, $\omega = \pi/k$. As we can see from Figure 3.8 a-c, the dependences found in this way indicate that the wavelength increases linearly with the diffusion coefficient, D, and decreases with the chemotactic coefficient, χ_0 (which can be approximated by a hyperbola), and the reproduction rate, r (which appears as linear), as predicted by linear analysis in Section 3. Regarding the dependence on the reproduction rate, r, the prediction made by the implicit formula (3.11), rather than the explicit (3.9) (see Figure 3.4), was confirmed both by simulations and analytically. It is evident that the predictions made using nonlinear analysis (based on equation (3.15)) are far more accurate compared to those made using linear analysis (based on equation (3.11)) in reproducing numerical results.

The dependence of the amplitude of the periodic pattern on model parameters is shown in Figure 3.8 d-f. The amplitude is predominantly defined by the maximal value of α_i ($i > 0$) when the size of the domain L is varied (see Figure 3.6). As found in Section 5, for the default values of the model parameters, the maximal value of α_i is $\alpha_{max} = 0.385$ for $i = 1, 2, 3, 4$, and evidently for all other modes. The main question we address now is how α_{max} depends on the model parameters. Figure 3.8 d-f show how α_{max}, which is represented here by the value of α_1, depends on the model parameters. In addition, we have presented the values of α_0, α_2, and α_3, which contribute to the shape of the n-profile. We do not consider the contributions of α_2 and α_3 to the amplitude of the periodic pattern for the following reasons: (1) Due to symmetry in the Fourier expansion, even modes do not contribute to the amplitude at all, and therefore α_2 has no impact on the amplitude of the pattern; (2) According to Table 3.2, α_3 is an order of magnitude smaller than α_1, which means it contributes only about 10% to the amplitude of the patterns. Furthermore, the plots in Fugure 3.8 d-f indicate that this contribution remains roughly the same for any set of model parameters, and thus we can consider α_1 as an indicator of the behaviour of the pattern's amplitude.

The main conclusion drawn from the plots presented in Figure 3.8 d-f is that the amplitude of the periodic pattern (given by the value of α_1) saturates at low values of the diffusion coefficient, D, and reproduction rate, r, and at high values of the chemotactic sensitivity, χ_0. The amplitude increases with an increase in D and r, while it decreases with an increase in χ_0. Another notable conclusion from the plots is that the average value of cell density, n, given by the value of α_0, increases with the diffusion coefficient, D, and the reproduction rate, r, while

decreasing with the chemotactic sensitivity, χ_0. It saturates at low values of D and high values of χ_0, while it depends linearly on r.

Figure 3.8 g-i shows how the shape of the n-profile depends on the model parameters. The plots in Figure 3.8 g confirm that the amplitude of the profile decreases, and the average value of the cell density, n, increases with the increase of the diffusion coefficient, D. The plots in Figure 3.8 h confirm that the amplitude of the profile increases, and the average value of the cell density, n, decreases with the increase of chemotactic sensitivity, χ_0. Finally, the plots in Figure 3.8 i confirm that the amplitude of the profile decreases, and the average value of the cell density, n, increases with the increase of the reproduction rate, r. The dependence of the wavelength of the patterns on the model parameters cannot be seen in Figure 3.8 g-i, as the profiles, although obtained for media of different sizes, are spatially scaled and presented as $n(x) = n(\xi)$ in the scaled variable $\xi = x/L$.

3.8 Discussion

In this chapter, we have introduced a prototype model that reproduces the formation of periodic patterns due to advection. A prototype model is a minimalistic model that can capture the essential features of the phenomenon under study, and as such, it is often used in mathematical biology. For example, the FitzHugh-Nagumo model is a prototype model for the study of excitability in biological systems [34], and, in addition, it is often used to reproduce other phenomena requiring cubic nonlinearity [132]. The formation of periodic patterns in reaction-diffusion systems also requires cubic nonlinearity, and a corresponding prototype model was introduced in [103]. The formation of periodic patterns in diffusion-advection-reaction systems requires only quadratic nonlinearity, and in the present work, we have introduced the corresponding prototype model, which is also designed to reproduce dynamics in a growing population of motile bacteria. The growth of the modelled population follows the logistic law, while the migration of cells is due to chemoattraction by the chemical produced by the cells themselves. The model used in this study is a prototype model because it is the simplest model that allows the formation of physically justified (bound and non-negative) periodic patterns. For example, the periodic patterns forming in our one-dimensional model can be considered as reproducing and explaining the formation of stripes of cell density in the experiments presented in [75], although it is simpler than the three-variable model used in that publication.

In our analysis of the model (3.4), we have identified the condition for the formation of stationary periodic patterns (or Turing instability), presented as a

certain expression, which we denoted as R_T (3.8). This is given in terms of the model parameters, with $R_T > 1$ required for the pattern to emerge. The main conclusion of this analysis is that for periodic patterns to form, chemoattraction must be sufficiently strong, while the diffusion of the chemical and the reproduction of cells must be slow and below a certain threshold, as defined by the condition $R_T > 1$. This result aligns with the known fact that for periodic pattern formation, the advection term should represent chemoattraction [59], while chemorepulsion only leads to the formation of moving bands of cells [58, 44, 131].

We have also presented our analysis of the spatial characteristics of the periodic patterns. Commonly, the wavelength of such patterns is estimated based on linear analysis using the formula (3.9) [87]. We have suggested a correction to this estimate, which is also based on linear analysis and is given by the implicit formula (3.11). Comparison with the wavelengths of simulated patterns has indicated that the formula (3.11) provides a better approximation of the wavelength of the periodic pattern, not only quantitatively but also qualitatively, particularly when checking the dependence of the wavelength on model parameters (see Figure 3.4 and Figure 3.8 c). The wavelength of the periodic pattern was also estimated based on nonlinear analysis presented in Section 6. The first-order approximation can be made analytically by finding the value of k corresponding to the maximal value of α_1 in equations (3.17). The link between this value of k and the wavelength is given by the formula $k = \pi/\Lambda_0$, where Λ_0 is a characteristic length, which is half the wavelength. The dependence of α_1 on the domain size, L, found from this approximation is shown by the dashed plot in Figure 3.7 b. It is evident from this figure that the length of the medium for which α_1 reaches its maximum value (and which gives the value of Λ_0) is much higher than the one found numerically ($\Lambda_0 = 5.5$, see Figure 3.6). However, when we find the characteristic length using the model (3.15) truncated at $M = 3$, we find that it is very close to the value obtained numerically (compare the locations of the maxima for dashed blue and cyan lines in Figure 3.7 b).

One of the most important problems addressed in this work concerns the analytical estimation of the amplitude of periodic patterns forming in Turing systems. Many researchers use multi-scale analysis to derive the amplitude equation for this purpose, although this technique often appears technically complex and not always entirely convincing [30, 137, 142]. For a certain class of kinetic terms, this approach can be significantly simplified, and has been applied with some success [19]. Generally, in terms of the system (3.4), these techniques allow for the derivation of a differential or algebraic equation for α_1, which is reasonably accurate in the vicinity of the Turing bifurcation point, where the homogeneous solution becomes unstable. In this work, we have proposed the use of Fourier

series analysis, which, in our view, despite its simplicity, offers many advantages compared to weakly nonlinear techniques.

As the amplitude equation is derived based on weakly nonlinear analysis and represents the equation for the amplitude of the most unstable mode, it should be compared with the Fourier series truncated at $M = 1$, that is, with the system (3.16). As we know (see [142]), the amplitude equation for the system (3.4) suggests a supercritical pitchfork bifurcation, meaning that when the homogeneous state becomes unstable, two stable stationary periodic patterns of equal amplitude but differing in sign would form. While it would require tedious algebra to determine the dependence of the amplitude on model parameters, one could expect it to increase with chemotactic sensitivity, as shown in (3.3). Solving the system (3.16) leads to the same result but in a much more efficient way. As we found earlier, $\chi^* = (\sqrt{D} + \sqrt{r})^2$ is the bifurcation value of χ_0 when the homogeneous state, $(n = 1, c = 1)$, loses its stability. By solving the system (3.16), we find that if $\chi_0 < \chi^*$, there are only two solutions, both with $\alpha_1 = 0$, corresponding to the homogeneous solutions of the system (3.4). However, when $\chi_0 > \chi^*$, two additional solutions emerge, for which α_1 can be approximated as:

$$\alpha_1 \approx \sqrt{\frac{2k^2\epsilon}{(Dk^2 - r)(1 + k^2)}}$$

where $\epsilon = \chi_0 - \chi^*$ is a small variable indicating proximity to the Turing bifurcation point, and $k = (r/D)^{1/4}$ is the wavenumber of the first unstable mode. This shows that the amplitude of the periodic pattern can be approximated using Fourier series in a way that saves a lot of time and effort. While we can't conclude on the stability of periodic patterns using only Fourier series, the preliminary linear stability analysis pointing to Turing bifurcation helps clarify this point. Furthermore, truncating the Fourier series at higher values of M allows for a more accurate approximation of the periodic pattern without resulting in any physically irrelevant solutions, as all extra solutions appear to be complex. For example, the amplitude found from the system (3.15) truncated at $M = 3$ is far more accurate when compared with that found using the system (3.16), and the periodic pattern reproduced using this solution is almost indistinguishable from the one obtained in numerical simulations (see Figure 3.7 a). The only concern when solving the algebraic system (3.15) is that this solution can only be expressed explicitly when the system is truncated at $M = 1$ (see (3.17)). For $M > 1$, solutions can only be found numerically. This is particularly true for the dependence of the wavelength and amplitude of the periodic patterns found for the system (3.15), as presented in Figure 3.8. All corresponding plots are drawn based on sets of solutions to the system (3.15) truncated at $M = 3$, which were found numerically.

As the presented model is a prototype model, it is representative of a wide class of models, and our results are, at least qualitatively, applicable to many biological systems. The analysed one-dimensional patterns shown in Figure 3.1 can be directly compared with the stripe patterns observed in expanding cell populations, as reported in [75]. Furthermore, in that paper, it was found that the wavelength of the emerging patterns increases (i.e., the number of stripes in the same physical domain reduces) with an increase in the diffusion rate of cells, which is also in agreement with the results shown in Figure 3.4 a. Generally, our results on the dependence of the wavelength and amplitude of periodic patterns on model parameters could be tested in experiments with different strains of *E. coli* that have varying chemotactic sensitivity, proliferation rate, or motility.

The analytical methods used in this chapter, particularly the representation of periodic patterns by means of Fourier series, have proven to be very useful. They can be applied to the analysis of other classes of models where the formation of stationary periodic patterns is observed. In particular, they can be extended to the analysis of patterns forming in a system of two competing species, where one produces a chemical agent and the other responds to it chemotactically. This study is presented in the next chapter.

Chapter 4

Modelling pattern formation in a system of two competing species

One of the classical models in mathematical biology is the Lotka-Volterra competition model, which describes the dynamics of two populations competing for resources. This system has two possible regimes: coexistence or the extinction of the weaker population. In this work, we extend the competition model by introducing an additional interaction between the populations through chemotactic coupling, specifically, assuming that one species produces a chemical agent that induces taxis in the other. It is well known that in a single-species model (i.e. the Keller-Segel model), the production of a chemoattractant leads to the formation of stationary periodic (or Turing-type) patterns. Here, we investigate the conditions under which stationary periodic patterns emerge in a two-species competition model with chemotaxis.

Pattern formation in reaction-diffusion-advection systems involving two interacting species has been previously demonstrated in the case of weak competition. However, little research has been conducted to determine the conditions that lead to a breakdown of stability or to characterise the patterns that emerge. In the weak competition regime, the novelty of our work lies in identifying a domain of instability, dependent on the competition rates, where pattern formation is possible. Beyond establishing the conditions for stability breakdown, we also conduct a detailed analysis of the effects of model parameters on this instability domain. Additionally, we obtain key insights into pattern characteristics, such as wavelength and amplitude, using nonlinear Fourier analysis, an approach that is commonly applied to one species systems, rather than two species.

Moreover, some of the most intriguing results in this study concern pattern formation when the species producing the chemical agent is initially close to extinction. We demonstrate that such patterns arise in the case of strong competition, driven by finite-amplitude disturbances rather than infinitesimal perturbations.

We provide a detailed numerical analysis of how model parameters influence the minimum perturbation amplitude required to trigger stability breakdown. Furthermore, we use Fourier analysis to show that these reaction-diffusion-advection systems admit Turing-type patterns as solutions. This finding contradicts results from linear analysis, which predict that the system remains homogeneous in the strong competition regime.

4.1 Introduction

Ecological systems, such as bacterial biofilms, are often composed of multiple biological species whose interactions play a crucial role in the formation and properties of these systems [66]. The interactions between biological populations can take various forms, including predator-prey, competition, and symbiosis [86]. In this work, we consider the case of competitive interactions between two populations, which is commonly modelled by the classical Lotka-Volterra model [76, 135], represented by the following (nondimensional) equations:

$$\begin{cases} u_t = u(1 - u - b_1 v), \\ v_t = rv(1 - v - b_2 u), \end{cases} \tag{4.1}$$

in which variables u and v represent sizes of two species, parameter r gives the ratio of reproduction rates of v and u, parameter b_1 represents the competition strength of v on u and b_2 - of u on v. The case when $0 < b_1 < 1$ and $0 < b_2 < 1$ is referred to as a weak competition regime; the case of $b_1 > 1$ and $b_2 > 1$ corresponds to strong competition regime, and intermediate cases as string-weak or weak-strong regimes. It is well known that this model has four steady states and their stability is defined by model parameters as follows [50, 86, 113]:

- $(u_1, v_1) = (0, 0)$ (both species are extinct) is always unstable;
- $(u_2, v_2) = \left(\dfrac{b_1 - 1}{b_1 b_2 - 1}, \dfrac{b_2 - 1}{b_1 b_2 - 1} \right)$ (coexistence) is stable if $b_1, b_2 < 1$ (weak competition) and unstable otherwise.
- $(u_3, v_3) = (1, 0)$ (the second species is extinct) is stable if $b_2 > 1$, and unstable otherwise;
- $(u_4, v_4) = (0, 1)$ (the first species is extinct) is stable if $b_1 > 1$ and unstable otherwise;

The system (4.1) is often extended by adding spatial variable so that the variables $u = u(x, t)$ and $v = v(x, t)$ represent densities of species, which depend on the coordinate x as well as on time t. Spatial coupling is commonly given by

diffusion and cross-diffusion (or cross-taxis) and mathematically represented by Shigesada-Kawasaki-Teramoto, or SKT system [113], which can be reduced to Potts-Petrovskii model [98]:

$$\begin{cases} u_t = u_{xx} - \chi_1(uv_x)_x + u(1 - u - b_1 v), \\ v_t = dv_{xx} - \chi_2(vu_x)_x + rv(1 - v - b_2 u). \end{cases} \tag{4.2}$$

Here parameter d represents the rate of random motion of species v relative to that of u and parameters χ_1 and χ_2 give the strengths of cross-taxis between species. The case of $\chi_1 = \chi_2 = 0$ is referred to as a classical competition-diffusion model known by travelling front solutions corresponding to transitions between stationary states of system (4.1), which were studied in many papers [47, 106, 4, 2]. Cross-taxis terms affect the speed, direction and shape of travelling fronts [138] and, under certain conditions, also cause the loss of stability of equilibrium states resulting to formation of stationary periodic patterns [71, 12].

Going one step further, mathematical models have been introduced for two competing species with extra interaction mediated by chemical produced by one or both species. This chemical can affect the kinetic terms resulting, for example, to inhibition of one species by the other [24]. It can also act as a chemotactic agent, as it is assumed in a class of so called two-species chemotaxis model, which can be represented by the following (non-dimensional) system [61]:

$$\begin{cases} u_t = D_1 u_{xx} - \chi_1(uc_x)_x + u(1 - u - b_1 v), \\ v_t = D_2 v_{xx} - \chi_2(vc_x)_x + rv(1 - v - b_2 u), \\ c_t = c_{xx} + \mu_1 u + \mu_2 v - \gamma c, \end{cases} \tag{4.3}$$

where parameters D_1 and D_2 define the rate of random motion of species u and v, χ_1 and χ_2 the strength of their chemotactic response to the chemical c, which is produced by both species (with production rates μ_1 and μ_2) and degrades with rate γ [65]. This system models spatio-temporal evolution of two competitive species, which migrate along (chemoattraction, $\chi > 0$) or against (chemorepulsion, $\chi < 0$) the concentration gradient of the chemical produced by themselves.

The impact of chemotactic terms on the shape and speed of travelling fronts, which represent transitions between the steady states of (4.1), has been in the focus of many studies of system (4.3) and other similar systems [53, 69, 73, 74, 120]. An analytical study of system (4.3), conducted in [92], demonstrated that in the case of chemoattraction ($\chi_1 > 0$, $\chi_2 > 0$) and strong competition ($b_1 > 1$, $b_2 > 1$), the stable steady states can lose their stability when the chemoattraction is sufficiently strong. The loss of steady-state stability due to special coupling (given by the chemotactic term in the given case) is commonly referred to as Turing instability, with the stationary periodic patterns forming as a result known as Turing

patterns [128]. In [92], it was shown that a stationary periodic pattern may arise when the steady state $(u,\ v,\ c) = (1,\ 0,\ 1)$ becomes unstable if χ_1 is sufficiently large, and similarly, such patterns may arise from $(u,\ v,\ c) = (0,\ 1,\ 1)$ when χ_2 is sufficiently large. Moreover, it was numerically demonstrated that in the case of weak competition, stationary periodic patterns can arise from the coexistence state if either of the parameters χ_1 or χ_2, defining the chemotactic response, is sufficiently large. These findings are not surprising, as by setting $u = 0$ or $v = 0$, the system (4.3) is reduced to a one-species model, aligning with the classical result [60, 15] that strong chemoattraction in a single species with logistic growth leads to Turing-type instability.

The formation of stationary periodic patterns in the case of mutual repulsion between species was reported in [70]. The model presented in that paper included two chemicals, each produced by one of the bacterial species and acting as a chemorepellent to the other. It was shown that, in the case of weak competition, the coexistence state can become unstable, leading to the formation of periodic patterns when the strengths of chemorepulsion are sufficiently high. The study of these patterns in [70] included an estimation of their amplitude using the amplitude equation, as well as their numerical reproduction in one- and two-dimensional domains. The phenomenon reported in [70] is quite novel, as it is not observed in single-species systems, where chemorepulsion does not result to formation of periodic patterns.

In this chapter, we focus on the formation of periodic patterns in system (4.3) in the most basic scenario, where only one species produces a chemical agent which repels the second species. In line with the results reported in [70], we found that Turing-type instability occurs only in the case of weak competition, where strong chemorepulsion causes the coexistence state to become unstable, resulting in the formation of periodic patterns. We have also found that both steady states, corresponding to the extinction of one of the species (in the case of strong competition), remain stable in the presence of chemotaxis. However, we have shown that, even in this case, stationary periodic patterns can be initiated by finite perturbations. We have also analysed the wavelengths and amplitude of the forming patterns using Fourier series analysis, as done in [15].

4.2 Model and linear stability analysis of its steady states

We consider a two-species competition model with chemotaxis where one of species produces chemotaxtic agent for the other. This is represented by a slightly

modified version of the system (4.3) given as:

$$\begin{cases} u_t = D_1 u_{xx} - \chi(uc_x)_x + r_1 u(1 - u - b_1 v), \\ v_t = D_2 v_{xx} - r_2 v(1 - v - b_2 u), \\ c_t = c_{xx} + v - c, \end{cases} \tag{4.4}$$

where the chemical agent c is produced by species v and affects chemotactically u. This system is considered on a one-dimensional domain $x \in (0, L)$ under no-flux boundary conditions. In the well-mixed case, when the solution is homogeneous, the first two equations of this system transform into the system (4.1), last equation gives $c = v$, and therefore it has four steady states:

$$(u^*,\ v^*,\ c^*) = \left\{ (0,0,0),\ \left(\frac{b_1 - 1}{b_1 b_2 - 1}, \frac{b_2 - 1}{b_1 b_2 - 1}, \frac{b_2 - 1}{b_1 b_2 - 1} \right),\ (1,0,0),\ (0,1,1) \right\},$$

with their stability given by the same conditions as for the Lotka-Volterra model (4.1).

Classical Turing instability analysis refers to the formation of stationary periodic patterns in a reaction-diffusion-advection system, when the steady states loose their stability due diffusion and advection terms [128, 60]. Linear stability analysis involves consideration of the perturbation given by cosinusoidal function, $\sim \exp(\lambda t)\cos(kx)$ [87], so that the stability of the steady state, (u^*, v^*, c^*), is defined by the signs of eigenvalues of the characteristic matrix at this state, which, for the system (4.4), is given as following:

$$M = \begin{pmatrix} -D_1 k^2 + r_1(1 - 2u^* - b_1 v^*) & -r_1 b_1 u^* & -\chi u^* k^2 \\ -r_2 b_2 v^* & -D_2 k^2 + r_2(1 - 2v^* - b_2 u^*) & 0 \\ 0 & 1 & -k^2 - 1 \end{pmatrix}. \tag{4.5}$$

The steady state is unstable if at least one of eigenvalues is positive. Since the steady state $(u_1, v_1, c_1) = (0, 0, 0)$ is always unstable and can't loose its stability due to diffusion and advection terms we don't need to consider it. However, stationary periodic patterns can emerge from other steady states when they are stable in the well-mixed system and become unstable in the presence of diffusion and advection.

4.2.1 Analysis of the coexistence state

The aim of this section is to obtain conditions for Turing-type instability of the coexistence steady state,

$$(u_2,\ v_2,\ c_2) = \left(\frac{b_1 - 1}{b_1 b_2 - 1},\ \frac{b_2 - 1}{b_1 b_2 - 1},\ \frac{b_2 - 1}{b_1 b_2 - 1} \right). \tag{4.6}$$

It is known that in the absence of diffusion and advection this state is stable if $b_1 < 1$ and $b_2 < 1$ (weak competition). The natural step is to evaluate the characteristic matrix (4.5) at the coexistence state and investigate under what conditions it will have positive eigenvalues. As the matrix (4.5) is 3x3 matrix its eigenvalues are roots of the cubic polynomial:

$$\lambda^3 + a_1\lambda^2 + a_2\lambda + a_3 = 0, \tag{4.7}$$

where coefficients a_1, a_2 and a_3 are defined by the entries of matrix (4.5) where $(u^*, v^*, c^*) = (u_2, v_2, c_2)$. Analytical expression for these coefficients are awkwardly long to be presented here, however their numerical values can always be found for any given set of parameter values of model (4.4). The Routh-Hurwitz criteria states that if

$$\begin{cases} a_1,\ a_2,\ a_3 > 0, \\ a_3 - a_1 a_2 < 0, \end{cases} \tag{4.8}$$

then all roots of (4.7) are negative and the steady state is stable. If any of these conditions is violated, then at least one eigenvalue is positive and the steady state is unstable. For a set of parameter values $D_1 = D_2 = 1$, $r_1 = r_2 = 0.1$, $\chi = -10$ and $k = 0.2$, we have found numerically how the coefficients $a_1,\ a_2,\ a_3$ and the expression $a_3 - a_1 a_2$ depend on the model parameters b_1 and b_2. Figure 4.1 a shows that the region of interest, $b_1 < 1$, $b_2 < 1$, is split into two domains δ_1 and δ_2. In domain δ_1 all conditions of the Routh-Hurwitz criteria for stability (4.8) are met, so the coexistence state is stable if $(b_1, b_2) \in \delta_1$. However, in domain δ_2 the Routh-Hurwitz criteria for stability are violated, namely, $a_3 < 0$. This means that if $(b_1, b_2) \in \delta_2$ then the coexistence steady state is unstable and stationary periodic patterns are expected to form. This conclusion is confirmed by numerical simulations shown in Figure 4.1 b.

The shape and size of the domain δ_2 depend not only on the model parameters but also on the wavenumber k. An important question is: what is the domain δ_2, encompassing all possible (b_1, b_2) values that will trigger a breakdown of stability and the formation of patterns for a given set of model parameters D_1, D_2, r_1, r_2 and χ and any value of the wavenumber k? Formally, this domain is a union of domains for all possible values of k. However it can be estimated as a domain for the value of k, which gives the highest positive value for eigenvalue of matrix (4.5). Figure 4.2 a shows how the real part of this eigenvalue depends on the wavenumber for three values of chemotactic sensitivity χ. Wavenumber k corresponding to the most unstable mode for each of these plots is that giving their maxima. The domain δ_2 for this value of k could be considered as a domain of instability for given set of parameters. As we can see from Figure 4.2 a, as chemotaxtic sensitivity χ increases, the value of most unstable wavenumber also increases,

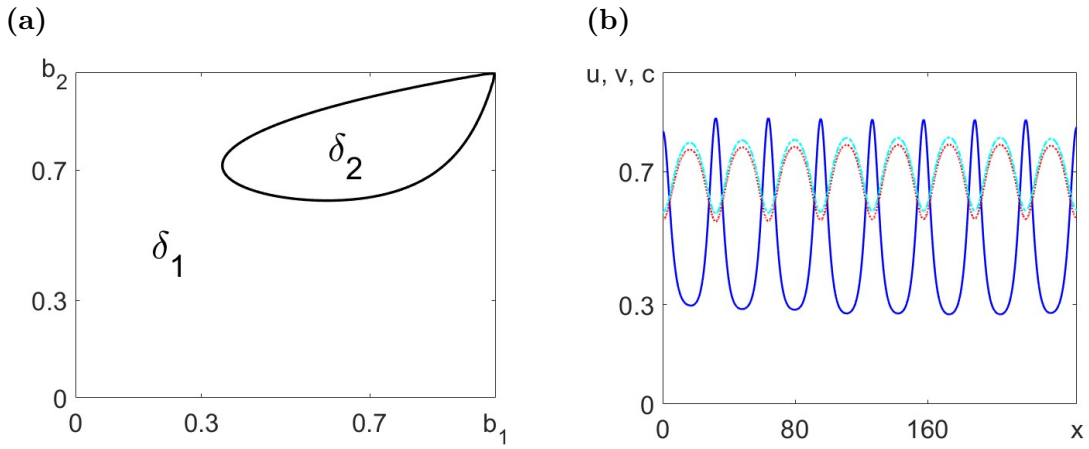

Figure 4.1: ***Stability of the coexistence steady state depending on interspecific competition.*** ***(a)****: Conditions (4.8) are verified for fixed parameters* $D_1 = D_2 = 1$, $r_1 = r_2 = 0.1$, $\chi = -10$ *and* $k = 0.2$, *in the region* $b_1,\ b_2 < 1$. *In domain* δ_2, *condition for* a_3 *is violated, i.e.* $a_3 < 0$. ***(b)****: stationary periodic pattern obtained from numerical simulations by fixing* $b_1 = b_2 = 0.7 \in \delta_2$. *Solid blue and dotted red lines represent the density of* u *and* v, *respectively. Dash-dotted cyan line shows the concentration profile of the chemical* c. *Initial conditions such that* $v(x,\ 0) = (b_2 - 1)/(b_1 b_2 - 1) + 0.1$ *for* $100 < x < 140$ *and* $(u,\ v,\ c)(x,\ 0)$ *is at coexistence everywhere else.*

resulting in smaller wavelengths and, consequently, more spikes. Additionally, as shown in the previous chapter, $k = \dfrac{i\pi}{L}$ satisfies the boundary conditions. The most unstable wavenumber can provide a rough estimate of how many spikes are expected in the system. For example, when $\chi = -10$, the most unstable wavenumber is $k = 0.2$. The number of half spikes can be predicted using $i = \dfrac{kL}{\pi}$; for a medium of length $L = 250$, $i \approx 16$, resulting in 8 full spikes. This prediction aligns well with the results shown in Figure 4.1 b.

Figure 4.2 b demonstrates another method for determining the domain δ_2 where the coexistence state of the system (4.4) becomes unstable. The presented analysis is performed using an assumption that $b_1 = b_2 = b$. As the loss of stability is associated with the sign change of a_3 (in (4.7)) we plot the line $a_3 = 0$ on (b, k) plane and note that a_3 is positive on the side of this plot corresponding to larger values of b. Minimal value of b on this plot gives the the minimal value of b in the domain δ_2. The way to find this value is to draw another line where the partial derivative $\dfrac{\partial a_3}{\partial k} = 0$. By examining the intersection between these two curves (see Figure 4.2 b), both the most unstable wavelength and the minimum value of b required for pattern formation can be found. For instance, in Figure 4.2 b, it can be observed that for $D_1 = D_2 = 1$, $r_1 = r_2 = 0.1$, and $\chi = -10$, the maximum size of δ_2 is reached when $k \approx 0.2$, which is consistent with the results

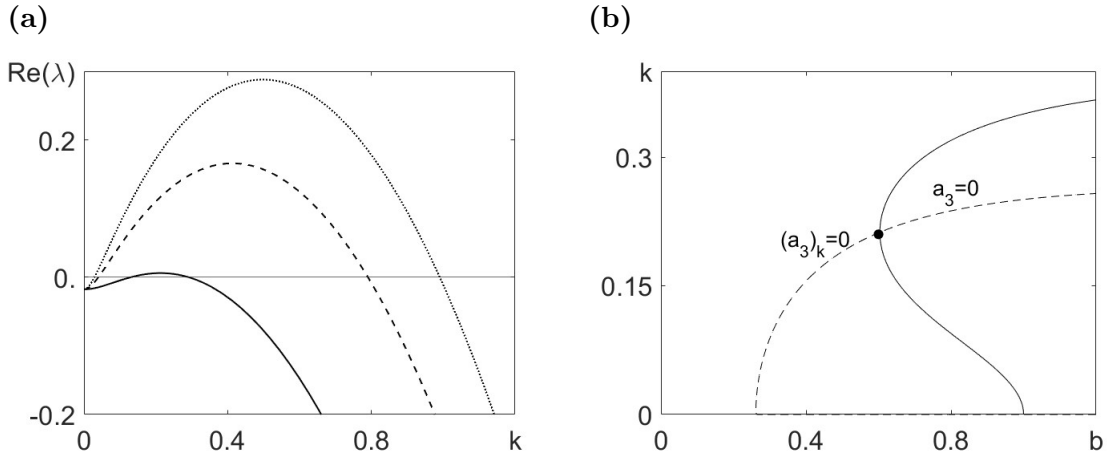

Figure 4.2: ***Most unstable wavenumber*** k ***for different chemotactic strengths and competition factors.*** ***(a)****: The real part of wavelength* λ *from equation* (4.7)*, as function of the wavenumber* k *for different chemotactic strengths:* $\chi = \{-10$ *(solid)* $, -50$ *(dashed)* $, -90$ *(dotted)* $\}$. ***(b)****: Minimum value of* b *that initiates formation of patterns and the most unstable wavenumber* k *that ensures maximal size of* δ_2*. Plots of parameter* a_3 *from* (4.8)*, such that* $a_3 = 0$ *(solid line) and derivative of* a_3 *with respect to* k*,* $(a_3)_k = 0$ *(dashed line). Fixed parameters:* $D_1 = D_2 = 1$*,* $r_1 = r_2 = 0.1$*,* $\chi = -10$ *and* $b_1 = b_2 = b$*.*

in Figure 4.2 a. Additionally, Figure 4.2 b predicts that the minimum value of the competition rate b needed to initiate periodic patterns is $b = 0.6$.

So far, using the Routh-Hurwitz criteria, we have identified a domain, δ_2 on the plane (b_1, b_2), where stationary periodic patterns are expected to emerge. Our next task is to examine how the size of this domain is affected by the remaining model parameters. We will perform this study using the technique illustrated in Figure 4.2 b, that is by assuming that both species exert the same competitive effect on one another, i.e. $b_1 = b_2 = b$, and examining the intersection point between $\dfrac{\partial a_3}{\partial k} = 0$ and $a_3 = 0$. In what follows we will use the following default set of parameters: $D_1 = D_2 = 1$, $r_1 = r_2 = 0.1$ and $\chi = -10$.

Model (4.4) accounts for two different diffusion coefficients, D_1 and D_2, corresponding to the two species u and v, respectively. Both analytical and numerical results show that fixing D_1 and varying D_2 has the same effect on the stability of the coexistence steady state as fixing D_2 and varying D_1. Figure 4.3 a shows how the minimal value of b in the domain δ_2 depends on the diffusion rate D_1 keeping the default values for other parameters. It shows a good match between the analytical and numerical results with both indicating that as diffusion increases the size of the domain δ_2 decreases and it disappears when $D_1 = 2.6$ (shown by the vertical dashed line) and indicating that no periodic patterns will form for diffusion values greater than this. If $D > 2.6$, then model (4.4) relaxes back to a

homogeneous state after disturbance.

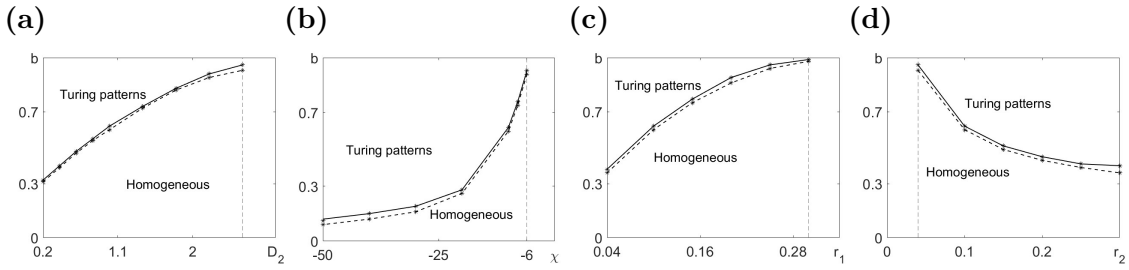

Figure 4.3: ***Domains for pattern formation after disturbance of the coexistence state in the weak competition case in model*** (4.4)**.** *Domains for the formation of stationary periodic patterns on the planes* ***(a)****:* (b, D_1)*;* ***(b)****:* (b, χ)*;* ***(c)****:* (b, r_1)*;* ***(d)****:* (b, r_2)*. Used default set of parameters:* $D_1 = D_2 = 1$*,* $r_1 = r_2 = 0.1$ *and* $\chi = -10$*. Solid lines represent results from numerical simulations of system* (4.4) *and dashed lines represent analytical results looking at the intersection between the two lines in Figure 4.2 b.*

In a similar manner, we have investigated the effects of chemotaxis on the size of the domain δ_2. Plots shown in Figure 4.3 b indicate that the minimal value of b increases (and, therefore, the size of δ_2 decreases) when the chemotactic response gets weaker (χ increases). This means that it is more likely to obtain periodic patterns for a stronger chemotactic response, while weaker chemotaxis can only result in the formation of travelling waves. Periodic patterns cannot be obtained if χ is below the threshold $\chi = -6$. Again, the shown plots indicate a good match between analytical and numerical results.

In Figure 4.3 c and d, the effects of species reproduction, r_1 and r_2, on the minimal value of b in the domain δ_2 are shown. We see that the reproduction rates r_1 and r_2 have opposite effects on the size of δ_2. Increasing r_1 results to the shrinkage of δ_2 with the threshold value of $r_1 = 0.3$ above which no periodic patterns can be obtained. On the other hand, increasing r_2 shows that the value of b decreasing and therefore the size of the domain δ_2 increasing. In this case, there is a threshold value $r_2 = 0.04$ below which no periodic patterns (only travelling waves) can be observed.

Thus far, classical Turing-type instability analysis has been employed to demonstrate the formation of stationary periodic patterns caused by disturbances to the coexistence steady state of model (4.4). The Routh-Hurwitz criteria have been used to show that, for fixed parameters, a domain of instability δ_2 exists, and any competition values within this domain will result in a breakdown of stability. The maximal size of this domain has been determined by identifying the most unstable wavenumber k, ensuring that all possible $(b_1,\ b_2)$ values are considered, along with the minimum value of $b = b_1 = b_2$ required for pattern formation.

4.2.2 Analysis of the extinction steady states

Now we investigate whether the pattern formation can take place in system (4.4) when the competion is not weak, that is when either $b_1 > 1$ and/or $b_2 > 1$. Linear analysis would point to this possibility if the stability of any of the extinction steady states, $(1, 0, 0)$ and $(0, 1, 1)$, is affected by the diffusion or advection terms. This implies that when $b_2 > 1$ periodic patterns can form if the steady state $(1, 0, 0)$ is unstable. Similarly, when $b_1 > 1$ periodic patterns can form if the steady state $(0, 1, 1)$ is driven unstable in the presence of diffusion and/or advection terms. Linear stability analysis involves examination of the eigenvalues of the characteristic matrix (4.5) evaluated at each extinction steady state to identify conditions under which at least one eigenvalue has a positive real part. The analysis of the steady state $(1, 0, 0)$ is done by investigating the eigenvalues of the characteristic matrix (4.5) evaluated at $(n, v, c) = (1, 0, 0)$, i.e.:

$$M_{(1,0,0)} = \begin{pmatrix} -D_1k^2 - r_1 & -r_1b_1 & -\chi k^2 \\ 0 & -D_2k^2 - r_2(b_2 - 1) & 0 \\ 0 & 1 & -1 - k^2 \end{pmatrix}, \tag{4.9}$$

which has 3 eigenvalues:

$$\begin{cases} -1 - k^2, \\ -D_1k^2 - r_1, \\ -D_2k^2 - r_2(b_2 - 1), \end{cases} \tag{4.10}$$

with negative real parts if $b_2 > 1$. This means that the steady state $(1, 0, 0)$ remains stable when perturbed in the full reaction-diffusion-advection system and we should not expect formation of stationary patterns from this state. This result also holds for the other extinction steady state, $(0, 1, 1)$: if $b_1 > 1$ this steady state is stable irrespective on the strengths of both diffusions and chemotaxis.

One characteristic of the periodic patterns obtained so far is that they have formed from infinitesimal perturbations, meaning that as long as the conditions for the breakdown of stability have been met, the size of the perturbation did not matter and has not been a factor to consider. However, when investigating the steady state $(1, 0, 0)$, one question to consider is whether a large enough perturbation in the second species, v, would result in the formation of patterns, or if the perturbation would decay and the system would return to being homogeneous. The biological idea behind this is that in experiments, if the starting point were a Petri dish with a species of bacteria, u, distributed homogeneously, introducing a large enough quantity of the second species of bacteria, v, could produce enough chemotactic agent to start repelling the first species, and with the aid of competition, the second species could survive and reproduce. The repulsion of the first

species, u, by the chemical, c, could launch the aggregation and hence, the formation of spots. In order to test this hypothesis, computational simulations have been performed with fixed parameters: $D_1 = D_2 = 1$, $\chi = -10$, $r_1 = r_2 = 0.1$, $b_1 = 0.7$, $b_2 = 1.7$, such that $b_2 > 1$ and $v = 0 + \tilde{v}$, where the perturbation $\tilde{v} = 0.9$. Simulated profiles are shown in Figure 4.4.

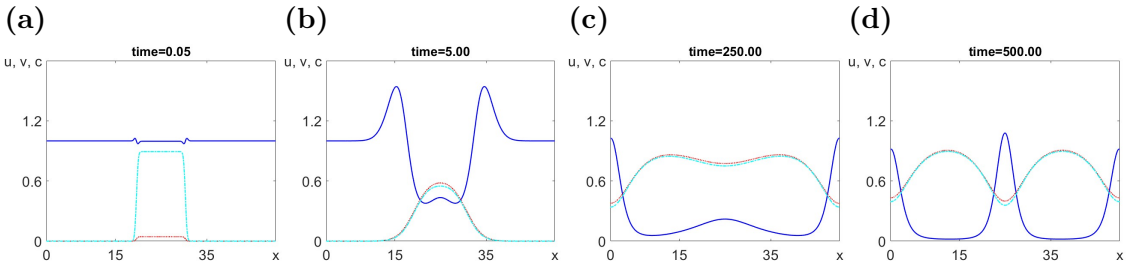

Figure 4.4: ***Simulation of pattern formation from system*** (??) ***in the weak-strong competition case when*** $b_2 > 1$***.*** ***(a)****: An initially large perturbation of the steady state* $(1, 0, 0)$ *(dash-dotted cyan line).* ***(b)****: v starts producing a chemical agent c (dotted red line) which repels species u (solid blue line).* ***(c)****: Density of u slowly starts increasing in the middle, while the density of v and concentration of c slowly start decaying* ***(d)****: Stationary pattern consisting of two full spikes has formed. Parameter values:* $D_1 = D_2 = 1$, $r_1 = r_2 = 0.1$, $\chi = -10$, $b_1 = 0.7$, $b_2 = 1.7$, *medium size,* $L = 50$, *and initial conditions such as:* $v(x, 0) = 0.9$ *for* $20 < x < 30$ *and* $(u, v, c)(x, 0) = (1, 0, 0)$ *for* $x < 20$ *and* $x > 30$.

Figure 4.4 shows that, contrary to linear analysis, stationary periodic patterns can emerge from finite perturbation of the stable extinction steady state $(1, 0, 0)$. An important characteristic of this pattern is that aggregation can only be initiated by the perturbation of species v. Perturbing species u, or the chemical c, results in the system decaying back to homogeneity, regardless of the amplitude of the perturbation. This leads us to the next question, which is how the minimal amplitude required for pattern formation is affected by changes in the model parameters.

Next, with the aid of computational simulations, the effect of model parameters on the minimal perturbation amplitude required for pattern formation is investigated. The default set of model parameters used in these simulations are: $D_1 = D_2 = 1$, $r_1 = r_2 = 0.1$, $\chi = -10$, $b_1 = 0.7$, $b_2 = 1.7$ and medium size, $L = 50$. By varying these parameters one at a time, we note the minimal amplitude required for a breakdown of stability. It is also important to note that, unlike patterns around the coexistence steady state, travelling waves do not emerge from the extinction steady state. This means that, depending on the amplitude of the perturbation, the system can exhibit pattern formation or return to a homogeneous state.

The plots in Figure 4.5 a show the minimum perturbation amplitude required in simulations for periodic patterns to emerge from the extinction steady state $(1, 0, 0)$ when both diffusion coefficients are varied one at a time and the other parameters are fixed. We see that the impacts of diffusion coefficients are similar with the increase of the threshold perturbation, $\tilde{v}$, with the increase of the diffusion. An important observation is that for $D_1 > 1.3$ or $D_2 > 1.3$, the system does not show the formation of patterns, meaning that from any perturbation the system relaxes back to homogeneous state.

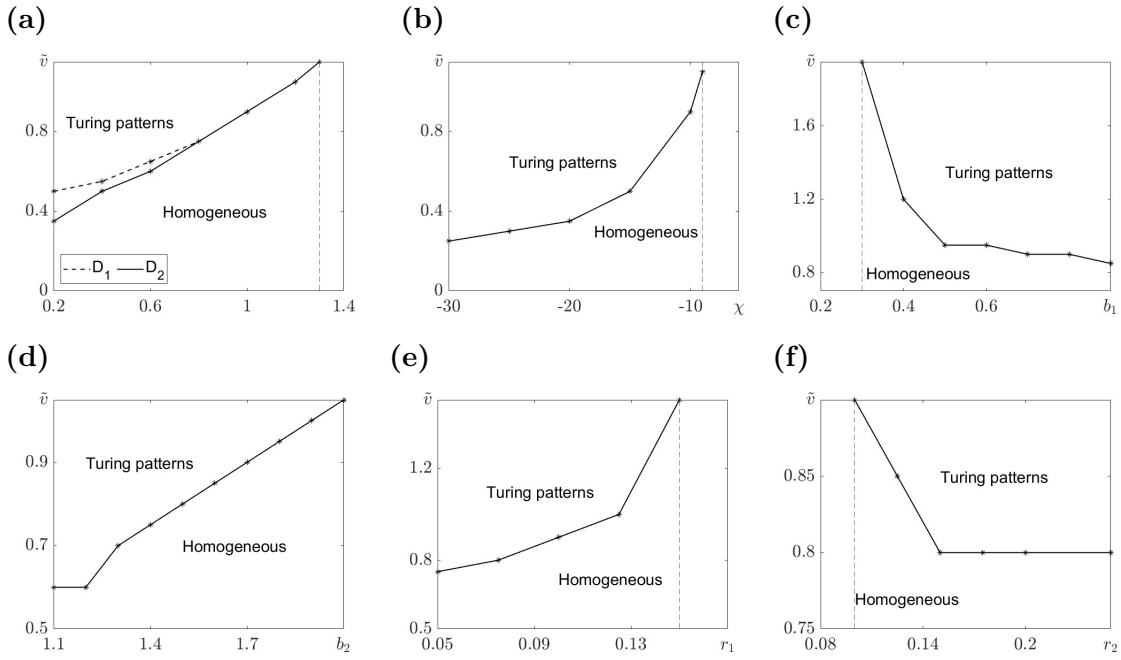

Figure 4.5: ***The dependence of the minimal perturbation amplitude,*** $\tilde{v}$***, from the steady state*** $(1, 0, 0)$***, required to generate periodic patterns, on the model parameters.*** *Dependence on the diffusion coefficients (panel* (a)*), chemotactic sensitivity (panel* (b)*), competition strength* b_1 *(panel* (c)*), and* b_2 *(panel* (d)*), reproduction rate* r_1 *(panel* (e)*) and* r_2 *(panel* (f)*). Default set of parameters:* $D_1 = D_2 = 1$*,* $\chi = -10$*,* $r_1 = r_2 = 0.1$*,* $b_1 = 0.7$ *and* $b_2 = 1.7$*. Results from numerical simulations of system* (4.4)*.*

The effect of chemotaxis on the perturbation amplitude is shown by the plot in Figure 4.5 b. For chemoattraction, or weak chemorepulsion, when $\chi > -9$, the system cannot be perturbed from the homogeneous state, no matter how large the perturbation is. However, for stronger chemorepulsion, when $\chi < -9$, the system can be transformed into inhomogeneous state provided the disturbance is large enough. As chemorepulsion increases, a smaller perturbation amplitude is needed to generate pattern formation.

Similarly, the effects of reproduction rates on the threshold perturbation am-

plitude are also investigated with the results presented in Figure 4.5 c and d . It appears that the two reproduction coefficients, r_1 and r_2, corresponding to species u and v, respectively, have opposite effects on the threshold amplitude. If the reproduction rate of the species u is high ($r_1 > 0.15$), then the system cannot be transformed into stationary inhomogeneous state no matter how large is perturbation. Additionally, as r_1 decreases, the minimal perturbation amplitude required for the formation of stationary periodic pattern decreases, meaning that if u reproduces more slowly, it is more likely to initiate aggregation through perturbation. On the other hand, if $r_2 < 0.1$, no pattern formation in the system can be observed. Moreover, as r_2 increases, the amplitude required for a breakdown of stability decreases, converging to $\tilde{v} = 0.8$ for $r_2 \geq 0.15$.

The effect of the competition rates, b_1 and b_2, on the threshold perturbation amplitude is presented by plots in Figure 4.5 e and f. Numerical results show that pattern can form only if b_1 is large enough, $b_1 \geq 0.3$. if $b_1 < 0.3$, the system relaxes back to a homogeneous state from any initial state. Conversely, as b_2 increases, the perturbation amplitude required for instability also increases. This means that, in order to initiate pattern formation, higher competition of u on v, represented by b_2, requires a larger disturbance for species v to survive and reproduce.

In this section, we have shown that, contrary to linear analysis, which suggests that the steady state $(1, 0, 0)$ of system (4.4) remains stable if $b_2 > 1$, stationary inhomogeneous pattern can emerge in the system (4.4) from a finite amplitude disturbance of this steady state. This phenomenon has been demonstrated in numerical simulations. Using numerical simulations, the effect of model parameters on the minimum perturbation amplitude required to generate a breakdown of stability and, consequently, pattern formation has been investigated. We have also found that if the strong-weak competition case when $b_2 < 1$ and $b_1 > 1$ we don't observe pattern formation no matter what initial conditions are set.

While linear analysis focuses on the breakdown of stability and formation of inhomogeneous patterns, Fourier analysis can be used to describe the pattern once it has formed and stabilized. In particular, Fourier analysis can be applied to obtain information about the pattern's characteristics, such as amplitude and wavelength.

4.3 Fourier analysis of patterns obtained in numerical simulations

In this section we will focus on Fourier series representing stationary periodic patterns obtained in numerical simulations, like those shown in Figure 4.1 b and

Figure 4.4 d. As the stationary pattern is that which does not change over time, it satisfies the simplified version of model (4.4):

$$\begin{cases} D_1 u_{xx} - \chi(uc_x)_x + r_1 u(1 - u - b_1 v) = 0, \\ D_2 v_{xx} + r_2 v(1 - v - b_2 u) = 0, \\ c_{xx} + v - c = 0, \end{cases} \tag{4.11}$$

and can be represented by Fourier series:

$$\begin{cases} u = \sum_{i=0}^{M} \alpha_i \cos\left(\frac{i\pi}{L} x\right), \\ v = \sum_{i=0}^{M} \gamma_i \cos\left(\frac{i\pi}{L} x\right), \\ c = \sum_{i=0}^{M} \beta_i \cos\left(\frac{i\pi}{L} x\right). \end{cases} \tag{4.12}$$

The coefficients α_i, γ_i and β_i define the amplitudes of mode i for the variables u, v and c. For smooth profiles, these coefficients quickly tend to zero as i increases, allowing us to truncate the series by considering only the first M terms, where M should be carefully chosen. For a known profile, $u(x)$, the coefficients are found using the formulas:

$$\alpha_0 = \frac{1}{L} \int_0^L u(x) dx,$$

and for $i > 0$

$$\alpha_i = \frac{2}{L} \int_0^L u(x) \cos \frac{i\pi x}{L} dx. \tag{4.13}$$

In the rest of this chapter, we will focus on profiles $u(x)$ (and coefficients α_i), keeping in mind that the analysis of the profiles $v(x)$ and $c(x)$ is done in the same way.

Formulas (4.13) can be used for the spectral decomposition of patterns obtained numerically. A typical stationary solution obtained from numerical simulations of the system (4.4) is shown in Figure 4.1 b. Spectral decomposition of this profile reveals that only four modes have reasonably high coefficients:

$$\begin{cases} \alpha_0 = 0.4777, \ \alpha_{16} = 0.2445, \ \ \alpha_{32} = 0.0842, \quad \alpha_{48} = 0.0225; \\ \gamma_0 = 0.6719, \ \gamma_{16} = -0.1024, \ \gamma_{32} = -0.0145, \ \gamma_{48} = -0.0010; \\ \beta_0 = 0.6719, \ \beta_{16} = -0.0984, \ \beta_{32} = -0.0124, \ \beta_{48} = -0.0006, \end{cases} \tag{4.14}$$

while all other coefficients are considerably smaller (all other α-s are less than 0.01). α_0 represents the average level of u for the entire pattern, α_{16} defines the amplitude of the mode with a characteristic length of 1/16th of the domain size, which corresponds to the 8 spikes observed. This matches the number of spikes

seen in Figure 4.1 b. Finally, α_{32} and α_{48} correspond to the second and third harmonics of the main harmonic given by α_{16}. Thus, the amplitude of the pattern shown in Figure 4.1 b can be estimated as $2\alpha_{16}$. Varying the size of the domain will change the number of observed spikes but will not affect their amplitude or spatial periodicity. This is illustrated by the patterns shown in Figure 4.6 b and c, which are obtained in simulations of smaller domains where only half (b) and one (c) spike can fit.

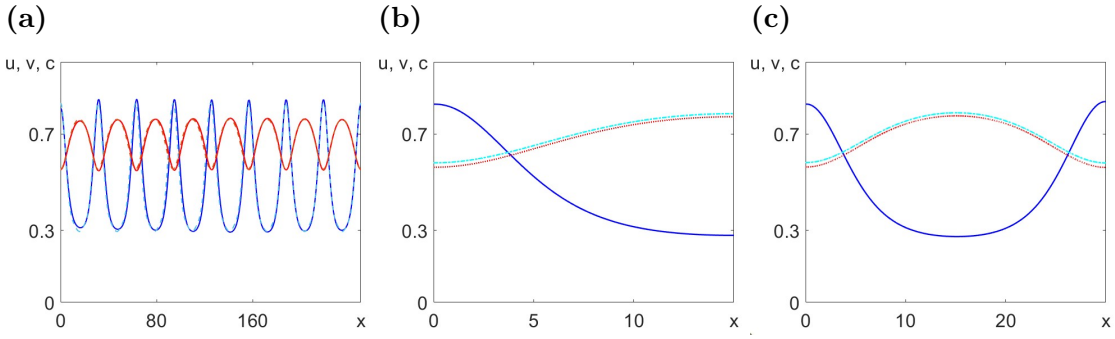

Figure 4.6: ***Numerical simulations of the stationary patterns formed in model (4.4) for different medium lengths.*** ***(a)****: Comparison between the numerical profile from simulations (solid) and the profile including only the highest three modes (dashed) given in* (4.14) *for a large medium* $L = 250$. ***(b)****: Reduced medium length such that only half a spike produced* $L = 15$. ***(c)****: Full spike for medium length* $L = 30$. *Blue and red lines represent the densities of* u *and* v*, respectively, while cyan lines the concentration of the chemical* c. *Used parameter values:* $D_1 = D_2 = 1$, $r_1 = r_2 = 0.1$, $\chi = -10$ *and* $b_1 = b_2 = 0.7$.

Patterns occurring in a small domain (like those shown in Figure 4.6 b and c) are of particular interest, as the corresponding Fourier series can be truncated at a reasonably low value of M (see Eq. (4.12)). Using Fourier decomposition of numerically obtained patterns, we investigated how the coefficients of Fourier modes depend on the domain size. In Fig. 4.7, we show plots of α_i for $i = 0, 1, 2, 3, 4, 6, 9$ against the domain size, L, which varies from 0 to 50. We observe that while α_0 does not vary much (staying in the range between 0.5 and 0.6) and the omitted α-coefficients are always negligibly small, the displayed coefficients vary significantly. For $L < 10$, $\alpha_0 = 0.6$ and all other coefficients are zero, indicating that the system is in a homogeneous state with no spikes formed. For $10 < L < 20$, the first coefficient, α_1, is larger than any subsequent coefficient ($\alpha_1 > \alpha_i$, $\forall i > 1$), reflecting the fact that only half of a spike can fit in. Within this range of domain sizes, the value of α_1 increases from zero, reaches a maximum value $\alpha_1 (= \alpha_{\max}) = 0.2445$ at $L = 15$, and then decreases to zero. This domain size, which corresponds to the maximal value of α_1, will be considered the characteristic length (or half-wavelength) of the periodic pattern and will be

denoted as Λ_0, i.e., $\Lambda_0 = 15$ for the system (4.4) with the model parameters used in simulations to produce Figure 4.7.

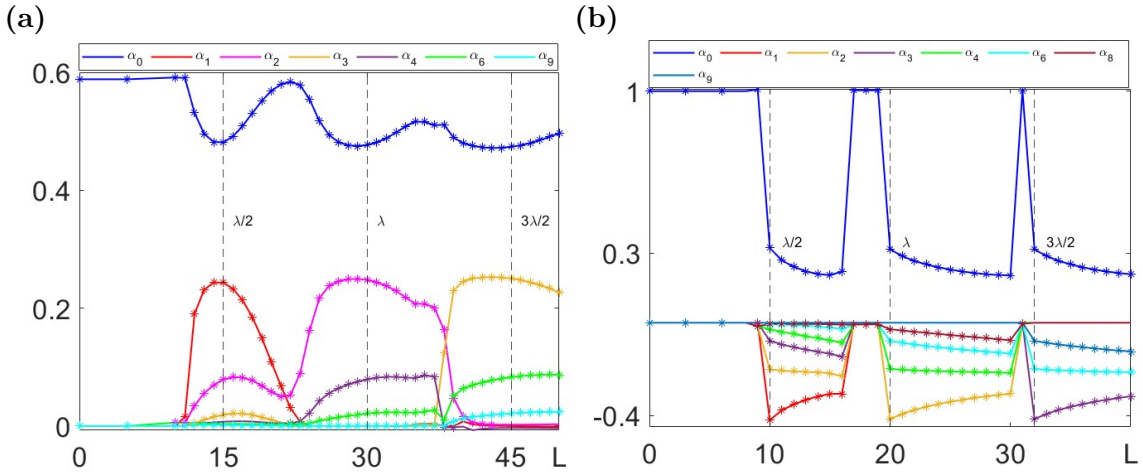

Figure 4.7: ***Dependence of Fourier coefficients*** α_i ***on medium size*** L ***for numerically simulated*** u***-profiles in model*** (4.4)***.*** *For patterns forming* ***(a)****: in weak competition case,* $b_2 = 0.7$ *and* ***(b)*** *in weak-strong competition case,* $b_2 = 1.7$*. Other model parameter:* $D_1 = D_2 = 1$*,* $r_1 = r_2 = 0.1$*,* $\chi = -10$*,* $b_1 = 0.7$*.*

As we seen earlier, stationary periodic patterns in the system (4.4) form under two regimes: in the case of weak competition ($b_1 < 1$ and $b_2 < 1$, see Figure 4.1 b and Figure 4.6) and in the case of weak-strong or strong competition when $b_2 > 1$. In the latter case despite the stability of homogeneous state $(1, 0, 0)$ we observe the formation of stationary periodic patterns (see Figure 4.4). Characteristics of the patterns forming in these two regimes are significantly different. Figure 4.7 b shows how the first 9 α-coefficients describing u-profile in the pattern obtained for $b_2 > 1$ depend on the medium size. As we can see the spectral decomposition of the profiles in panel (b) is considerable different from those shown in the panel (a). For $L \in [10, 17)$, α_1 is the largest mode and in this case only half of the spike can fit into the simulated medium. We note that α_0 drops significantly when pattern forms: for $L \in [17, 20)$, $\alpha_0 = 1$ is the only non-zero coefficient, meaning the system relaxes back to a homogeneous steady state. For $L \in [20, 30]$, α_2 is the highest frequency mode, and patterns emerging for medium lengths in this region will exhibit one full spike. Additionally, the fastest-growing mode corresponds to $L = 20$, as α_2 is largest at this point.

So far, we have shown that we can use Fourier decomposition to obtain information about the amplitude and wavelength of a stationary periodic pattern obtained in numerical simulations and express the solution of system (4.4) as a Fourier series. Our next aim is to to solve this system analytically by finding out

the Fourier coefficients of solution to the system (4.11).

4.4 Analytical solution represented by Fourier series

The analytical solution of the system (4.11) can be found using substitution (4.12), which transforms this system into:

$$\begin{cases} -D_1 \sum_{i=0}^{M} (ik)^2 \alpha_i \cos(ikx) + \chi \dfrac{\partial}{\partial x} \left(\sum_{i=0}^{M} \alpha_i \cos(ikx) \sum_{i=0}^{M} ik\beta_i \sin(ikx) \right) = 0 \\ \qquad\qquad + r_1 \sum_{i=0}^{M} \alpha_i \cos(ikx) \left(1 - \sum_{i=0}^{M} \alpha_i \cos(ikx) - b_1 \sum_{i=0}^{M} \gamma_i \cos(ikx) \right), \\ -D_2 \sum_{i=0}^{M} (ik)^2 \gamma_i \cos(ikx) + r_2 \sum_{i=0}^{M} \gamma_i \cos(ikx) \left(1 - \sum_{i=0}^{M} \gamma_i \cos(ikx) - b_2 \sum_{i=0}^{M} \alpha_i \cos(ikx) \right) = 0, \\ -\sum_{i=0}^{M} (ik)^2 \beta_i \cos(ikx) + \sum_{i=0}^{M} \gamma_i \cos(ikx) - \sum_{i=0}^{M} \beta_i \cos(ikx) = 0, \end{cases} \tag{4.15}$$

where $k = \pi/L$. Truncation of the system (4.15) at $M = 0$ gives the system of three algebraic equations:

$$\begin{cases} r_1 \alpha_0 (1 - \alpha_0 - b_1 \gamma_0) = 0, \\ r_2 \gamma_0 (1 - \gamma_0 - b_2 \alpha_0) = 0, \\ \gamma_0 - \beta_0 = 0, \end{cases} \tag{4.16}$$

which has four solutions:

$$(\alpha_0,\ \gamma_0,\ \beta_0) = \left\{ (0,0,0),\ (1,0,0),\ (0,1,1),\ \left(\frac{b_1 - 1}{b_1 b_2 - 1}, \frac{b_2 - 1}{b_1 b_2 - 1}, \frac{b_2 - 1}{b_1 b_2 - 1} \right) \right\},$$

corresponding to the steady states of model (4.4), as expected. Note, that the third equation in the system (4.15) gives:

$$-(ik)^2 \beta_i + \gamma_i - \beta_i = 0 \Longrightarrow \beta_i = \frac{\gamma_i}{1 + (ik)^2}, \tag{4.17}$$

which allows to reduce the system to equations in terms of unknowns α_i and γ_i. Truncating the system (4.15) at $M > 0$ we get $2M$ simultaneous equations that

need to be solved:

$$
\begin{cases}
\alpha_0 - \alpha_0^2 - \sum_{i=1}^{M} \frac{\alpha_i^2}{2} - b_1 \left(\alpha_0\gamma_0 + \sum_{i=1}^{M} \frac{\alpha_i\gamma_i}{2} \right) = 0, \\
\gamma_0 - \gamma_0^2 - \sum_{i=1}^{M} \frac{\gamma_i^2}{2} - b_2 \left(\alpha_0\gamma_0 + \sum_{i=1}^{M} \frac{\alpha_i\gamma_i}{2} \right) = 0, \\
-D_1\alpha_1 k^2 + \chi k^2 \left(\alpha_0\beta_1 + \sum_{i=1}^{M-1} \frac{i+1}{2}\alpha_i\beta_{i+1} - \sum_{i=2}^{M} \frac{i-1}{2}\alpha_i\beta_{i-1} \right) - \\
\qquad r_1 b_1 \left(\alpha_0\gamma_1 + \alpha_1\gamma_0 + \sum_{i=1}^{M-1} \left(\frac{\alpha_i\gamma_{i+1}}{2} + \frac{\alpha_{i+1}\gamma_i}{2} \right) \right) + \\
\qquad r_1 \left(\alpha_1 - 2\alpha_0\alpha_1 - \sum_{i=1}^{M-1} \alpha_i\alpha_{i+1} \right) = 0, \\
-D_2\gamma_1 k^2 - r_2 b_2 \left(\alpha_0\gamma - 1 + \alpha_1\gamma_0 + \sum_{i=1}^{M-1} \left(\frac{\alpha_i\gamma_{i+1}}{2} + \frac{\alpha_{i+1}\gamma_i}{2} \right) \right) + \\
\qquad r_2 \left(\gamma_1 - 2\gamma_0\gamma_1 - \sum_{i=1}^{M-1} \gamma_i\gamma_{i+1} \right) = 0, \\
-4D_1\alpha_2 k^2 + \chi k^2 \left(4\alpha_0\beta_2 + \alpha_1\beta_1 + \sum_{i=1}^{M-2} (i+2)\alpha_1\beta_{i+2} - \sum_{i=3}^{M} (i-2)\alpha_i\beta_{i-2} \right) - \\
\qquad r_1 b_1 \left(\alpha_0\gamma_2 + \alpha_2\gamma_0 + \frac{\alpha_1\gamma_1}{2} + \sum_{i=1}^{M-2} \left(\frac{\alpha_i\gamma_{i+2}}{2} + \frac{\alpha_{i+2}\gamma_i}{2} \right) \right) + \\
\qquad r_2 \left(\alpha_2 - \frac{\alpha_1^2}{2} - 2\alpha_0\alpha_2 - \sum_{i=1}^{M-2} \alpha_i\alpha_{i+2} \right) = 0, \\
-4D_2\gamma_2 k^2 - r_2 b_2 \left(\alpha_0\gamma_2 + \alpha_2\gamma_0 + \frac{\alpha_1\gamma_1}{2} + \sum_{i=1}^{M-2} \left(\frac{\alpha_i\gamma_{i+2}}{2} + \frac{\alpha_{i+2}\gamma_i}{2} \right) \right) + \\
\qquad r_2 \left(\gamma_2 - \frac{\gamma_1^2}{2} - 2\gamma_0\gamma_2 - \sum_{i=1}^{M-2} \gamma_i\gamma_{i+2} \right) = 0, \\
...
\end{cases}
\tag{4.18}
$$

where the first two equations represent the balance for coefficients of $\cos(0)$, the third and fourth equations - for the coefficients of $\cos(kx)$, the following two equations - the coefficients of $\cos(2kx)$ and so on up to coefficients of $\cos(Mkx)$.

Analytical solutions expressed in terms of model parameters for the simultaneous system (4.18) cannot be found for $M \geq 1$, but numerical values of α_i, γ_i, and β_i can be determined with the aid of Maple for any given set of model parameters D_1, D_2, χ, r_1, r_2, b_1, and b_2. This method can be used to compare the Fourier series coefficients obtained analytically by solving system (4.18) with those obtained through Fourier decomposition of the simulated profile, as presented in Figure 4.7. To quantify the difference between the profiles obtained from sim-

ulations and those predicted analytically, the error between the two curves is calculated using the formula:

$$ER = \int_0^L (P_A - P_N)^2 dx, \tag{4.19}$$

where P_A represents the profile found analytically as a solution of the system (4.18) and P_N - the profile from numerical simulations.

Figure 4.7 shows that the half-wavelength of the periodic pattern obtained numerically using parameter values: $D_1 = D_2 = 1$, $r_1 = r_2 = 0.1$, $\chi = -10$, and $b_1 = b_2 = 0.7$ is equal to 15. In addition, this figure indicates that for an accurate approximation of the profile $u(x)$, coefficients up to and including α_3 need to be considered. For the fixed parameters mentioned, we have used Maple to find coefficients up to and including α_3 (to describe the profile $u(x)$) and γ_3 (to describe the profile $v(x)$) by solving the system (4.18) for the medium of size, $L = 15$, using truncations at $M = 1, 2, 3$. Found solutions for α-s are presented in Table 4.1.

$L = 15$	α_0	α_1	α_2	α_3
Numerical	0.4813	0.2431	0.0787	0.0191
$M = 1$	0.1878	0.3330	0	0
$M = 2$	0.4753	0.2446	0.0961	0
$M = 3$	0.4702	0.2532	0.0849	0.0241

Table 4.1: ***First four Fourier coefficients describing*** u***-profile in the case of weak competition****. Numerical coefficients are obtained by Fourier decomposition of the profile* $u(x)$ *obtained in simulations of system* (4.4) *and shown in Fig.4.6(b), while analytical coefficients are obtained by solving system (4.18) truncated at* $M = 1, 2$ *and* 3*. Model parameters:* $D_1 = D_2 = 1,\ r_1 = r_2 = 0.1,\ \chi = -10,\ b_1 = b_2 = 0.7$ *and medium length* $L = 15$*.*

Analysing the coefficients presented in Table 4.1, one can clearly see that truncating at $M = 1$, including only α_0 and α_1, does not accurately reproduce the corresponding coefficients found from numerical simulations. However, increasing the truncation to $M = 2$, such that the simultaneous system is extended to solve for α_0, α_1, and α_2, produces a much better match to Fourier decomposition of simulated profiles. Our next aim is to determine how many α coefficients are needed to accurately reproduce the pattern shown by the curve $u(x)$. It is difficult to say whether increasing the truncation further, with $M > 2$, would result in a better match between numerical and analytical results. To quantify the discrepancy and better visualise the difference between the numerical and

analytical profiles, the numerical profile is compared against the four analytical profiles obtained from different truncations, and the error between the two curves is calculated according to (4.19).

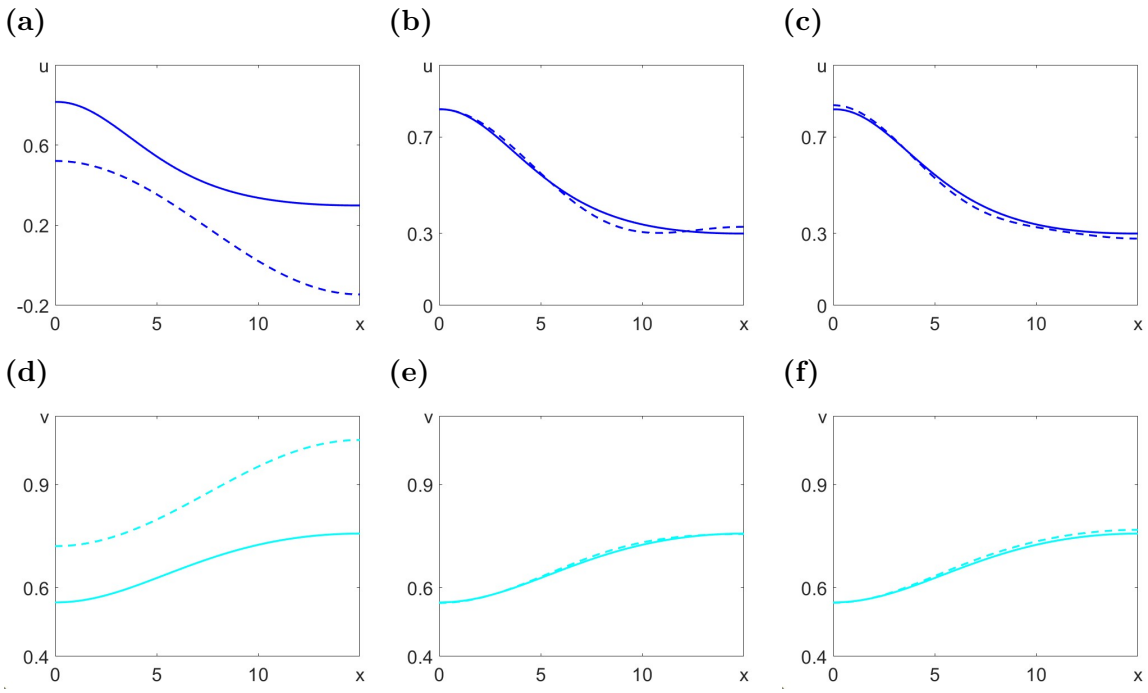

Figure 4.8: ***Comparison between the numerical and analytical profiles of*** $u(x)$ ***and*** $v(x)$***.*** ***(a)****: Numerical u-profile (solid) versus analytical u-profile (dashed) obtained by truncating the system* (4.18) *at* $M = 1$*. Error between the curves is* $ER = 1.3830$*.* ***(b)****: Increasing the truncation to* $M = 2$ *significantly reduces the error between the numerical and analytical u-profiles to* $ER = 0.0061$*.* ***(c)****: Further increase in truncation to* $M = 3$ *reduces the error between the two curves to* $ER = 0.0035$*. Similar results for v-profiles: truncation at* $M = 1$ *with error* $ER = 0.6566$ *on panel* ***(d)****,* $M = 2$ *with error* $ER = 0.0003$ *on panel* ***(e)*** *and* $M = 3$ *with error* $ER = 0.0009$ *on panel* ***(f)****. Parameter values:* $D_1 = D_2 = 1,\ r_1 = r_2 = 0.1,\ \chi = -10$ *and* $b_1 = b_2 = 0.7$*.*

Figure 4.8 a-c show that solving the system (4.18) for $M = 3$ is sufficient to accurately reproduce the $u(x)$ pattern, as increasing the truncation further to $M = 4$ results in solving a system of 10 simultaneous equations, which is more computationally expensive and does not significantly affect the error between the two curves. This result matches the one obtained through the numerical integration of the profile from simulations, as Figure 4.7 a shows that only coefficients up to and including α_3 influence the amplitude of the half spike. A similar analysis is performed for the pattern produced by the second species, $v(x)$, which has a smaller amplitude compared to that of the first species, $u(x)$ (see Figure 4.8 d-f).

Patterns forming in the case when $b_2 > 1$ can also be found as solutions

of the system (4.15). Again for $M > 0$ these solutions can't be expressed as an explicit function of model parameters. However, numerical solutions can be found for fixed set of parameter values with the aid of Maple. We have made such calculations for the set of parameter values $D_1 = D_2 = 1$, $r_1 = r_2 = 0.1$, $\chi = -10$, $b_1 = 0.7$, $b_2 = 1.7$ and truncations $M = 1, 2, 3$ and 4 of the system (4.18). In Table 4.2 obtained α coefficients (for a medium length $L = 10$, representing the half-wavelength of the numerically simulated pattern) are compared against coefficients found by Fourier decomposition of the numerical solution represented in Figure 4.7 b. It is evident that the truncation at $M = 1$ gives a significant discrepancy between the numerical and analytical coefficients, indicating that the truncation needs to be increased to include contributions from higher frequency modes. The coefficients obtained by truncating the series at $M = 2, 3$ and 4 provide much better approximations of the numerical ones, suggesting that this analytical solution is a closer representation of the numerical solution. It is evident from comparison of the u-profiles, representing solutions of (4.18) with the profile obtained in numerical simulations. The discrepancy between these profiles can be calculated using equation (4.19).

$L = 10$	α_0	α_1	α_2	α_3	α_4
Numerical	0.3234	-0.4206	0.2015	-0.0779	0.0283
$M = 1$	0.6419	-0.5806	0	0	0
$M = 2$	0.3248	-0.4128	0.2878	0	0
$M = 3$	0.3139	-0.4367	0.2208	-0.1080	0
$M = 4$	0.3208	-0.4419	0.2241	-0.0916	0.0342

Table 4.2: ***First five Fourier coefficients describing*** u***-profile in the case when the competition is not weak.*** *Numerical coefficients are obtained by Fourier decomposition of the simulated profile* $u(x)$*, while analytical coefficients are obtained by solving system (4.18) truncated at* $M = 1, 2, 3$ *and* 4*. Parameter values:* $D_1 = D_2 = 1$, $r_1 = r_2 = 0.1$, $\chi = -10$, $b_1 = 0.7$, $b_2 = 1.7$ *and medium length* $L = 10$*.*

Figure 4.9 provides a graphical comparison between the numerical profile from simulations and the analytical profiles given as solutions of the system (4.18), in the strong competition case when $b_2 > 1$. As expected, Figure 4.9 a shows a significant difference between the profile from simulations and the profile given by the Fourier series truncated at $M = 1$, with the discrepancy between the two curves being $ER = 1.3928$. In Figure 4.9 b, with $M = 2$ such that coefficient $\alpha_2 \neq 0$, there is a considerable improvement in the shape of the analytical profile,

as well as a reduction in the discrepancy between the two curves, which is now $ER = 0.0717$. The analytical profile in Figure 4.9 c represents the Fourier solution when the series for u is truncated at $M = 3$, and the error between the curves is further reduced to $ER = 0.0155$. Increasing the truncation further in Figure 4.9 d does not significantly improve the error between the two curves, $ER = 0.0113$, but it does produce a smoother analytical profile. Since increasing to $M = 4$ did not have a substantial effect on the discrepancy between the curves, we conclude that truncation at $M = 4$ is sufficient to capture the analytical solution corresponding to species $u(x)$ that emerges when $b_2 > 1$.

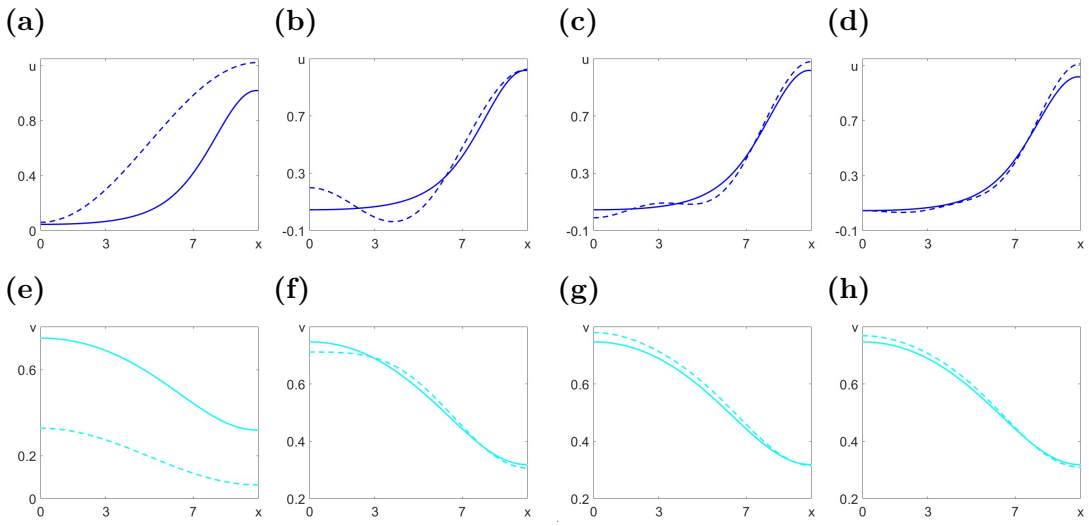

Figure 4.9: ***Comparison between the numerical and analytical profiles of*** $u(x)$ ***and v(x).*** ***(a)****: Numerical u-profile (solid) versus analytical u-profile (dashed) obtained by truncating the system* (4.18) *at* $M = 1$*. Error between the curves is* $ER = 1.3928$*.* ***(b)****: Increasing the truncation to* $M = 2$ *significantly reduces the error between the numerical and analytical curves to* $ER = 0.0717$*.* ***(c)****: Further increase in truncation to* $M = 3$ *reduces the error between the two curves further to* $ER = 0.0155$*.* ***(d)****: Increasing the truncation to* $M = 4$ *does not have a significant effect on the difference between the two curves,* $ER = 0.0113$*, but makes a smoother analytical profile. Fixed parameters:* $D_1 = D_2 = 1$, $r_1 = r_2 = 0.1$, $\chi = -10$ *and* $b_1 = 0.7$, $b_2 = 1.7$*. Similar results for v-profiles: truncation at* $M = 1$ *with error* $ER = 1.3482$ *on panel* ***(e)****,* $M = 2$ *with error* $ER = 0.0031$ *on panel* ***(f)****,* $M = 3$ *with error* $ER = 0.0047$ *on panel* ***(g)*** *and* $M = 4$ *with error* $ER = 0.0019$ *on panel* ***(h)****. Parameter values:* $D_1 = D_2 = 1$, $r_1 = r_2 = 0.1$, $\chi = -10$, $b_1 = 0.7$ *and* $b_2 = 1.7$.

In this section we has demonstrated that nonlinear Fourier analysis is a powerful method for describing the periodic patterns forming in the model (4.4). We obtained Fourier coefficients describing profiles for the species, u and v, both in weak and non-weak competition cases. We have found that these coefficients

found as roots of the algebraic system (4.18) is in good agreement with those found by Fourier decomposition of profiles found in numerical simulations. A comparison between numerical and analytical results has shown that to accurately describe the pattern containing half spike a truncation of $M = 3$ is necessary in the weak competition case and $M = 4$ in the case when $b_2 > 1$. This result was demonstrated for a certain fixed set of model parameters. Our next task is to investigate the impact of model parameters on amplitude and wavelength of forming periodic patterns.

4.5 Effect of model parameters on amplitude and wavelength of periodic patterns

In this section, the effect of model parameters on amplitude and wavelength is investigated. The system (4.18) can be solved only when it is truncated at low numbers ($M \leq 4$) and to make this truncation meaningful we have considered patterns in small media containing only half of the spike. However, we note, that the obtained results hold for patterns with multiple spikes. The effect of parameters is explored by running simulations for different medium lengths, performing Fourier decomposition of obtained profiles using (4.13), and detecting the medium length L when the values of the dominating node, α_1 and γ_1, get their highest values. The lengths that produce the largest node correspond to the most unstable wavelength, which is the fastest-growing medium length, resulting in the highest pattern amplitude. Numerical results have been verified using analytical Fourier analysis by solving system (4.18) for $M = 4$ and similarly investigating the effects of L on α_1 and γ_1, corresponding to the profiles $u(x)$ and $v(x)$, respectively.

Figure 4.10 a and b show the effects of diffusion on the amplitude and wavelength of the half-spike pattern found for both species, $u(x)$ and $v(x)$. Dependences of the wavelength of pattern formed by profiles, $u(x)$ and $v(x)$, which are obtained in numerical simulations, shown by the plots $L(u, S)$ and $L(v, S)$ in Figure 4.10 a. Same dependences, found analytically by solving the system (4.18) truncated at $M = 4$. $\alpha_1(n, S)$ shown by the plots $L(u, S)$ and $L(v, S)$ in the same panel. Figure 4.10 b shows dependences of the amplitudes of both profiles ($u(x)$ and $v(x)$), as given by the plots of Fourier coefficients of the main mode (which is a first mode for the pattern represented by the half-spike), which are α_1 for the u-profile and γ_1 for the v-profile. Again, $\alpha_1(S)$ and $\gamma_1(S)$ are plots obtained by Fourier decomposition of profiles obtained numerically, while $\alpha_1(A)$ and $\gamma_1(A)$ are obtained analytically. If the absolute value of α_1 increases, the amplitude of u-profile also increases, and if the absolute value of α_1 decreases,

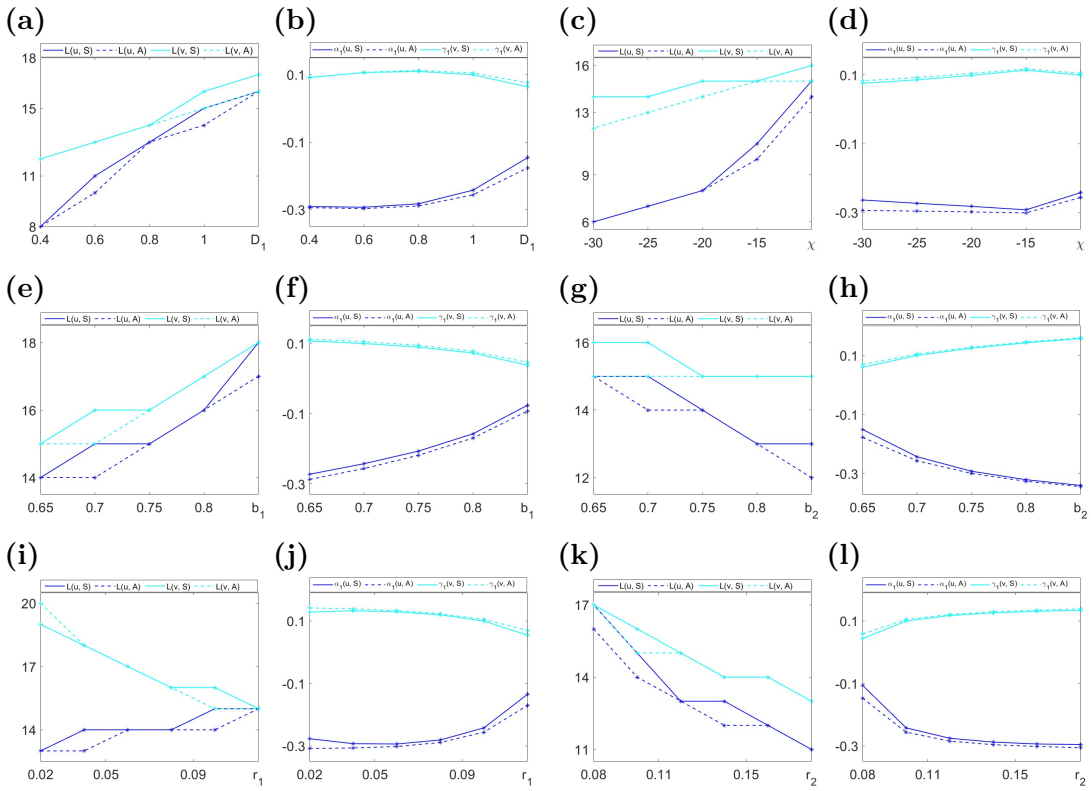

Figure 4.10: ***Dependence of the wavelength and amplitude of periodic patterns on model parameters.*** *The effect of* ***(a-b)*** *the diffusion coefficient, D_1;* ***(c-d)*** *chemotaxtic sensitivity, χ;* ***(e-f)*** *competition rate, b_1;* ***(g-h)*** *competition rate, b_2;* ***(i-j)*** *proliferation rate, r_1, and* ***(k-l)*** *proliferation rate, r_2. Default set of parameters: $D_1 = D_2 = 1$, $r_1 = r_2 = 0.1$, $b_1 = b_2 = 0.7$ and $\chi = -10$.*

the amplitude of u-profile also decreases. The same can be said about plots of γ_1 and the amplitude of v-profile. Figure 4.10 a and b demonstrate that the wavelength of pattern increases with increasing diffusion of u, represented by D_1. An interesting characteristic of the patterns corresponding to species u and v is that, for small values of D_1, the most unstable wavelengths of the two species differ significantly. This suggests that irregularities in the patterns are expected if the diffusion of u is small.

Similarly, Figure 4.10 c and d show that an increase in D_2 leads to an increase in the most unstable wavelength, while the amplitude of the pattern decreases. Additionally, irregularities are expected to appear for small values of D_2. All panels display good correlation between numerical and analytical results, indicating that accurate solutions to system (4.4) can be found by solving (4.18).

Pattern formation in a two-species system arises as a result of chemorepulsion. As a reminder, chemorepulsion needs to be strong enough for system (4.4) to become unstable under perturbation. Therefore, the effects of chemotaxis on

wavelength and amplitude are investigated. Numerical and analytical results are represented graphically in Figure 4.10 c and d, which illustrates the effects of chemorepulsion on the amplitude and wavelength of patterns resulting from the disturbance of the coexistence steady state of system (4.4). Figure 4.10 c shows that as chemorepulsion increases, the most unstable wavelength decreases. Additionally, with increasing chemorepulsion, a significant difference arises between the most unstable wavelength of species u and that of species v, indicating that strong chemorepulsion leads to irregularities in pattern formation. Figure 4.10 d demonstrates that the maximal amplitude of the pattern formed by both species occurs at $\chi = -15$. As chemorepulsion deviates from this value, the amplitude of the pattern decreases. It is worth noting that the analytical Fourier solutions predict a slightly larger pattern amplitude than the one obtained from simulations, although there is a very good approximation between the numerical and analytical results.

Next, the effects of interspecific competition are examined, as these parameters play a crucial role in the formation of periodic patterns around the coexistence steady state. Figure 4.10 shows the effects of interspecific competition on the wavelength and amplitude of the half-spike pattern formed by an infinitesimal perturbation of the coexistence steady state. In Figure 4.10 e and f, the effects of the competition of v on u are investigated. As b_1 increases, the most unstable wavelength also increases, while the amplitude of the pattern decreases. Conversely, Figure 4.10 g and h show the effects of the competition of u on v, and in this case, as b_2 increases, the most unstable wavelength decreases, and the amplitude of the pattern increases. Additionally, in both cases, there are differences between the most unstable wavelength of u and that of v, which suggests that pattern irregularities are likely to appear. It is also evident that b_1 and b_2 have opposite effects on the characteristics of the pattern: b_2 enhances pattern formation, leading to larger pattern amplitudes, while b_1 leads to smaller ones.

The final set of parameters to investigate concerns the effects of reproduction on pattern formation. As shown in Figure 4.3, periodic patterns are more likely to appear when species u has a smaller reproduction rate, r_1, and species v has a larger reproduction rate, r_2. This leads to the prediction that an increase in r_1 would decrease the amplitude of the pattern, while an increase in r_2 would enhance it. Figure 4.10 illustrates the effects of species reproduction on pattern characteristics. Figure 4.10 i and j show that as the reproduction rate of the first species increases, the most unstable wavelength decreases, along with the amplitude of the pattern. These results are consistent with previous findings, which indicated that, for this set of fixed parameters, pattern formation is not possible for $r_1 > 0.15$. Similarly, Figure 4.10 k and l show that as r_2 increases,

the most unstable wavelength also decreases; however, in this case, the amplitude of the pattern increases. This aligns with earlier results showing that, for this set of fixed parameters, pattern formation is not possible for small values of $r_2 < 0.8$. See Figure 4.3.

This section has focused on understanding how patterns are affected by changes in parameters, specifically examining how characteristics such as amplitude and wavelength are influenced. This has been demonstrated through methods of numerical and analytical Fourier analysis, which show a good match between the two sets of results. This indicates that truncating system (4.18) at $M = 3$ and solving analytically accurately captures the characteristics of a half-spike pattern. Additionally, it has been shown that the parameters which enhance the amplitude of the pattern as they increase are b_2 and r_2, while all other parameters, D_1, D_2, χ, b_1, and r_1, reduce the amplitude as they increase. It has also been observed that species u and v exhibit different wavelengths under certain parameter regimes, suggesting that patterns formed from the coexistence steady state of model (4.4) are likely to display irregularities.

This concludes the analysis of pattern formation around the coexistence steady state, and the next section focuses on pattern formation around the extinction steady states.

4.6 Discussion

Understanding interactions between two or more bacterial species is crucial in the early stages of colonisation and biofilm formation. Systems of two competing bacterial species are often referred to as Lotka-Volterra models, and the stability of the steady states has been thoroughly analysed [76, 135]. In this chapter, the Lotka-Volterra model and the Keller-Segel model [59, 60] have been combined to investigate a system of two bacterial species, u and v, where the latter produces a chemical agent, c, which chemotactically affects the former. These interactions are modelled using a system of three partial differential equations (4.4), which has four steady states:

$$(u,\ v,\ c) = \left\{(0,0,0),\ (1,0,0),\ (0,1,1),\ \left(\frac{b_1-1}{b_1b_2-1},\ \frac{b_2-1}{b_1b_2-1},\ \frac{b_2-1}{b_1b_2-1}\right)\right\},$$

where the trivial steady state is always unstable, while the other three steady states are stable in the well-mixed system under specific conditions. Classical Turing pattern analysis states that pattern formation occurs if an initially stable steady state in the well-mixed system is driven unstable by a perturbation in the full reaction-diffusion-advection system [128]. In this chapter, methods of

linear analysis and nonlinear Fourier analysis have been used to demonstrate the formation of periodic patterns around both the coexistence steady state $(u, v, c) = \left(\frac{b_1 - 1}{b_1 b_2 - 1}, \frac{b_2 - 1}{b_1 b_2 - 1}, \frac{b_2 - 1}{b_1 b_2 - 1}\right)$ and the extinction steady state $(u, v, c) = (1, 0, 0)$, as a result of aggregation initiated by a breakdown of stability.

As demonstrated in the introductory chapter, the coexistence steady state is stable in the well-mixed system if the interspecific competition between the species is less than 1, i.e., $b_1, b_2 < 1$. This identifies the region of interest for the formation of stationary periodic patterns. The first section of this chapter focused on showing that model (4.4) at coexistence can be driven unstable by infinitesimal perturbations within this region. Since finding analytical conditions for instability proved difficult, the Routh-Hurwitz criteria [25] were used with fixed parameters to identify a domain, δ_2, in which the system is unstable and exhibits pattern formation. Using numerical simulations, we have shown that for competition rates $b_1, b_2 \in \delta_2$, stationary periodic patterns arise from infinitesimal disturbances as a result of chemorepulsion. An important question that followed was how to ensure we consider the largest domain of instability, δ_2, in order to capture all competition rates that lead to a breakdown of stability and initiate aggregation. To address this, we found the most unstable wavenumber, k, which represents the fastest-growing mode. By examining the intersection point between $a_3 = 0$ and $(a_3)_k = 0$, we determined the most unstable wavenumber k, as well as the minimum competition rates $b = b_1 = b_2$ that lead to pattern formation. This prompted further analysis of how the minimum b that leads to instability changes with other parameters. This analysis was conducted through numerical simulations and analytics, and the results showed strong correlation. As diffusion increases, the minimum requirement for b also increases, meaning that faster diffusing species require stronger competition to initiate aggregation. As the strength of chemorepulsion increases, the minimum requirement for b decreases. Additionally, an increase in the reproduction rate, r_1, of the repelled species u leads to an increase in the minimum requirement for b, whereas an increase in the reproduction rate, r_2, of the species producing the repellent reduces the minimum requirement for b. This means that as species v reproduces faster, more chemotactic agent is produced, and aggregation is initiated even with weaker competition between species.

Classical Turing pattern analysis has provided conditions under which the system is driven unstable by perturbation, leading to pattern formation. However, it offers no information about the characteristics of the pattern, such as amplitude and wavelength. Using nonlinear Fourier pattern analysis, the aim is to represent solutions of model (4.4) as Fourier series and identify the fastest-growing mode. Initially, the analysis was carried out numerically by integrating a simulated pro-

file to find the coefficients corresponding to the Fourier series solution. It has been shown that, in order to accurately reproduce a pattern formed by species u containing i half-spikes, α_i, α_{2i}, and α_{3i} must be determined, and similarly for patterns produced by v and c. For a pattern with many spikes, these coefficients are easy to obtain numerically, but much more difficult to derive analytically. Therefore, to obtain the analytical coefficients corresponding to the Fourier series solution, the medium length was reduced to obtain patterns containing at most one half-spike or a full spike. Analytical Fourier series are obtained by truncating at some M, which represents the highest frequency mode, and the goal is to determine which M provides a good approximation of the profile obtained from simulations. It has been shown that truncating at $M = 1$ results in a large discrepancy between the numerical and analytical profiles. However, including one more term in the series and truncating at $M = 2$ produces a much better approximation. Results were verified for truncations up to $M = 4$, and we concluded that this is an acceptable truncation parameter for representing a half-spike pattern, based on the discrepancy between numerical and analytical solutions. The effects of model parameters on the most unstable mode have also been investigated using numerical simulations and Fourier analysis. It has been shown that the analytically obtained Fourier solution for a half-spike pattern accurately captures the characteristics of the numerical solution. Moreover, for certain parameter regimes, the two species u and v have different most unstable wavelengths, a characteristic that explains why pattern irregularities appear in a system of two bacterial species. The most unstable wavelength is the one corresponding to the fastest-growing mode. This has been used to show that certain model parameters, such as b_2 and r_2, enhance pattern formation as they increase, meaning that the amplitude of the pattern increases. On the other hand, most other model parameters reduce the amplitude of the pattern as they increase.

The second part of the chapter has focused on pattern formation from the extinction steady state $(u, v, c) = (1, 0, 0)$ due to finite amplitude disturbance. This extinction steady state is stable in the well-mixed system if $b_2 > 1$ and remains stable under the same condition in the full reaction-diffusion-advection system. According to linear analysis, stationary periodic patterns do not emerge if this steady state is perturbed by an infinitesimal disturbance. However, numerical simulations have shown that if species v is perturbed by a finite amplitude disturbance, $\tilde{v}$, stationary periodic patterns emerge, provided the disturbance is large enough. Initially, this phenomenon was analysed using computational simulations, and one of the first questions addressed was how the minimum perturbation amplitude $\tilde{v}$ is affected by parameters. It was shown that if diffusion increases, the minimum perturbation amplitude also increases. This means that

for more diffusive species, a larger density of species v needs to be introduced into the system to prevent it from decaying back to a homogeneous state before aggregation is initiated. As expected, an increase in chemorepulsion strength decreases the minimum perturbation amplitude required to initiate aggregation. For an increase in b_1, which represents the competition of v on u, there is a decrease in $\tilde{v}$, since this indicates that v is more competitive for resources and is more likely to survive and produce enough chemical agent to initiate aggregation. Conversely, for an increase in b_2, which represents the competition of u on v, there is an increase in the minimum perturbation amplitude required to initiate aggregation. Similarly, an increase in the reproduction rate of the first species, r_1, results in an increase in $\tilde{v}$, whereas an increase in the reproduction rate of the second species, r_2, decreases the minimum perturbation amplitude required to initiate aggregation. Solutions around this steady state have been investigated using nonlinear Fourier analysis, following the same procedure as for patterns emerging from the coexistence steady state. In this case, exact analytical solutions were found by solving a system of simultaneous equations (4.18) for fixed parameters, and it was shown that truncating the series at $M = 4$ produces accurate results with small discrepancies between numerical and analytical profiles. The most important result of this section is that, contrary to linear analysis, stationary periodic patterns can emerge from the steady state $(n, v, c) = (1, 0, 0)$ due to finite amplitude disturbances.

This chapter has focused on the analysis of stationary periodic patterns around the coexistence steady state and one of the extinction steady states, $(u, v, c) = (1, 0, 0)$. However, there is one more extinction steady state, $(u, v, c) = (0, 1, 1)$, which is stable in the well-mixed system if $b_1 > 1$. Classical Turing pattern analysis suggests that stationary periodic patterns can emerge from this steady state if the system can be driven unstable by perturbation in the full reaction-diffusion-advection system under the same condition. However, according to linear analysis, this steady state remains stable when perturbed in the full diffusive system for $b_1 > 1$, and pattern formation is not possible. This result is consistent with findings from computational simulations and nonlinear Fourier analysis, even in the presence of finite amplitude disturbances.

In conclusion, this chapter has analysed pattern formation in a system consisting of two bacterial species interacting with a chemical agent. Pattern formation has been proven to emerge from two steady states, and characteristics of these patterns have been identified using nonlinear Fourier analysis. Analytical results have been supported by numerical computations.

Chapter 5

Discussion

Pattern formation from an almost uniformly homogeneous steady state is one of the fundamental questions in developmental biology. A key aim of this thesis was to understand the mechanisms underlying spatio-temporal pattern formation and the conditions under which different patterns can emerge as a result of a disturbance. The patterns thoroughly investigated in this work are stationary periodic (Turing) patterns and travelling wavefronts. Mathematical models, as well as computational simulations, have been used to investigate cell-cell and cell-chemical interactions to show the conditions for the formation of spatio-temporal patterns depending on model parameters, as well as to find information about the characteristics of such patterns, such as amplitude and wavelength in the case of Turing patterns, and minimum wave speed in the case of travelling wavefronts. In this final chapter, we present an overview of our main results and their applications and discuss potential future work.

5.1 An overview of the research presented in this thesis

This thesis began with an introductory chapter to present the motivation behind this work, as well as to introduce the reader to some basic biological and mathematical concepts used throughout. This was then followed by three research chapters.

Chapter 2 represents the first research chapter, and the aim was to thoroughly investigate travelling wavefronts admitted as solutions to systems of partial differential equations, representing single as well as two interacting bacterial populations. The formation and existence of travelling waves admitted as solutions to biological systems have been thoroughly researched over the years, as this is one of the simplest ways to describe the spatial distribution of biological species. For a single species, it is common to use the well-known Fisher-Kolmogorov equation

[33, 62] to describe its spatial distribution. Using linear analysis methods, it has been shown that the minimum wave speed of a species with diffusion coefficient D and reproduction rate r, transitioning from the unstable trivial steady state to a stable steady state, is given by $s_{min} \geq 2\sqrt{Dr}$ [86, 87]. On the other hand, by expressing the solution of the Fisher-Kolmogorov equation as a sum of hyperbolic functions, the wave speed has been shown to be $s = \sqrt{\frac{25Dr}{6}}$ [64, 121].

In the single species case, we considered a system of two decoupled partial differential equations, one representing the density of the bacterial species, formulated as the Fisher-Kolmogorov equation, and the second representing the concentration of the chemical produced by the bacteria, which can decay. Our work focused on understanding the effects of model parameters on the shape of the fronts admitted as solutions in the absence of chemotaxis, as well as the effects of chemotaxis on the minimum wave speed of the wavefronts when the chemical produced by the bacteria acts as an attractant or repellent. In the case of no chemotaxis, we showed that the distance between the two wavefronts, n and c, increases as r increases but remains unchanged when D varies. Additionally, the minimum wave speed increases as D and r increase, as expected and given by the formula above. In terms of the shape of the fronts, a small reproduction coefficient results in significantly smoother fronts, while a small diffusion coefficient results in slightly sharper fronts. These results are highly valuable for analysing the chemotactic system, since we assume that for very small diffusion and reproduction, $n \approx c$, as the distance between the fronts is assumed to be very small, and the shapes are assumed to be similar. This allowed us to express n in terms of an exponential function: $n(z) = \dfrac{1}{1 + a\exp(\alpha z)}$ and obtain a formula for the wave speed of the fronts: $s = -D\sqrt{-\dfrac{r}{2\chi}} + \sqrt{-\dfrac{r\chi}{2}} + \sqrt{-2\chi r}$, where $\chi < 0$ represents the case of chemorepulsion. One of the main results of this chapter was that as the strength of chemorepulsion increases, the wave speed also significantly increases, and we provided a comparison between the wave speeds obtained analytically and those obtained from computational simulations.

The second section of this chapter focused on investigating travelling wavefronts in a two-species system, both with and without chemotaxis. The simplest and most common way to describe the spatial spread of two competing species is the well-known Lotka-Volterra system [76, 135]. The existence of travelling wavefronts in systems with Lotka-Volterra dynamics has been thoroughly investigated, and minimum wave speeds (when waves transition from the unstable steady state or one of the extinction steady states) have been found in terms of model parameters using methods of linear analysis [86, 87]. In addition, an exact

solution and wave speed of travelling wavefronts making the transition between the two extinction states have been found by expressing the solution in terms of hyperbolic functions [106]. This method is not as powerful as linear analysis since the wave speed is given for fixed model parameters, providing only one possible solution to the system. Other researchers have investigated the direction of invasion and minimum wave speed dependence on model parameters in degenerate and near-degenerate systems with Lotka-Volterra kinetics. In degenerate systems (where one of the species is assumed not to diffuse), three zones of response have been found: in the central zone, the direction of invasion depends on motility, and in the outer two zones, it depends on competition [4]. On the other hand, in near-degenerate systems (where the ratio of diffusion coefficients is very small), the wave direction is determined by a general energy function for the full system [2].

More recently, Lotka-Volterra systems with chemotaxis have attracted the attention of researchers. Typically, these systems are represented by three partial differential equations: two equations describing the interaction between the two species and their response to the chemical agent, and a third equation describing the change in the concentration of the bacterial agent. Travelling wavefronts have been proven to exist when both bacterial species degrade a chemical agent that acts as an attractant [73]. In this work, regions where travelling wavefronts appear have been shown to depend on both chemotactic sensitivities and competition between species. On the other hand, when the bacteria produce the chemical rather than degrade it, the existence of travelling wavefronts has been proven numerically using the perturbation method in computational simulations and under the assumption that the chemical concentration does not change over time [69, 123]. Moreover, the minimum wave speed of travelling wavefronts between two spatially homogeneous steady states has been given as $s_{min} \geq s\sqrt{1-b_1}$ in [53].

Rather than proving the existence of travelling wavefronts in systems with Lotka-Volterra dynamics, our work has focused on finding the minimum wave speed of fronts transitioning between various steady states. In the case where the chemical has no effect on the spatial distribution of either bacterial species, we have shown analytically, as well as numerically, that if $Dr \neq 1$, then wavefronts transitioning from the unstable trivial steady state to coexistence move with different speeds, and we have provided minimum wave speed formulas using linear analysis methods. On the other hand, we have shown that when both competition rates $b_1,\ b_2 > 1$, coexistence is unstable, and wavefronts appear to transition from coexistence to one of the stable extinction states. In this case, the minimum wave speed has been obtained analytically using the dispersion curve as a

function of the wavenumber. In the case of chemotaxis, we have assumed that the chemical agent is produced by one of the species and has a chemotactic effect on the other species. We have shown that when the system transitions from the unstable trivial state, in the long run, waves tend to move at the same speed due to chemoattraction, and the speed converges to that obtained in the case of no chemotaxis. However, when waves transition from the unstable coexistence state, as chemoattraction increases, the minimum wave speed also increases. This increase has been proven analytically using the dispersion curve as a function of the wavenumber. Additionally, the effect of model parameters on the minimum wave speed has been investigated, and a comparison between numerical and analytical speeds has been provided, which shows that the analytical speed obtained using the dispersion curve accurately captures the speed of the waves from numerical simulations.

Chapter 3 of this thesis was concerned with modelling stationary periodic (Turing) patterns in a system of two partial differential equations, representing one species producing a chemical agent. It is well known that pattern formation appears in such systems if cell migration is due to chemoattraction [59]. A number of models have been presented as variations of the original Keller-Segel model [60] from a biological perspective [46]. More recently, characteristics of stationary periodic patterns such as wavelength and amplitude have also been investigated. For example, linear analysis methods for wavelength estimation have been presented in [87]. As for the estimation of pattern amplitude, sophisticated methods using the amplitude equation have been presented in [30, 137], and an oversimplified method is described in [19].

In our work, we considered a number of nonlinear reaction-diffusion-advection systems to describe the interaction of a single species with a chemical agent produced by itself. Using classical Turing pattern analysis, we obtained conditions under which stability breaks down and aggregation is initiated, such that $R_T > 1$ represents the threshold value for pattern formation. We presented the advantages and disadvantages of various forms of chemotactic sensitivity and concluded that the simplest way to represent migration due to chemotaxis from a biologically relevant perspective is to assume that the chemotactic sensitivity is proportional to the density of the bacteria, $\chi(n,\ c) = \chi_0(nc_x)_x$. In this chapter, we also estimated the wavelength of the pattern using three different methods: linear, nonlinear, and computational, and showed that nonlinear Fourier analysis represents the most accurate method. Additionally, using nonlinear Fourier analysis, we demonstrated that the three highest frequency modes are sufficient to accurately reproduce the profiles from numerical computations. The highest frequency mode is responsible for the amplitude of the pattern as well as the

number of spikes produced. The impact of parameters on the pattern was also analysed, and we proved that an increase in the diffusion coefficient results in an increase in wavelength and a decrease in amplitude; an increase in chemotaxis results in a decrease in wavelength and an increase in amplitude; and an increase in reproduction results in a decrease in both wavelength and amplitude. We believe this work to be highly important for understanding bacterial responses to chemotactic agents and how spatial patterns can be affected by the diffusivity and proliferation properties of the species in question. Although the results presented in this thesis are based on a one-dimensional model, we believe they remain relevant, as mathematical modelling on a line is a common starting point for understanding and investigating biological processes due to its simplicity. These basic models can be refined using experimental data for parameter estimation, followed by comparisons of computational simulations with experimental findings. Furthermore, to enhance the relevance of these results, this work could be extended to higher dimensions, as biological models are often described in two- and three-dimensional spatial systems. In addition, biological processes involve numerous interacting variables and nonlinear dynamics, making them difficult to study directly. Breaking these processes down into simpler, more manageable mathematical models helps reveal underlying mechanisms and fundamental principles while filtering out unnecessary complexity. This approach also improves computational efficiency, enabling faster and more accessible analysis. This work has been extended to model interactions between two species in the final research chapter.

The aim of Chapter 4 was to investigate a competition model extended by additional interactions between populations, given by chemotactic coupling, in which one species produces a chemical agent that causes the taxis of the other species. This is biologically relevant for understanding the formation of ecological systems through competitive interactions between multiple species [66]. Researchers have shown spatial distribution due to diffusion and cross-diffusion (cross-taxis) using models such as the SKT systems [113] or the Potts-Petrovskii models [98]. In these cases, the formation of spatial patterns is due to the properties of the cross-taxis terms, which affect the speed, direction, and shape of the travelling fronts [2, 4, 12, 71]. On the other hand, other mathematical models have introduced an extra equation to model the change in the concentration of the chemical produced by one of the species [61, 65]. It has been shown that Turing instabilities can arise from extinction states when there is strong chemoattraction and strong competition between the species [92, 128]. Conversely, where there is weak competition between species and one of the chemotactic sensitivities is sufficiently large, Turing patterns can emerge from the coexistence state by re-

ducing the system to a two-variable model [60]. Recently, a novel result has been presented in [70] showing that Turing instabilities can emerge from the coexistence state if the species have mutually repulsive effects and chemorepulsion is sufficiently strong. Additionally, the amplitude of the pattern has been discussed using the amplitude equation.

The aim of our research was to better understand the conditions under which stability breaks down and patterns emerge in a system of two competitive species, where one produces a chemical agent affecting the other. Using methods of linear analysis, we identified instability domains $(b_1,\ b_2)$ where Turing patterns can emerge from the coexistence steady state. We demonstrated the importance of considering the most unstable wavenumber to ensure the largest domain of instability is obtained. Using these domains, we identified the minimum model parameters that lead to the formation of stationary periodic patterns. Moreover, employing nonlinear Fourier analysis, we obtained characteristics of the pattern such as amplitude and wavelength. Supported by results from computational simulations, we showed that an increase in any of D_1, D_2, χ, or b_1 results in an increase in wavelength and a decrease in amplitude. An increase in the reproduction rate of the first species, r_1, results in decreases in both wavelength and amplitude, while an increase in all other model parameters leads to a decrease in wavelength and an increase in amplitude.

One of the most important results of this chapter was the formation of stationary periodic patterns when the species producing the chemical agent is initially close to extinction. According to linear analysis, Turing patterns cannot emerge from this steady state when $b_2 > 1$; however, with the aid of computational simulations and nonlinear Fourier analysis, we showed that the steady state can be driven unstable by finite amplitude disturbances rather than infinitesimal perturbations. We used computational simulations to investigate the minimum disturbance required for a breakdown of stability and demonstrated its dependence on model parameters. On the other hand, such patterns cannot emerge when the species undergoing taxis is initially close to extinction.

5.2 Future work

So far, we have discussed important research regarding modelling pattern formation in growing bacterial populations and how our work contributes to this field. One of the most significant techniques developed in this thesis is the use of nonlinear Fourier analysis to obtain information about the characteristics of stationary periodic patterns, such as amplitude and wavelength. We have shown that this technique can be used to identify the most unstable wavelength, which

is responsible for the pattern with the highest amplitude and also determines the number of half-spikes expected to be produced. Future research could focus on using the amplitude equation to obtain further information about the amplitude of a Turing pattern and comparing these results with those obtained from Fourier analysis and numerical computations.

Future work could also involve applying the nonlinear Fourier analysis technique developed in this thesis to a broader range of mathematical models, such as SKT models or systems combining bacterial diffusion, cross-diffusion, and chemotaxis. The latter model is more analytically sophisticated, and it would be interesting to explore the conditions under which Turing patterns can emerge and whether stability breakdown occurs as a result of cross-diffusion, chemotaxis, or both. I believe this model is valuable for understanding spatial pattern formation, as bacteria are rarely stationary, and their motility is influenced by various environmental factors and mutual interactions between species.

In the two-species system, we have shown with the aid of computational simulations and Fourier analysis that when $b_2 > 1$, Turing instabilities can appear when the species producing the chemical agent is initially extinct, under the influence of finite amplitude disturbances. We have demonstrated how the minimum perturbation amplitude required for a breakdown of stability depends on model parameters using results from computational simulations. In the future, I aim to develop an analytical method to determine the minimum perturbation amplitude required for pattern formation and compare this with the analytical results presented in Chapter 4. Additionally, this thesis focuses on understanding the effects of competition on pattern formation in a system of two species, one of which produces a chemical agent that influences the other. Future research could explore pattern formation in predator-prey models or investigate the effects of symbiosis.

The results presented in this thesis primarily concern the use of a one-dimensional system to study pattern formation in systems of one and two interacting bacterial populations, with the computational simulations effectively illustrating pattern formation on a line. While this approach is biologically relevant due to its simplicity in breaking down complex biological systems into manageable mathematical models, I would welcome the opportunity to extend these results and simulations into higher dimensions, such as two- and three-dimensional models. To achieve this, the numerical methods employed for the computational simulations in this thesis would need refinement, and the numerical scheme would need to shift to implicit methods, which are generally more difficult to implement, but faster and more computationally efficient than explicit methods. Comparing results from a one-dimensional model with those from a two-dimensional model would offer

valuable insights into the strengths and limitations of each approach. Some questions that could be explored include: Would simpler, more time-efficient methods be more appropriate for investigating processes like biofilm formation, or would two-dimensional methods, which require more careful analytical and numerical treatment, be more beneficial?

Moreover, investigating pattern formation is a crucial step in understanding the early stages of biofilm formation and the interactions between species within an ecosystem. While mathematical models provide a valuable tool for analysing these processes by simplifying them into easier models to investigate fundamental principles, there remains uncertainty regarding how environmental factors, rather than just interspecies interactions and taxis, affect pattern formation. A promising area of development would be to refine mathematical models to incorporate environmental factors such as temperature, light, nutrient availability, and surface properties. For example, how does the smoothness of a surface influence bacterial pattern formation? Are bacteria more likely to aggregate on rougher surfaces, or do the effects of surface adhesion remain negligible?

Finally, throughout my research, I would have liked the opportunity to compare my analytical results with experimental data, which I have not had the chance to work with. In future work, I hope to validate the analytical and numerical results presented in this thesis against experimental data, as the lack of experimental validation in mathematical models remains a common challenge.

Bibliography

[1] M.J. Ablowitz and A. Zeppettela. Explicit solutions of fisher equation for a special wave speed. *Bulletin of Mathematical Biology*, 41, 1979.

[2] E.O. Alzahrani, F.A. Davidson, and N. Dodds. Travelling waves in near-degenerate bistable competition models. *Mathematical modelling of natural phenomena*, 5, 2010.

[3] E.O. Alzahrani, F.A. Davidson, and N. Dodds. A 3-species competition model for bio-control. *Applied Mathemativs and Computation*, 218, 2012.

[4] E.O. Alzahrani, F.A. Davidson, and N. Dodds. Reversing invasion in bistable systems. *Journal of Mathematical Biology*, 65, 2012.

[5] C.R. Ambruster and M.R. Parsek. New insight into the early stages of biofilm formation. *PNAS*, 115, 2018.

[6] A. Aotani, M. Mimura, and T. Mollee. A model aided unedrstanding of spot pattern formation in chemotactic *E. coli* colonies. *Japan Journal of Industrial and Applied Mathematics*, 27, 2010.

[7] J.P. Armitage and K.J. Hellingwerf. Light-induced behavioural responses ('phototaxis') in prokaryotes. *Photoshynthesis Research*, 76, 2003.

[8] C. Atkinson, G.E.H. Reuter, and C.J. Ridler-Rowe. Travelling wave solutions for some nonlinear diffusion equations. *Society for Industrial and Applied Mathematics*, 12, 1981.

[9] F.J. Ayala. Competition, coexistence, and evolution. *Essays in Evolution and Genetics in Honor of Theodosius Dobzhansky: A Supplement to Evolutionary Biology*, 1970.

[10] G.P. Bodey, R. Bolivar, V. Fainstein, and L. Jadeja. Infections caused by *Pseudomonas aeruginosa*. *Review of Infectious Diseases*, 5, 1983.

[11] J.J. Bramburger. Exact minimum speed of travelling waves in a keller-segel model. *Applied Mathematics Letters*, 111, 2021.

[12] M. Breden, C. Kuehn, and C. Soresina. On the influence of cross-diffusion in pattern formation. *Journal of Computational Dynamics*, 8, 2021.

[13] M. Breuss. The correct use of the lax–friedrichs method. *ESAIM:Mathematical Modelling and Numerical Analysis*, 38, 2004.

[14] P. Broadbridge, B.H. Bradshaw, F. Fulford, and G.K. Aldis. Huxley and fisher equations for gene propagation: An exact solution. *The ANZIAM Journal*, 44, 2002.

[15] V. Bucur and Vasiev B. Modelling formation of stationary periodic patterns in growing population of motile bacteria. *arXiv:2406.07182*, 2024.

[16] E.O. Budrene and H.C. Berg. Complex patterns formed by motile cells of *Escherichia coli*. *Letters to Nature*, 349, 1991.

[17] E.O. Budrene and H.C. Berg. Dynamics of formation of symmetrical patterns by chemotactic bacteria. *Letters to Nature*, 376, 1995.

[18] J. Canosa. Diffusion in nonlinear multiplicative media. *Journal of Mathematical Physics*, 10, 2003.

[19] Y. Chen and J. Buceta. A non-linear analysis of turing pattern formation. *Plos One*, 14, 2019.

[20] E.Y.M. Chiang. Lecture notes in fourier analysis and applications. *The Hong Kong University of Science and Technology*.

[21] J.H. Connell. On the prevalence and relative importance of interspecific competition: Evidence from field experiments. *The American Naturalist*, 122, 1983.

[22] J.C. Conrad and et al. Flagella and pili-mediated near-surface single-cell motility mechanism in *P. aeruginosa*. *Biophysics Journal*, 100, 2011.

[23] R. Courant, K. Friedrichs, and H. Lewy. On the partial difference equations of mathematical physics. *IBM Journal of Research and Development*, 11, 1967.

[24] A. Dean, M.J. Horsburg, and B. Vasiev. Toxin-mediated competition in weakly motile bacteria. *Journal of Theoretical Biology*, 480, 2019.

[25] E.X. DeJesus and C. Kaufman. Routh-hurwitz criterion in the examination of eigenvalues of a system of nonlinear ordinary differential equations. *Physical Review A*, 35, 1987.

[26] R.M. Donlan. Biofilms: Microbial life on surfaces. *Emerging Infectious Diseases*, 8, 2002.

[27] S. Doron. Bacterial infections: Overview. *International Encyclopedia of Public Health*, 2008.

[28] A.E. Douglas. *Symbiotic Interactions*. Oxford University Press, 1994.

[29] D.B. Dusenbery. *Living at Micro Scale: The Unexpected Physics of Being Small*. Harvard University Press, 2011.

[30] A. K. Dutt. Amplitude equation for a diffusion-reaction system: The reversible sel'kov model. *AIP Advances*, 2, 2012.

[31] L. Edelstein-Keshet. *Mathematical Models in Biology*. Society for Industrial and Applied Mathematics, 2005.

[32] P.C. Fife. Asymptotic states for equations of reaction and diffusion. *Bulletin of the Americal mathematical society*, 84, 1978.

[33] R.A. Fisher. The wave of advance of advantageous genes. *Annalf of Eugenics*, 7, 1937.

[34] R. Fitzhugh. Impulses and physiological states in theoretical models of nerve membrane. *Biophysical Journal*, 1, 1961.

[35] G.B. Folland. *Fourier analysis and its applications*. Brooks/Cole Publishing Company, 1992.

[36] J. Fourier. *The analytical theory of heat*. Cambridge University Press, 1878.

[37] B Franz, C. Xue, K.J. Painter, and R. Erban. Travelling waves in hybrid chemotaxis models. *Bulletin of Mathematical Biology*, 2013.

[38] M.K.A. Gavina, T. Tahara, K.-I. Tainaka, H. Ito, S. Morita, G. Ichinose, T. Okabe, T. Nagatani, and J. Yoshimura. Multi-species coexistence in lotka-volterra competitive systems with crowding effects. *Scientific Reports*, 2018.

[39] A. Gierer and H. Meinhardt. Theory of biological pattern formation. *Kybernetik*, 12, 1972.

[40] A.F. Gorter, M. Manhart, and M. Ackermann. Understanding the evolution of interspecies interactions in microbial communities. *Philosophical Transactions of the Royal Society B*, 375, 2020.

[41] A. Gupta and S. Chakraborty. Linear stability analysis of high- and low-dimensional models for describing mixing-limited pattern formation in homogeneous auticatalytic reactors. *Chemical Engineering Journal*, 145, 2009.

[42] L. Hall-Stoodley, J.W. Costerton, and P. Stoodley. Bacterial biofilms: from the natural environment to infectious diseases. *Nature Reviews*, 2, 2004.

[43] G. Hardin. The competitive exclusion principle. *Science*, 1960.

[44] N. C. Harrison, R. Diez del Corral, and B. Vasiev. Coordination of cell differentiation and migration in mathematical models of caudal embryonic axis extension. *Plos One*, 6, 2011.

[45] J-H. He and X-H. Wu. Exp-function method for nonlinear wave equations. *Chaos, Solitons and Fractals*, 30, 2006.

[46] T. Hillen and K.J. Painter. A user's guide to pde models for chemotaxis. *Journal of Mathematical Biology*, 58, 2009.

[47] Y. Hosono. The minimal speed of travelling fronts for a diffusive lotka-volterra competition model. *Bulletin of Mathematical Biology*, 60, 1998.

[48] Y. Hosono. Travelling waves for a diffusive lotka-volterra competition model i: Singular perturbations. *Discrete and Contionuous Dynamical Systems Series B*, 3, 2003.

[49] Y. Hosono. Traveling waves for the lotka-volterra predator-prey system without diffusion of the predator. *Discrete and Continuous Dynamical Systems*, 20, 2015.

[50] S.B. Hsu, S.P. Hubbell, and P. Waltman. A contribution to the theory of competing predators. *Ecological Monographs*, 48, 1978.

[51] J.A. Hulzebos. *Keller-Segel models for chemotaxis*. PhD thesis, Iowa State University, 2017.

[52] L-C. Hung. Exact travelling wave solutions for diffusive lotka-volterra systems of two competing species. *Japan Journal of Industrial and Applied Mathematics*, 29, 2012.

[53] T.B. Issa, R.B. Salako, and W. Shen. Travelling wave solutions for two species competitive chemotaxis systems. *Nonlinear Analysis*, 212, 2021.

[54] K. Ito and F. Kappel. *Evolution equations and approximations*. Singapore: World Scientific Publishing Company, 2002.

[55] J. Jaishankar and P. Srivastava. Molecular basis of stationary phase survival and applications. *Frontiers in Microbiology*, 8, 2017.

[56] G.A. James, L. Beaudette, and J.W. Costerton. Interspecies bacterial interactions in biofilms. *Journal of Industrial Microbiology*, 15, 1995.

[57] G. Kaiser. *Microbiology.* Community College of Baltimore County, LibreTexts, 2024.

[58] E.F Keller. Traveling bands of chemotactic bacteria: A theoretical analysis. *Journal of Theoretical Biology*, 30, 1971.

[59] E.F. Keller and L.A. Segel. Initiation of slime mold aggregation viewed as an instability. *Journal of Theoretical Biology*, 26, 1970.

[60] E.F. Keller and L.A. Segel. Model for chemotaxis. *Journal of Theoretical Biology*, 30, 1971.

[61] F.X. Kelly, K.J. Dapsis, and D.A. Lauffenburger. Effect of bacterial chemotaxis on dynamics of microbial competition. *Microbial Ecology*, 16, 1988.

[62] A. Kolmogorov, I. Petrovskii, and N. Piskunov. A study of the diffusion equation with increase in the amount of substance. *Bulletin of Moscow University*, 1, 1993.

[63] A.N. Kolmogorov, I.G. Petrovskii, and N.S. Piskunov. A study of the diffusion equation with increase in the quantity of matter, and its application to a biological problem. *Moscow University Mathematics Bulletin*, 1, 1937.

[64] E.V. Krishnan. On some diffusion equations. *Journal of the Physics Society of Japan*, 63, 1993.

[65] H.I. Kurt and W. Shen. Two species chemotaxis-competition system with singular sensitivity: Global existence, boundedness, and persistence. *Journal of Differential Equations*, 355, 2023.

[66] J.M. Lang and M.E. Benbow. Species interactions and competition. *Nature Education Knowledge*, 4, 2013.

[67] D.A. Larson. Transient bounds and time-asymptotic behaviour of solutions to nonlinear equations of fisher type. *SIAM Journal of Applied Mathematics*, 34, 1978.

[68] P.D. Lax. Weak solutioms of nonlinear hyperbolic equations and their numerical computation. *Communications on Pure and Applied Mathematics*, 7, 1954.

[69] D. Li, X. He, X. Li, and S. Guo. Travelling wavefronts in a two-species chemotaxis model with lotka-volterra competitive kinetics. *Applied Mathematics Letters*, 114, 2021.

[70] G. Li and Y. Yao. Two-species competition model with chemotaxis: well-posedness, stability and dynamics. *Nonlinearity*, 35, 2022.

[71] Qing Li and Yaping Wu. Stability analysis on a type of steady state for the skt competition model with large cross diffusion. *Journal of Mathematical Analysis and Applications*, 462, 2018.

[72] T. Li and J. Park. Travelling waves in a chemotaxis model wtih logistic growth. *Discrete and Continuous Dynamical Systems Series B*, 24, 2019.

[73] T.-C. Lin. Development of travelling waves in an interacting two-species chemotaxis model. *Discrete and Continuous Dynamical Systems*, 34, 2014.

[74] T.-C. Lin and Z.-A. Wang. Development of travelling waves in an interacting two-species chemotaxis model. *Discrete and Continuous Dynamical Systems*, 34:2907–2927, 2014.

[75] C. Liu, X. Fu, L. Liu, X. Ren, C. K. L. Chau, S. Li, L. Xiang, H. Zeng, G. Chen, L.-H. Tang, P. Lenz, X. Cui, W. Huang, T. Hwa, and J.-D. Huang. Sequential establishment of stripe patterns in an expanding cell population. *Science*, 334, 2011.

[76] A.J. Lotka. A contribution to the theory of periodic reaction. *Journal of Physical Chemistry*, 14, 1910.

[77] P.S. Lovely and F.W. Dahlquist. Statistical measures of bacterial motility and chemotaxis. *Journal of Theoretical Biology*, 50, 1975.

[78] X. Lu, B. Dong, B. Mao, and X. Zhang. Convergence improved lax-friedrichs scheme based numerical schemes and their applications in solving the one-layer and two-layer shallow-water equations. *Mathematical Problems in Engineering*, 1, 2015.

[79] W.X. Ma and B. Fuchssteiner. Explicit and eaxct solutions to a kolmogorov-petrovskii-piskunov equation. *International Journal of Non-Linear Mechanics*, 31, 1996.

[80] R.M. Macnab and Jr Koshland, D.E. The gradient-sensing mechanism in bacterial chemotaxis. *PNAS*, 69, 1972.

[81] V.S. Manoranjan and A.R. Mitchell. A numerical study of the belusov-zhabotinskii reaction using galerkin finite elements methods. *Journal of Mathematical Biology*, 16, 1983.

[82] W.F. Marshall. Pattern formation and complexity in single cells. *Current Biology*, 30, 2020.

[83] K. Mattsson and Y.L. Rydin. Implicit summation by parts operators for finite difference approximations of first and second derivatives. *Journal of Computational Physics*, 473, 2023.

[84] H.P. McKean. Application of brownian motion to the equation of kolmogorov-petrovskii-piskunov. *Communications of pure and applied mathematics*, 28, 1975.

[85] W. Milne. *Numerical calculus*. Princeton University Press, 1949.

[86] J.D. Murray. *Mathematical Biology: I. An Introduction*. Springer, third edition edition, 2003.

[87] J.D. Murray. *Mathematical Biology: II. Spatial Models and Biomedical Applications*. Springer, third edition edition, 2003.

[88] E.K. Nelso, C.E. Matthews, and J.A. Rosenheim. Predators reduce prey population growth by inducing changes in prey behaviour. *Ecology*, 85, 2004.

[89] A. Okubo, P.K. Maini, M.H. Williamson, and J.D. Murray. On the spatial spread of the grey squirrel in britain. *Proceedings of the Royal Society of London*, 238, 1989.

[90] K.J. Painter, P.K. Maini, and H.G. Othmer. Stripe formation in juvenile *pomacanthus* explained by a generalized turing mechanism with chemotaxis. *Proceedings of the National Academy of Sciences of the United States of America*, 96, 1999.

[91] V. Palma, M. S. Gutiérrez, O. Vargas, R. Parthasarathy, and P. Navarrete. Methods to evaluate bacterial motility and its role in bacterial–host interactions. *Microorganisms*, 10, 2022.

[92] X. Pan, C. Mu, and W. Tao. On the strongly competitive case in a fully parabolic two-species chemotaxis system with lotka-volterra competitive kinetics. *Journal of Differential Equations*, 354.

[93] D.R. Peart. Species interactions in a successional grassland. i: Seed rain and seedling recruitment. *Journal of Ecology*, 77, 1989.

[94] D.R. Peart. Species interactions in a successional grassland. ii: Colonization of vegetated sites. *Journal of Ecology*, 77, 1989.

[95] V. Piskovsky and N.M. Oliweira. Bacterial motility can govern the dynamics of antibiotic resistance evolution. *Nature Communications*, 14, 2023.

[96] A. Piunovskiy and B. Vasiev. Modelling ethnogenesis. *Biosystems*, 219, 2022.

[97] A.A. Polezhaev, R.A. Pashkov, A.I. Lobanov, and I.B. Petrov. Spatial patterns formed by chemotactic bacteria escherichia coli. *International Journal of Developmental Biology*, 50, 2006.

[98] J. R. Potts and S. V. Petrovskii. Fortune favours the brave: Movement responses shape demographic dynamics in strongly competing populations. *Journal of Theoretical Biology*, 420, 2017.

[99] R. Pound. Symbiosis and mutualism. *The American Naturalist*, 27, 1893.

[100] W.H. Press, S.A. Teukolsky, W.T. Vetterling, and B.P. Flannery. *Numerical Recipes in C; The Art of Scientific Computing*. Cambridge University Press, second edition edition, 1992.

[101] M.A.M. Qasem and I.S. Muhammasd. Sine-cosine method for finding the soliton solutions of the generalized fifth-order nonlinear equation. *Chaos, Solitons and Fractals*, 33, 2007.

[102] N. Rabin, Y. Zheng, C. Opoku-Temeng, Y. Du, E. Bonsu, and H. O Sintim. Biofilm formation mechanisms and targets for developing antibiofilm agents. *Future Medicinal Chemistry*, 7, 2015.

[103] M. Rasolonjanahary and B. Vasiev. Scaling of morphogenetic patterns in reaction-diffusion systems. *Journal of Theoretical Biology*, 404, 2016.

[104] E. Renshaw. Pearl-verhulst logistic process. *Encyclopaedia of Mathematics Supplement Vol. 1 (ed. M. Hazewinkel)*, 1999.

[105] W. J. M. Ridgway, M. P. Dalwadi, P. Pearce, and S. J. Chapman. Motility-induced phase separation mediated by bacterial quorum sensing. *Physical Review Letters*, 131, 2023.

[106] M. Rodrigo and M. Mimura. Exact solutions of a competition-diffusion system. *Hiroshima Mathematical Journal*, 30, 2000.

[107] C. Romsics, J. Makk, M. Palatinszky, É. Ács, and K. Jáger. *Practical Microbiology based on the Hungarian practical notes entitled "Mikrobiológiai Laboratóriumi Gyakorlatok"*. Eötvös Loránd University, 2013.

[108] P.W.W. Rushton, S.P. ad Lurz, R. Fuller, and P.J. Garson. Modelling the distribution of the red and grey squirrel at the landscape scale: A combined gis and population dynamics approach. *Journal of Applied Ecology*, 34, 1997.

[109] I. Sampedro, R.E Parales, T. Krell, and J.E. Hill. Pseudomonas chemotaxis. *FEMS Microbiology Reviews*, 39, 2015.

[110] J. Sapp. *Evolution by Association: A History of Symbiosis*. Oxford University Press, 1994.

[111] L.A. Segel. Simplification and scaling. *SIAM Review*, 14, 1972.

[112] L.F. Shampine. Two-step lax-friedrichs method. *Applied Mathematics Letters*, 18, 2005.

[113] N. Shigesada, K. Kawasaki, and E. Teramoto. Spatial segregation of interacting species. *Journal of Theoretical Biology*, 79, 1979.

[114] S.J. Siegel and J.N. Weiser. Mechanisms of bacterial colonization of the respiratory tract. *Annual Review of Micobiology*, 69, 2015.

[115] F. Siegert, B. Vasiev, and C.J. Weijer. The morphogenesis of dictyostelium discoideum — pattern formation in a biological excitable system. In J. Parisi, S.C. Müller, and W. Zimmermann, editors, *A Perspective Look at Nonlinear Media*. Springer Berlin Heidelberg, 1998.

[116] L. Smolin. Galactic disks as reaction-diffusion systems. *arXiv:astro-ph/9612033*, 1996.

[117] J. Smoller. *Shock waves and reaction-diffusion equations*. Springer Science and Busniess Media, 2012.

[118] V. Sourjik and N.S. Wingreen. Responding to chemical gradients: bacterial chemotaxis. *Current Opinion in Cell Biology*, 24, 2012.

[119] E.A. Soutourina, O.A. amd Semenova, V.V. Parfenova, A. Danchin, and P. Bertin. Control of bacterial motility by environmental factors in polarly flagellated and peritrichous bacteria isolated from lake baikal. *Applied and environmental microbiology*, 2001.

[120] C. Stinner, J.I. Tello, and M. Winkler. Competitive exculsion in a two-species chemotaxis model. *Journal of Mathematical Biology*, 68, 2014.

[121] N. Taghizadeh and M. Mirzazadeh. The modified extended tanh method with the riccati equation for solving nonlinear partial differential equations. *Mathematica Aeterna*, 2, 2012.

[122] N. Taghizadeh and M. Mirzazadeh. Travelling wave solutions of kdvs using sine-cosine method. *Journal of the Assocition of Arab Universities for Basic and Applied Sciences*, 15, 2014.

[123] J.I. Tello and M. Winkler. Stabilization is a two-species chemotaxis system with a logistic source. *Nonlinearity*, 25, 2012.

[124] G. Teschl. *Ordinary Differential Equations and Dynamical Systems*. American Mathematical Society, 140 edition, 2012.

[125] M.T.T. Thi, D. Wilbowo, and B.H.A. Rehm. Pseudomonas aeruginosa biofilms. *International Journal of Molecular Sciences*, 21, 2020.

[126] G.P. Tolstov. *Fourier series*. Dover Publications, New York, 1976.

[127] G.J. Tortora, B.R. Funke, and C.L. Case. *Microbiology: An Introduction*. Harlow:Pearson Education LImited, 2021.

[128] A. Turing. The chemical basis of morphogenesis. *Royal Society of London*, 237, 1952.

[129] G.A. Turnbull, A.W. Morgan, and J.R. Wjipps, J.M. ad Saunders. The role of bacterial motility in the survival and sperad of *pseudomonas fluorescens* in soil and in the attachment and colonisation of wheat roots. *FEMS Micobiology Ecology*, 36, 2001.

[130] R. Tyson. *Pattern formation by E. coli; Mathematical and numerical investigation of a biological phenomenon*. PhD thesis, University of Washington, 1996.

[131] B. Vasiev. Modelling chemotactic motion of cells in biological tissues. *Plos One*, 11, 2016.

[132] B.N. Vasiev, P. Hogeweg, and A.V. Panfilov. Simulation of dictyostelium-discoideum aggegation via reaction-diffusion model. *Physical Review Letters*, 73, 1994.

[133] O.O. Vasieva, B.N. Vasiev, V.A. Karpov, and A.N. Zaikin. A model of dictyostelium discoidem aggregation. *Journal of Theoretical Biology*, 171, 1994.

[134] A.I. Volpert, V.A. Volpert, and V.A. Volpert. *Travelling wave solutions of parabolic systems*. American Mathematical Society, 1994.

[135] V. Volterra. Variations and fluctuations of the number of individuals in animal species living together. *Animal Ecology by Chapman, R.N.*, 1931.

[136] G.H. Wadhams and J.P. Armitage. Making sense of it all: bacterial chemotaxis. *Nature Reviews Molecular Cell Biology*, 5, 2004.

[137] Y. Wang and H. Li. Travelling wave fronts of lotka-volterra reaction-diffusion system in the weak competition case. *The Royal Society of Edinburgh Section A*, 152, 2022.

[138] Z.A. Wang. Mathematics of travelling waves in chemotaxis - review paper. *Discrete and Continuous Dynamical Systems*, 18, 2013.

[139] N. Weiland-Bräuer. Friends or foes—microbial interactions in nature. *Biology*, 10, 2021.

[140] A. White, P. Lurz, H. Jones, M. Boots, J. Bryce, J. Tonkin, K. Ramoo, L. Bamforth, and A. Jarrott. *The use of mathematical models in red squirrel conservation: Assessing the threat from grey invasion and disease to the Fleet basin stronghold.* 2015.

[141] I.N. William. Some exact solutions to a non-linear diffusion problem in population genetics and combustion. *Journal of Theoretical Biology*, 85, 1980.

[142] T.E. Woolley. Boundary conditions cause different generic bifurcation structures in turing systems. *Bulletin of Mathematical Biology*, 84, 2022.

[143] C. Xue, H.J. Hwang, K.J. Painter, and R. Erban. Travelling waves in hyperbolic chemotaxis equations. *Bulletin of Mathematical Biology*, 73, 2011.

[144] M. Yamaguchi, E. Yoshimoyo, and S. Kondo. Pattern regulation in the stripe of zebrafish suggests an underlying dynamic and autonomous mechanism. *Applied Physical Sciences*, 104, 2007.

[145] G. Yusuf and M. Emine. Exp-function method for solving nonlinear evolution equations with higher order nonlinearity. *Computers and Mathematics with Applications*, 61, 2011.

[146] A. Zaikin and A.M. Zhabotinsky. Concentration wave propagation in 2-dimensional liquid-phase self-oscillating system. *Nature*, 225, 1970.

[147] H. Zang, A. Kosmrlj, and S. S. Datta. Chemotactic motility-induced phase separation. *Physical Review Letters*, 131, 2023.

[148] K. Zegadło, M. Gieroń, P. Żarnowiec, K. Durlik-Popińska, B. Kręcisz, W. Kaca, and G. Czerwonka. Bacterial motility and its role in skin and wound infections. *International Journal of Molecular Sciences*, 24, 2023.

[149] L. Zhou, T. Wang, Z. Lyu, and J. Yu. A modified lotka-volterra model for the evolution of coordinate symniosis in energy enterprise. *IOP Conference Series: Earth and Environmental Science*, 113, 2018.